Development and Application of Coupled Cluster Ground- and Excited-State Models

Christopher E. Smith

Dissertation submitted to the Faculty of the

Virginia Polytechnic Institute and State University

in partial fulfillment of the requirements for the degree of

Doctor of Philosophy

in

Chemistry

T. Daniel Crawford, Chair

Paul Carlier

Alan Esker

John Morris

Brian Tissue

April 24, 2006

Blacksburg, Virginia

Keywords: EOM, Coupled Cluster Theory, CC3

Development and Application of Coupled Cluster Ground- and Excited-State Models

Christopher E. Smith

(ABSTRACT)

We give an overview of quantum chemical methods with a particular emphasis on the development of high-accuracy quantum chemical models. The reliability of these methods often hinges on whether enough electron correlation is included in the truncated wave function. As an example, we investigate the structures of *m*-benzyne and its fluorinated derivative, tetrafluoro-*m*-benzyne where the inclusion of triple excitations is paramount to correctly describe through-bond delocalization of the monocyclic form. At the CCSDT/6-31G** level of theory, the C1−C3 distance of the minimum energy form of *m*-benzyne is 2.0 Å and the profile of the PES along the C1−C3 distance is that of an asymmetric, single-well, in agreement with previous density-functional theory and coupled cluster studies. In addition, the calculated CCSD(T) fundamental frequencies are in excellent agreement with the measured infrared frequencies, thus confirming the monocyclic form of *m*-benzyne. For tetrafluoro-*m*-benzyne, however, the increased eclipsing strain between the ring-external C−X bonds stabilizes the bicyclo[3.1.0]hexatriene form: the C1−C3 distance is calculated at the CCSD(T)/cc-pVTZ level to be approximately 1.75 Å, which is in the range of elongated CC bonds. Computed harmonic vibrational frequencies compare reasonably well with the experimental neon-matrix

difference spectrum and provide further evidence for the existence of a bicyclic form.

We also report an extension of the coupled cluster iterative-triples model, CC3, to excited states of open-shell molecules, including radicals. We define the method for both spin-unrestricted Hartree-Fock (UHF) and spin-restricted open-shell Hartree-Fock (ROHF) reference determinants and discuss its efficient implementation in the PSI3 program package. The program is streamlined to use at most $\mathcal{O}(N^7)$ computational steps and avoids storage of the triple-excitation amplitudes for both the ground-and excited-state calculations. The excitation-energy program makes use of a Löwdin projection formalism (comparable to that of earlier implementations) that allows computational reduction of the Davidson algorithm to only the single- and double-excitation space, but limits the calculation to only one excited state at a time. However, a root-following algorithm may be used to compute energies for multiple states of the same symmetry. Benchmark applications of the new methods to the lowest valence $^2B_1$ state of the allyl radical, low-lying states of the CH and CO^+ diatomics, and the nitromethyl radical show substantial improvement over ROHF- and UHF-based CCSD excitation energies for states with strong double-excitation character or cases suffering from significant spin contamination. For the allyl radical, CC3 adiabatic excitation energies differ from experiment by less than 0.02 eV, while for the $^2\Sigma^+$ state of CH, significant errors of more than 0.4 eV remain.

Finally, ground- and excited-state dipole moments are derived diagramatically and were recently developed within the PSI3 quantum chemistry package. However, convergence problems with computing the left-hand excited-state has prevented us from reporting any mean-

ingful results. Thus, future work includes solving this convergence problem before the effects of triple excitations on one-electron properties can be reported with certainty.

Acknowledgments

This dissertation was achieved thanks to the hard work and commitment of many individuals.

- Dr. Daniel Crawford for his dedication to his students and providing strong leadership in developing both research and communication skills
- Dr. Rollin King for his guidance and involvement in developing the CC3 code
- Group members Mary Tam and Nicholas Russ for their extensive help in lab and providing an enjoyable work environment
- Dr. Micah Abrams for many helpful discussions involving methods development.
- My committee members Dr. Paul Carlier, Dr. Alan Esker, Dr. John Morris, and Dr. Brian Tissue
- My roommate Shane Thompson for our many late-night escapades and insightful billiards discussions
- My brother-in-law Jim Burghard for teaching me the true meaning of patience and of course his financial support

- My fond Grandfather and Uncle for their involvement in my life
- My family, especially my parents Charles and Nancy Smith and sister Christina Smith, for their guidance and everlasting love and support

Preface

> "Today, the situation has been reached where, in many cases, the computational chemist can substitute the computing machine for the test tube. Not that the computational approach to the study of chemistry should be regarded as a rival to the traditional experimental techniques. Often the two approaches are complementary, one approach providing data which are not available from the other, and *vice versa*.[1]"
>
> -Stephen Wilson

The field of computational chemistry has progressed to the point that scientists are now capable of exploring important chemical concepts that would be otherwise left untouched. For some molecules, such as species that occur in interstellar space, frequently the only available data is obtained from theoretical calculations. Identifying possible carriers of diffuse interstellar bands, for example, are sometimes only possible by high-level theory. Could other isoelectronic species exist? Theory can provide us with the fingerprints needed to detect them. Thus, much research effort is devoted towards developing and improving these

high-accuracy chemical models.

In this dissertation, we will focus on the development of high-level quantum chemical methods and described approximate techniques for solving many-body problems. What approximations are made in developing these models? Can we systematically improve the reliability of these approximations or is the price of obtaining such accuracy impractical or unrealistic? These are just a few of the questions which we will address. Of particular interest are the experimental observables and phenomena which stem from the molecule's electronic excited-states. We have developed a model for obtaining some excited-state properties which will be compared to previous theoretical results. First, however, we will review some ground-state methods and address the importance of properly correlating the motion of the electrons.

Chapter 1 reviews notation and basic equations in quantum chemistry. A review of spin-restricted and spin-unrestricted Hartree-Fock theory is used to define our reference wave functions. Subsequent methods for improving the Hartree-Fock reference will also be discussed including many-body perturbation theory and coupled cluster theory. Computational considerations are reported with a focus on symmetry exploitation. Finally, we present a discussion of Feynman-like diagrams and their role in quantum chemistry.

A particular emphasis in Chapter 3 is on extending the high-accuracy coupled cluster model to include higher-level excitations. The chapter compares a few different techniques for incorporating the effects of triples in the coupled cluster wave function. The chapter includes a diagrammatic derivation and some key computational details of our implementation of a high-accuracy EOM-CC model.

Chapter 3 is an application of the techniques described in Chapter 1. The chapter focuses on two radicals (m-benzyne and tetra-fluoro-m-benzyne) which are two examples that elucidate the importance of making systematic improvements to the electronic wave function. These improvements are shown to make qualitative differences along the C_1-C_3 coordinate path of its potential energy surface. Comparisons with experimental infrared data are utilized to reveal the reliability of each model.

The profound effects observed in Chapter 3 will also carry over for excited-state models. Chapters 4 and 5 include applications of the EOM-CC models. The chapters focus on open-shell molecules which are known to create many modeling difficulties. Chapter 4 focuses on comparing the predicted EOM-CC excitation energies to other theoretical techniques. In Chapter 5, we will reveal and characterize the excited states of the allyl radical through its ionization potential.

Finally, in Chapter 6 we conclude with a discussion on density matrices and excited-state one-particle properties. This chapter contains the diagrammatic details of the ground-state and excited-state one-particle density matrices.

Contents

1 Introduction to Many-Electron Wave Functions **1**

1.1 Born-Oppenheimer Approximation 2

1.2 Hartree-Fock Theory 4

1.2.1 Roothaan-Hall Equations 6

1.2.2 Pople-Nesbet Equations 8

1.3 Correlated Wavefunctions 12

1.3.1 Perturbation Theory 15

1.3.2 Coupled Cluster Theory 17

1.4 Formalism of the EOM Eigenvalue Equation 20

1.4.1 Davidson Method 23

1.5 Efficient Program Implementation 25

1.5.1 Direct Product Decomposition 26

1.5.2 Spin Factorization 28

1.6 Coupled Cluster Diagrams 29

1.6.1 EOM-CCSD Sigma Equations 37

2 Approximate Triples Corrections **40**

2.1 Perturbative Energy Correction 42

2.1.1 Ground-State Equations 42

2.1.2 Excited-State Equations 46

2.2 Iterative Triples Correction 47

2.2.1 CCSDT-n Methods 48

2.2.2 CC3 50

2.3 CC3 Diagrams 51

3 The Structures of *m*-Benzyne and Tetrafluoro-*m*-Benzyne **55**

3.1 Introduction 55

3.2 Computational Approach 61

3.3 Results and Discussion: *m*-Benzyne 62

3.3.1 Electronic Structure of *m*-Benzyne 64

3.3.2 Biradical Character of *m*-Benzyne 67

3.3.3 The Infrared Spectrum of *m*-Benzyne 68

3.4 Results and Discussion: Tetrafluoro-*m*-Benzyne 73

3.4.1 The Infrared Spectrum of Tetrafluoro-*m*-Benzyne 77

3.4.2 Biradical Character of Tetrafluoro-*m*-Benzyne 81

3.5 Conclusions 82

4 Coupled Cluster Methods Including Triple Excitations for Excited-States of Radicals 85

4.1 Introduction 85

4.2 Theory 90

4.3 Benchmark Calculations 99

4.3.1 The Valence $^2B_1$ State of the Allyl Radical 99

4.3.2 The CH and CO^+ Radicals 102

4.3.3 Low-Lying Doublet States of the Nitromethyl Radical 104

4.4 Conclusions 106

5 Coupled Cluster Excitation Energies of the Allyl Radical Including Single-

Double- and Approximate Triple Excitations **108**

5.1 Introduction 108

5.2 Computational Details 113

5.3 Discussion 115

5.3.1 The $^2A_1$ States 115

5.3.2 The $^2A_2$ States 119

5.3.3 The $^2B_1$ States 120

5.3.4 The $^2B_2$ States 121

5.4 Conclusions 121

6 One Electron Density Properties **123**

6.1 General Theory 124

6.2 One-Particle Density Matrix 126

6.2.1 Transition Dipole Moments 129

6.3 Computer Implementation 129

7 Summary and Concluding Remarks **131**

Bibliography 135

List of Figures

1.1 RHF and UHF potential energy curves illustrating the dissociation of H_2 . . 9

1.2 Short range dynamic correlation energy curves for the exact and Hartree-Fock wave functions. The energy (vertical distance) is a function of the distance between electrons (cusp occurs at $r_{12} = 0$). 12

1.3 H_2 molecular orbital energy profiles illustrating static correlation effects; (a) is at equilibrium R_e; (b) and (c) occur at stretched bond lengths creating a near-degeneracy between the MOs. 14

1.4 Matrix representation of the totally symmetric amplitudes. 27

2.1 Ground-state triples contributions to the CC3 amplitude equations. The squiggly interaction lines refer to the T_1-transformed intermediates, defined by equation (2.15). 53

2.2 Excited-state triples contributions to the CC3 sigma equations. The three-body terms are given in literature by Christiansen, Koch, Jørgensen and co-workers.[2–4] 54

3.1 Possible structural forms of *m*-benzyne: a monocyclic singlet biradical (**1**) vs. a bicyclic closed-shell singlet (**2**); the σ-allylic structure of Winkler and Sander[5] (**I**) vs. a σ-delocalized structure (**II**). In structure **2**, the ring denotes the π system, which remains essentially intact (relative to benzene) after the formation of the C1−C3 bond. In structure **I**, the dotted line indicates the presence of σ-through-bond coupling between C1−C3 and C1−C2/C2−C3. For structure **II**, the circle indicates the delocalized π system, the dashed hexagon through-bond delocalization, and the coupled arrows a strong degree of spin coupling leaving little, but still finite biradical character. 56

3.2 RHF-CCSD and RHF-CCSD(T) C1−C3 energy profiles for *m*-benzyne using a 6-31G(*d*,*p*) basis set. Structural parameters were optimized for fixed C1−C3 distances. Energies are reported relative to the global minimum on the respective PES. (a) Total energies; (b) SCF energies (left-hand *y*-axis) and change in correlation energy with respect to the C1−C3 distance, relative to the correlation energy at r(C1−C3) = 1.40 Å (right-hand *y*-axis). 65

3.3 RHF-CCSD and CCSD(T) infrared vibrational spectra for *m*-benzyne using a 6-31G(*d*,*p*) basis. The experimental infrared difference spectrum reported by Marquardt *et al.*[6] is compared to **(a)** the CCSD harmonic infrared spectrum and **(b)** the CCSD(T) harmonic and fundamental infrared spectra. 71

3.4 RHF-CCSD and RHF-CCSD(T) C1−C3 energy profiles for tetrafluoro-*m*-benzyne using the 6-31G(*d*,*p*) and cc-pVTZ basis sets. Structural parameters were optimized for fixed C1−C3 distances at the RHF-CCSD(T)/6-31G(*d*,*p*) level of theory. Energies are reported relative to the global minimum on the respective PES. 75

3.5 RHF-CCSD and RHF-CCSD(T) harmonic vibrational spectra for tetrafluoro-*m*-benzyne using a 6-31G(*d*,*p*) basis. The experimental infrared difference spectrum reported by Wenk and Sander[7,8] is compared to (**a**) the CCSD spectrum, (**b**) the CCSD(T) spectrum for the "inner" minimum, and (**c**) the CCSD(T) spectrum for the "outer" minimum. 79

4.1 Schematic diagram of the nine $M_S = \frac{1}{2}$ Slater determinants arising from the distribution of three electrons in three spatial orbitals (six spin-orbitals): (a) The ground doublet state, used as a reference determinant; (b) two "closed-shell" doublet determinants, both classified as single excitations relative to (a); (c) three "closed-shell" doublet determinants classified as double excitations relative to (a); and (d) three "low-spin" determinants that contribute to both doublet and quartet states, one of which is a double excitation relative to (a). 87

4.2 Generalized antisymmetrized diagrammatic representations of expressions for (a) X_3, Y_3 and T_3 triples given in Eqs. 4.10, 4.11, and 4.12; (b) triples contributions to Eq. 4.8; (c) triples contributions to Eq. 4.9 from two-electron intermediates; (d) triples contributions to Eq. 4.9 from the occupied-virtual block of the Fock matrix for non-Hartree-Fock references (e.g., ROHF). . . . 96

5.1 Geometric parameters were optimized at the CCSD(T)/aug-cc-pVDZ level; bond lengths are reported in Å; angles are reported in degrees. 112

6.1 Triples contributions to the ground-state one-particle density matrix elements. The thin upper and lower lines represent λ and T vectors. 127

6.2 Triples contributions to the excited-state CC3 one-particle density matrix. The ground-state amplitudes (T_1, T_2, and T_3) correspond to the thin horizontal lines while the thick upper and lower lines represent the L and R vectors. . . 128

List of Tables

1.1 H_2 correlation energies at equilibrium, R_e, two times equilibrium, $2*R_e$, and three times equilibrium, $3*R_e$ where R_e = 0.75 Å. Correlation energies obtained at the CCSD/cc-pVDZ level of theory 13

1.2 The Davidson-Liu iterative method for solving the lowest few eigenvalues and eigenvectors of real matrices. 24

1.3 Wall times (reported in seconds) to converge the CCSD amplitude equations. T_0 is the time before utilizing symmetry and spin adaptation. T_{DPD} is the time with symmetry exploitation of the amplitudes. T_{SA} is the time utilizing a spin adapted wave function. T_T is the time utilizing both symmetry and spin adaptation 29

2.1 CCSD(T) contributions to the CCSD excited-state amplitude equations. $\tilde{V} = (VT_2)_c + (VT_1T_2)_c + (VT_2^2/2)_c + (VT_1^2T_2/2)_c + (VT_1T_2^2/2)_c + (VT_1^3T_2/2)_c/3!$ 46

2.2 Triples contributions to the CCSD ground-state amplitude equations. 48

2.3 Triples contributions to the EOM-CCSD excited-state σ-equations. $\bar{W}=e^{-(T_1+T_2)}Ve^{(T_1+T_2)}$, $\hat{W}_{T-3}=(fT_3)_c+(VT_2)_c+(VT_1T_2)_c+(VT_1T_1T_2)_c+(VT_1T_1T_1T_2)_c+(VT_2T_2)_c+(VT_1T_2T_2)_c$, $\hat{W}_{CC3}=(fT_3)_c+(VT_2)_c+(VT_1T_2)_c+(VT_1T_1T_2)_c+(VT_1T_1T_1T_2)_c$ 49

3.1 Optimized geometrical parameters of m-benzyne (bond distances in Å, angles in degrees, and energies in E_h). 63

3.2 Computed harmonic vibrational frequencies (in cm^{-1}) for m-benzyne determined using the 6-31G(d,p) basis set. Normalized infrared absorption intensities (in km/mol) are given in parentheses. 69

3.3 Anharmonicities and fundamental vibrational frequencies (cm^{-1}) of m-benzyne computed at the RHF-CCSD(T)/6-31G(d,p) level of theory. 72

3.4 Optimized geometrical parameters of tetrafluoro-m-benzyne (bond distances in Å, angles in degrees, and energies in E_h) computed with the 6-31G(d,p) basis set. 74

3.5 Computed harmonic vibrational frequencies (in cm^{-1}) for tetrafluoro-m-benzyne determined using the 6-31G(d,p) basis set. Normalized infrared absorption intensities (in km/mol) are given in parentheses. 78

4.1 CCSD and CC3 vertical and adiabatic excitation energies (in eV) of the valence $^2B_1$ state of the allyl radical, computed at the CCSD/cc-pVDZ optimized C_{2v} geometry for the ground state (vertical) and the cc-pVDZ/EOM-CCSD optimized geometry for the excited state (adiabatic). The experimental UV absorption maximum reported in Ref.[9] is 3.05 eV. 100

4.2 CCSD and CC3 vertical excitation energies (in eV) of CO^+ and CH radicals with ROHF and UHF reference determinants.[1] 103

4.3 CCSD and CC3 vertical excitation energies (in eV) of three low-lying states of the nitromethyl radical relative to the $^2B_1$ ground state.[2] ROCIS, XCIS and G2 results.[10] 105

5.1 Vertical exciation energies (eV) for each state of the allyl radical. 114

[1]Calculations performed at the experimental ground-state geometries of r(C−O) = 1.115 Å and r(C−H) = 1.1198 Å. Core orbitals were held frozen in the CCSD and CC3 calculations.

[2]Computed at the UMP2/6-31++G(d,p) optimized geometry using the Sadlej-pVTZ basis set with core orbitals frozen.

Chapter 1

Introduction to Many-Electron Wave Functions

> "To those who do not know mathematics it is difficult to get across a real feeling as to the beauty, the deepest beauty, of nature... If you want to learn about nature, to appreciate nature, it is necessary to understand the language that she speaks in.[11]"
>
> -Richard P. Feynman

Quantum Chemistry is the application of quantum mechanics to explain the electronic structure and properties of molecules *via* Schrödinger's fundamental equation

$$H\Psi = E\Psi \tag{1.1}$$

This chapter will focus on finding approximate ground-state solutions to the electronic Schrödinger equation. Tools for deriving and implementing these methods will also be discussed. First, however, is a review of some basic formalisms in electronic structure theory.

1.1 Born-Oppenheimer Approximation

A major pursuit of quantum chemists is finding solutions to the non-relativistic time-independent Schrödinger equation. The Hamiltonian operator for N electrons and M nuclei is:

$$H = T_N + T_e + V(r, R). \tag{1.2}$$

In atomic units, T_N and T_e denote nuclear and electronic kinetic energy operators

$$T_N = -\frac{1}{2}\sum_{A=1}^{M}\frac{1}{M_A}\nabla_A^2 \tag{1.3}$$

$$T_e = -\frac{1}{2}\sum_{i=1}^{N}\nabla_i^2 \tag{1.4}$$

where M_A is the ratio of the mass of nucleus A to the mass of an electron, and ∇_i and ∇_A are Laplacian operators. The potential operator $V(r, R)$ denotes the nuclear-nuclear, electron-nuclear, and electron-electron interaction terms

$$V(r, R) = \sum_{A=1}^{M}\sum_{B>A}^{M}\frac{Z_A Z_B}{r_{AB}} - \sum_{i=1}^{N}\sum_{A=1}^{M}\frac{Z_A}{r_{iA}} + \sum_{i=1}^{N}\sum_{j>i}^{N}\frac{1}{r_{ij}}. \tag{1.5}$$

Here Z_A is the atomic number of nucleus A, r_{AB} is the distance between the A^{th} nucleus and B^{th} nucleus, r_{iA} is the distance between the i^{th} electron and the A^{th} nucleus, and r_{ij} is the distance between the i^{th} and j^{th} electrons.

The Hamiltonian appearing in equation (1.2) can be separated into two terms: one describing the motions of the electrons in an electrostatic field created by the fixed nuclei and the other determining the motion of the nuclei.

$$H = H_{elec} + H_{nucl} \tag{1.6}$$

The electronic Hamiltonian H_{elec} is defined as

$$H_{elec} = -\frac{1}{2}\sum_{i=1}^{N}\nabla_i^2 - \sum_{i=1}^{N}\sum_{A=1}^{M}\frac{Z_A}{r_{iA}} + \sum_{i=1}^{N}\sum_{j>i}^{N}\frac{1}{r_{ij}} \tag{1.7}$$

and the nuclear Hamiltonian H_{nucl} is

$$\begin{aligned} H_{nucl} &= -\sum_{A=1}^{M}\nabla_A^2 + \sum_{A=1}^{M}\sum_{B>A}^{M}\frac{Z_A Z_B}{r_{AB}} + \langle\psi(r,R)_{elec}|H_{elec}|\psi(r,R)_{elec}\rangle & (1.8)\\ &= -\sum_{A=1}^{M}\nabla_A^2 + \sum_{A=1}^{M}\sum_{B>A}^{M}\frac{Z_A Z_B}{r_{AB}} + E_{elec} & (1.9)\\ &= -\sum_{A=1}^{M}\nabla_A^2 + E_{tot} & (1.10) \end{aligned}$$

Equation (1.8) makes the assumption that the nuclei are stationary relative to the much-lighter electrons. Therefore, the electrostatic potential created from the electrons can be treated as an average field potential. From the above equations, it is clear that solutions to the nuclear Schrödinger equation are derived from solutions to the electronic problem. The total energy (which includes vibration, rotation, translation, and electronic energy) thus describes the potential created by nuclear motion. This approach is the most common use of the adiabatic approach originally proposed by Born and Oppenheimer.[12] Their "clamped nuclei" approximation is inherent in any molecular interpretation and has become essential to all of chemistry.

For our purposes, we will focus on only the electronic problem. We note that the electronic Schrödinger equation

$$H_{elec}\psi(r,R) = E_{elec}\psi(r,R) \tag{1.11}$$

determines a set of eigenvalues and eigenfunctions which depend explicitly on the electron coordinates and parametrically on the nuclear coordinates. Although the Born-Oppenheimer approximation has simplified the molecular Hamiltonian, exact solutions to the electronic Schrödinger equation are still only possible for one-electron systems. Further approximations must be made to solve for more complex structures.

1.2 Hartree-Fock Theory

Hartree-Fock theory is one of the simplest approximate methods for solving the many-body problem. It is based on the wave function being a single Slater determinant of N orthonormal spin orbitals,[13,14]

$$\Psi(x_1, x_2, ...x_N) = (N!)^{-1/2} \begin{vmatrix} \psi_i(x_1) & \psi_j(x_1) & \dots & \psi_N(x_1) \\ \psi_i(x_2) & \psi_j(x_2) & \dots & \psi_N(x_2) \\ \vdots & \vdots & & \vdots \\ \psi_i(x_N) & \psi_j(x_N) & \dots & \psi_N(x_N) \end{vmatrix}$$

where the parameter x_N encompasses both the spin and spatial coordinates of the electron. The Slater determinant captures much of the physics required for building antisymmetric wavefunctions. Most importantly, its structure can be shown to obey the Pauli exclusion

principle: if two electrons were to occupy the same column (molecular orbital), the determinant would equal zero. A general short hand notation for this determinant is often written as,

$$\Psi(x_1, x_2, \ldots x_N) = |\psi_1 \psi_2 \ldots \psi_N\rangle \tag{1.12}$$

where the normalization constant is implicitly included.

The Slater determinant is the simplest antisymmetric wave function used to describe the ground-state of an N-electron system. Based on Schrödinger's variational principle in quantum mechanics, the determinant can be variationally optimized

$$\Psi \rightarrow \Psi + \delta\Psi \tag{1.13}$$

giving the lowest possible energy for a trial wave function.

$$E(\Psi) = E(\Psi + \delta\Psi) \tag{1.14}$$

In other words, the energy is stationary with respect to any variation in the wave function.

The principles described here form the basic foundation to the Hartree-Fock approximation. The Hartree-Fock equation is an eigenvalue equation that yields a set of orthonormal spin orbitals with orbital energies ε_i.

$$f(i)\chi(x_1) = \varepsilon_i \chi(x_1) \tag{1.15}$$

The Fock operator $f(i)$ is a one-electron operator,

$$f(i) = -\frac{1}{2}\nabla_i^2 - \sum_{A=1}^{M} \frac{Z_A}{r_{iA}} + \upsilon^{HF}(i) \tag{1.16}$$

where $\upsilon^{HF}(i)$ is the average potential experienced by the i^{th} electron created from the field of other electrons. Now the complicated two-electron problem has been converted into a simpler one-electron problem. The basic idea behind the Hartree-Fock procedure is to calculate the average field felt by each electron for a trial wave function, and solve the Hartree-Fock equation (1.15) for a new set of spin orbitals. Using the new spin orbitals, recompute the fields for another set of orbitals and repeat the procedure until the fields no longer change. The final variationally optimized Hartree-Fock orbitals form the best possible approximation to the single-determinant ground-state wavefunction.

1.2.1 Roothaan-Hall Equations

An important contribution was a paper by Roothaan in 1951,[15] where he demonstrated that the Hartree-Fock equation (1.15) can be converted into a convenient set of algebraic matrix equations, which, as it turns out, are well suited for computers. By expanding the wave function into a basis set, the spin orbitals are calculated from the set of expansion coefficients $C_{\nu i}$.

$$\sum_{\nu} C_{\nu i} \int dr_1 \phi_{\mu}^{*}(1) f(1) \phi_{\nu}(1) = \varepsilon_i \sum_{\nu} C_{\nu i} \int dr_1 \phi_{\mu}^{*}(1) \phi_{\nu}(1) \tag{1.17}$$

$$\mathbf{FC} = \mathbf{SC}\varepsilon \tag{1.18}$$

where the Greek indices $\mu, \nu, \sigma, \lambda$ refer to the atomic orbitals (AO) and i is a doubly occupied molecular orbital (MO). Equation (1.18) is the Roothaan-Hall equation where $\mathbf{F}$ is defined as the Fock matrix and $\mathbf{S}$ is denoted as the overlap matrix between the orthonormal basis

functions ϕ_μ and ϕ_ν.

$$F_{\mu\nu} = \int dr_1 \phi_\mu^*(1) h(1) \phi_\nu(1) + \sum_i^{N/2} \sum_{\lambda\sigma} C_{\lambda i} C_{\sigma i}^* (2\langle \mu\sigma|\nu\lambda\rangle - \langle \mu\sigma|\lambda\nu\rangle) \tag{1.19}$$

$$= H_{\mu\nu}^{core} + \sum_{\lambda\sigma} P_{\lambda\sigma} (\langle \mu\sigma|\nu\lambda\rangle - \frac{1}{2}\langle \mu\sigma|\lambda\nu\rangle) \tag{1.20}$$

$$= H_{\mu\nu}^{core} + G_{\mu\nu}. \tag{1.21}$$

The core Hamiltonian matrix $H_{\mu\nu}^{core}$ includes the one-electron components (kinetic energy and electron-nuclear attraction terms) of the electronic Hamiltonian. Shown here and throughout the text, physicist's notation is used to denote the two electron integrals. The coefficients in the basis set make up the charge density matrix $P_{\lambda\sigma}$, which is used to construct the two-electron matrix $G_{\mu\nu}$.

Since the Fock matrix is a function of the expansion coefficients $C_{\nu i}$, the Roothaan equation is non-linear, $F(C)C = SC\varepsilon$, and must be solved iteratively, through what is termed a self-consistent field (SCF) procedure. The SCF requires an initial guess for the charge density, which can play a critical role in the efficiency of Hartree-Fock theory. Because the coulombic attractions are the most significant contributor to the Fock matrix, the simplest guess is to approximate the initial Fock matrix as a one-electron Hamiltonian operator and neglect the coulombic repulsions. However, for cases where the initial molecular geometry is significantly distorted from its equilibrium geometry, such as stretched bonds, the one-electron Hamiltonian may be a poor guess of the charge density, which could lead to nonsensical results.

Once the density and Fock matrix have converged the total Hartree-Fock electronic energy

is calculated as,

$$E_{elec} = \frac{1}{2}\sum_{\mu\nu} P_{\mu\nu}(H_{\mu\nu}^{core} + F_{\mu\nu}). \tag{1.22}$$

Repeating the SCF procedure for different nuclear positions gives a total energy as a function of geometry. Such an approach is useful for optimizing molecular geometries, finding transition states, and calculating infrared vibrational spectra.

With all computational methods it is important to understand rate-determining steps and storage requirements of the calculations. The bottleneck for Hartree-Fock calculations is the generation of the two-electron integrals with the number of integrals scaling as $O(N^4)$, where N is the total number of basis functions. This scaling can be drastically reduced to $O(N^2)$ for larger molecules by "throwing out" the integrals whose AO overlap is negligible. Consider the two-electron integral $\langle\mu\nu|\sigma\lambda\rangle$: if the overlap between either μ and σ or ν and λ is negligible, then that integral will vanish.

1.2.2 Pople-Nesbet Equations

Because the Hartree-Fock reference is the foundation for higher levels of theory, the choice of reference is essential for accurate descriptions of a system's molecular properties. The Hartree-Fock approximation discussed in section (1.2.1) is often the starting point for more accurate calculations. However, problems may arise from using an spin-restricted Hartree-Fock (RHF) reference. Constraining pairs of electrons to share the same spatial orbitals often raises the electronic energy of the molecule. For example, inherent to the Hartree-

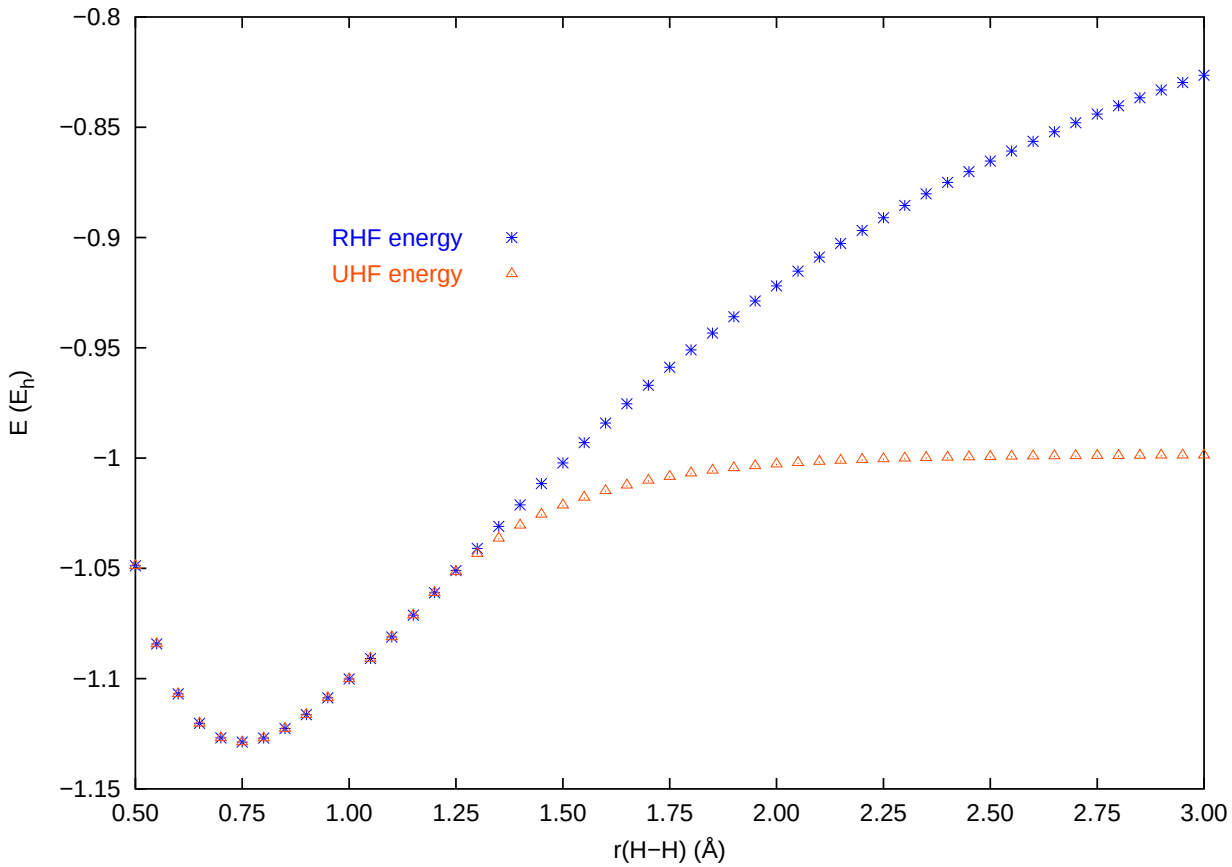

Figure 1.1: RHF and UHF potential energy curves illustrating the dissociation of H_2

Fock description, Slater determinants introduce an exchange correlation between two alpha electrons but no exchange interaction with the beta electron. Because the alpha and beta electron pair experience different electron potentials, they would prefer to have separate spatial distributions.

Figure (1.1) illustrates another RHF deficiency: at large interatomic distances the potential energy surface (PES) does not correctly describe the dissociation of molecules into open-shell fragments. By removing the spin symmetry constraint of the α and β electron pairs, an unrestricted Hartree-Fock (UHF) reference can give a more accurate description of the

potential energy surface. Separating the α and β electrons into linearly expanded molecular orbitals, Pople and Nesbet introduced a set of equations that can be derived in a similar manner as the Roothaan equations.[16]

$$F^{\alpha}C^{\alpha} = SC^{\alpha}\varepsilon^{\alpha} \tag{1.23}$$

$$F^{\beta}C^{\beta} = SC^{\beta}\varepsilon^{\beta} \tag{1.24}$$

Because the α and β electrons do not share the same spatial distribution, the spin density is a convenient way to describe the distribution of spins in an open-shell system.[17]

$$P^{S} = \sum_{i}^{N\alpha} C_{\mu i}^{\alpha}(C_{\nu i}^{\alpha})^{*} - \sum_{i}^{N\beta} C_{\mu i}^{\beta}(C_{\nu i}^{\beta})^{*} = P^{\alpha} - P^{\beta} \tag{1.25}$$

The total charge density for electrons of either spin is similarly defined as,

$$P^{T} = \sum_{i}^{N\alpha} C_{\mu i}^{\alpha}(C_{\nu i}^{\alpha})^{*} + \sum_{i}^{N\beta} C_{\mu i}^{\beta}(C_{\nu i}^{\beta})^{*} = P^{\alpha} + P^{\beta} \tag{1.26}$$

Expressions for the Fock matrices F^{α} and F^{β} are,

$$F^{\alpha} = H_{\mu\nu}^{core} + \sum_{\lambda}\sum_{\sigma} P^{T}(\mu\nu|\sigma\lambda) - P^{\alpha}(\mu\lambda|\sigma\nu) \tag{1.27}$$

$$F^{\beta} = H_{\mu\nu}^{core} + \sum_{\lambda}\sum_{\sigma} P^{T}(\mu\nu|\sigma\lambda) - P^{\beta}(\mu\lambda|\sigma\nu) \tag{1.28}$$

The procedure for finding solutions to the Pople-Nesbet equations is identical to that for the Roothaan equations. For the case where the number of α electrons, N^{α}, is not equal the number of β electrons, N^{β}, ρ^{α} and ρ^{β} can be initially set to zero with the core Hamiltonian as the initial guess at the Fock matrix. However, if N^{α} equals N^{β} then a non-zero initial guess must be made at the density matrices. For this case, it is possible that two independent

solutions exist, the restricted and unrestricted solutions, with the following electronic energy:

$$E_{elec} = \frac{1}{2}\sum_{\mu}\sum_{\nu}[P^{T}_{\nu\mu}H^{core}_{\mu\nu} + P^{\alpha}_{\nu\mu}F^{\alpha}_{\mu\nu} + P^{\beta}_{\nu\mu}F^{\beta}_{\mu\nu}] \tag{1.29}$$

As figure (1.1) illustrates, removing the spin symmetry constraint of the α and β electron pairs can give a more accurate description of the PES. Additionally, a UHF reference may be more reliable for systems with problematic orbital near-instabilities. In a report on *p*-benzyne,[18] an RHF-reference calculation led to orbital near-instabilities of the HOMO - LUMO, HOMO-1 - LUMO, and HOMO-2 - LUMO pairs, where the approximate wavefunction failed to maintain the spatial characteristics of the exact wavefunction which led to imaginary vibrational modes. These near-instabilities are an artifact of the single determinant RHF wavefunction and require a multireference approach that utilizes more than one determinant to accurately describe the exact wavefunction. The UHF-reference solution on the other hand predicted the structure to be a minimum on the potential energy surface. By relaxing the spatial symmetry constraint on the molecular orbitals, the energy gap between nearly degenerate orbitals widened and reduced *p*-benzyne's multireference character.

However, a UHF reference may not be appropriate for all molecular calculations. One of the deficiencies of a UHF description is that the wavefunction is generally contaminated by other spin states, although the exact wavefunction has no such contamination. The amount of spin contamination can be monitored by the expectation value of the S^2 operator. Due to its non-spin-adaptive nature, the UHF wavefunction could lead to an artifactual molecular structure.

1.3 Correlated Wavefunctions

A general deficiency of the Hartree-Fock model is its inability to correctly treat the Coulombic potential between the electrons (the $\frac{1}{r_{12}}$ term). At the point $r_{12} = 0$, the true wave function will incur a coalescence cusp where a negative singularity, due to the kinetic energy operator $-\nabla_i^2$, acts to balance the positive $\frac{1}{r_{12}}$ term. A Hartree-Fock wave function, however, shows a continuous smooth curve and does not display a coulombic hole. This indicates that the average-field approximation overestimates the positive interelectron repulsion term.

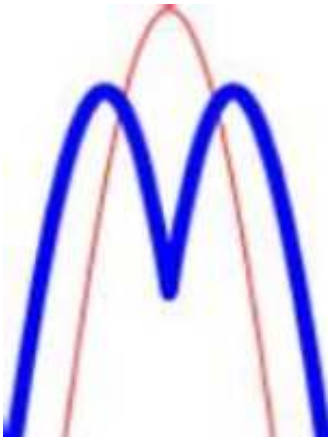

Figure 1.2: Short range dynamic correlation energy curves for the exact and Hartree-Fock wave functions. The energy (vertical distance) is a function of the distance between electrons (cusp occurs at $r_{12} = 0$).

Table 1.1: H_2 correlation energies at equilibrium, R_e, two times equilibrium, $2*R_e$, and three times equilibrium, $3*R_e$ where $R_e = 0.75$ Å. Correlation energies obtained at the CCSD/cc-pVDZ level of theory

Geometry	E_{corr} (Hartree) [1]
R_e	-0.03485
$2*R_e$	-0.05934
$3*R_e$	-0.11705

The Hartree-Fock description also suffers from long-range inadequacies or non-dynamical correlation effects. Consider the dissociation of molecular hydrogen. With stretched geometries, the interelectronic repulsion will decrease, and therefore one might expect a reduction in the correlation energy; but as shown in Table (1.1), just the opposite occurs. The origin of this problem stems from non-dynamical or static correlation effects which reflect deficiencies with using a single Slater determinant. The MO diagrams, illustrated in Figure 1.3, indicate that as the H_2 bond is stretched, the orbitals become closer and closer in energy. Both electronic configurations are important in the true wave function and therefore it should include a linear combination of determinants (b) and (c). To overcome problems associated with single reference models of degenerate or near-degenerate states, electron correlation effects must be included in the approximate wavefunction.

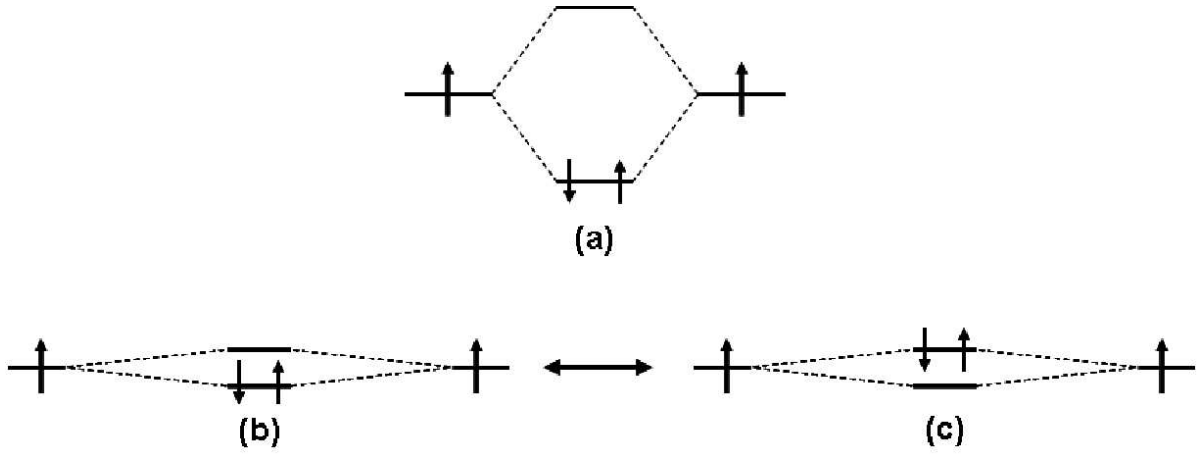

Figure 1.3: H_2 molecular orbital energy profiles illustrating static correlation effects; (a) is at equilibrium R_e; (b) and (c) occur at stretched bond lengths creating a near-degeneracy between the MOs.

The difference between the Hartree-Fock energy, E_{HF}, and the exact non-relativistic energy, E_0, is known as the correlation energy,

$$E_{corr} = E_0 - E_{HF}. \tag{1.30}$$

Since the variationally optimized Hartree-Fock energy is an upper bound to the exact energy, the correlation energy must be negative. Improvements to the single-determinant Hartree-Fock wave function are made by correlating the motion of the electrons in the approximate wave function. If we were to include all possible interactions between the electrons, then this would give us the exact answer within the space spanned by the basis set. However, except for the simplest of cases (like H_2), such an approach is computationally not plausible. Truncated correlation techniques have been the focus of substantial research efforts since

the early 1970s. The goal is to develop a method which is chemically accurate, yet scales reasonably with the size of the system. Sections 1.3.1 and 1.3.2 discusses some correlation models based on both perturbation theory and coupled cluster theory.

1.3.1 Perturbation Theory

Perturbation theory,[19] approximates the correlation problem as a perturbation to the Hartree-Fock solution. This approach has been alternatively referred to as many-body perturbation theory in which the perturbed Hamiltonian H consists of a series of corrections to the unperturbed Hamiltonian H_0,

$$H|\Phi\rangle = (H_0 + \lambda V)|\Phi\rangle = E|\Phi\rangle. \tag{1.31}$$

Accordingly, the exact wave function Φ and corresponding energy can be expanded as a Taylor series in terms of λ,

$$|\Phi\rangle = |\Psi^0\rangle + \lambda|\Psi^{(1)}\rangle + \lambda^2|\Psi^{(2)}\rangle + \ldots \tag{1.32}$$

$$E = E^0 + \lambda E^{(1)} + \lambda^2 E^{(2)} + \ldots. \tag{1.33}$$

The parameter λ is a dummy variable used for bookkeeping that is eventually set to unity. Substituting equations (1.32) and (1.33) into equation (1.31) and equating coefficients of λ^n, yields a set of n^{th}-order energy corrections. The first-order energy correction only gives the SCF energy, which is already known. The second-order energy equation is solved from the first-order wave function $|\Psi^{(1)}\rangle$. By expanding the first-order wavefunction in terms of all

possible excited determinants, it can be shown that the MP2 energy equation includes only doubly excited determinants ($T_2^{(1)}$).[17]

After transforming the AO integrals to the MO basis, the second-order energy for a closed-shell system is written as:

$$E^{(2)} = \sum_{ij}\sum_{ab} \frac{\langle ij|ab\rangle(2\langle ij|ab\rangle - \langle ij|ba\rangle)}{\varepsilon_i + \varepsilon_j - \varepsilon_a - \varepsilon_b} \tag{1.34}$$

$$= \sum_{ij}\sum_{ab} \langle ij|ab\rangle T_2^{(1)} \tag{1.35}$$

where the indices i and j refer to occupied MO's and a and b to the unoccupied or virtual MO's.

Higher-order energy terms are computed in a similar manner to the procedure described above. The even-ordered series are more commonly used since they will always include new correlation effects: MP2 includes two-electron correlation, MP4 three-electron correlation, MP6 four-electron correlation. Although the even series exaggerates electron correlation, the odd series over-corrects the even series thereby reducing its effects including: stronger separation of electrons, a more diffuse electron density, and a deshielding of the nuclei. Therefore, perturbation theory will generally predict longer bond lengths than those of the true geometry.[20]

While MP2 is a relatively cheap way to include electron correlation, the higher-order expressions become very expensive compared to other more accurate methods: the computational cost of the MPn energy is $O(N^{(n+3)})$. Futhermore, convergence of the perturbation series is dependent on the accuracy of the starting wavefunction, but even with a good reference

function, divergence may still occur. For example, when bonds are stretched the perturbative series has been known to oscillate. In reports by Olsen *et al.*,[21] and Forsberg *et al.*,[22] properties such as energy, geometry, and dipole moments were shown to oscillate at the lower orders of perturbation theory and eventually diverge at the higher orders. Thus, perturbation theory is often viewed as an unreliable method for including large amounts of correlation to the electronic wavefunction.

1.3.2 Coupled Cluster Theory

Čížek and Paldus introduced a method in the late 1960s that added dynamic electron correlation to the Hartree-Fock ground state $|\Phi_0\rangle$ *via* an exponential expansion of n-particle cluster functions.[23–25] These expansion functions are constructed from a product of spin orbitals, commonly referred to as configuration state functions (CSF), some of which are coupled to each other in some manner, e.g., we will show that the correlated wavefunction indirectly couples the singly and doubly excited determinants. Adding these n-particle cluster functions to the ground-state wavefunction gives an improved approximate wavefunction, with each cluster being a linear combination of n-tuply excited determinants. For example, the two-particle function f_{ij} is used to correlate the motion of any two electrons within occupied orbitals ϕ_i and ϕ_j,

$$f_{ij}(x_m, x_n) = \sum_{a>b} t_{ij}^{ab} \phi_a(x_m)\phi_b(x_n) \tag{1.36}$$

where t_{ij}^{ab} are the two particle coefficients that represent the excitation of electrons from occupied orbitals i and j into virtual orbitals a and b. The notation $a > b$ indicates that

only unique pairs of functions are included. The coupled cluster wavefunction includes products of these cluster operators making the wavefunction non-linear. For example, the coupled cluster ground-state wave function for a Li atom may be written as,

$$\begin{aligned}\Psi &= |\psi_i\psi_j\psi_k\rangle + |f_i\psi_j\psi_k\rangle + |\psi_i f_j\psi_k\rangle + |\psi_i\psi_j f_k\rangle + \\ &+ |f_i f_j\psi_k\rangle + |f_i\psi_j f_k\rangle + |\phi_i f_j f_k\rangle + |f_{ij}\psi_k\rangle + |f_{ik}\psi_j\rangle + \\ &+ |\psi_i f_{jk}\rangle + |f_i f_{jk}\rangle + |f_{ij}f_k\rangle + |f_{ik}f_j\rangle + |f_{ijk}\rangle \end{aligned} \tag{1.37}$$

Since the Hamiltonian is at most a two-electron operator, the last term will not directly contribute to the coupled cluster energy expression. Using second-quantized operators,[26] and defining the one and two orbital cluster operators as,

$$T_1 = \sum_i \sum_a t_i^a a_a^\dagger a_i \tag{1.38}$$

$$T_2 = \sum_{i>j} \sum_{a>b} t_{ij}^{ab} a_a^\dagger a_b^\dagger a_j a_i \tag{1.39}$$

the coupled cluster wave function is reduced to,

$$\Psi = (1 + T_1 + \frac{1}{2!}T_1^2 + \frac{1}{3!}T_1^3 + T_2 + T_2T_1)\Phi_0 \tag{1.40}$$

Since T_1 and T_2 commute, equation (1.40) matches those of an exponential function which can be written as,

$$\Psi = e^T\Phi_0 \tag{1.41}$$

where T is the sum of the cluster operators; $T = T_1 + T_2 + \ldots$. This exponential ansatz is central to coupled cluster theory and is used to approximate solutions to the exact wavefunction Ψ.[26]

$$He^T|\Phi_0\rangle = Ee^T|\Phi_0\rangle \tag{1.42}$$

Left projection of equation (1.42) by the reference $\langle\Phi_0|$, singly excited $\langle\Phi_i^a|$, and doubly excited $\langle\Phi_{ij}^{ab}|$ determinants reveals three coupled cluster equations for solving the three unknown variables,

$$E_{corr} = \langle\Phi_0|H(T_1 + T_2 + \frac{1}{2}T_1^2)|\Phi_0\rangle \tag{1.43}$$

$$t_i^a E_{corr} = \langle\Phi_i^a|H(T_1 + T_2 + \frac{1}{2}T_1^2 + \frac{1}{6}T_1^3)|\Phi_0\rangle \tag{1.44}$$

$$\begin{aligned}(t_{ij}^{ab} + t_i^a t_j^b - t_i^b t_j^a)E_{corr} &= \langle\Phi_{ij}^{ab}|H(1 + T_1 + T_2 + \frac{1}{2}T_1^2 + T_1T_2 + \\ &+ \frac{1}{6}T_1^3 + \frac{1}{2}T_2^2 + \frac{1}{2}T_2T_1^2 + \frac{1}{24}T_1^4)|\Phi_0\rangle\end{aligned} \tag{1.45}$$

While an exact solution is obtainable, the above equations are certainly not in the most efficient formulation. If instead equation (1.42) is multiplied by the inverse of the exponential operator,

$$e^{-T}He^T|\Phi_0\rangle = E|\Phi_0\rangle \tag{1.46}$$

a set of coupled cluster equations can now be defined by the connected cluster theorem developed by Čížek,[24]

$$E_{corr} = \langle\Phi_0|\{H_N e^T\}_c|\Phi_0\rangle \tag{1.47}$$

$$0 = \langle\Phi_i^a|\{H_N e^T\}_c|\Phi_0\rangle \tag{1.48}$$

$$0 = \langle\Phi_{ij}^{ab}|\{H_N e^T\}_c|\Phi_0\rangle \tag{1.49}$$

where H_N is the normal ordered Hamiltonian and $\{H_N e^T\}_c$ indicates that only the connected diagrams are included. This connectivity issue is addressed in section (1.6). The introduction of the similarity transformed Hamiltonian, $e^{-T}He^T$, thus allows the coupled cluster energy to

be decoupled from the amplitude equations. Now the coupled cluster equations are reduced to a more computer efficient form,

$$E_{corr} = \sum_{ia} f_{ia} t_i^a + \frac{1}{4} \sum_{aibj} \langle ij||ab\rangle t_{ij}^{ab} + \frac{1}{2} \sum_{aibj} \langle ij||ab\rangle t_i^a t_j^b \tag{1.50}$$

where f_{ia} is the occupied-virtual block of Fock matrix. The coupled cluster singles and doubles (CCSD) amplitude equations (1.48) and (1.49) are derived in a similar but more tedious manner [derived diagrammatically in section (1.6)]. The amplitude equations are solved simultaneously, where the initial guess of T_2 comes from the MP2 energy equation (1.35) and the T_1 single excitations are set to null. From this initial guess, a new set of T_2 and T_1 amplitudes are obtained which are then inserted back into equations (1.48) and (1.49). This procedure proceeds iteratively until the amplitudes have converged. Unlike perturbation theory, the exaggerated MPn bond lengths are not found at any coupled cluster level since the exponential form of the wavefunction includes coupling corrections up to infinite order.[26] Thus, the coupled cluster wavefunction allows for all possible coupling corrections without the need for higher cluster operators: CCSD includes triple and quadruple excitations through products of T_1 and T_2.

1.4 Formalism of the EOM Eigenvalue Equation

We now shift our focus from the ground-state methodology to excited-state coupled cluster models. While diagonalizing the Hamiltonian would provide a great deal of information regarding all the states of the molecule, computer limitations often prevent us from proceed-

ing in this manner. Furthermore, this is a terribly inefficient approach since chemists are generally interested in only the first few states of a molecule and not the entire spectrum. Alternatively, one might try solving the excited-state problem similar to the ground-state: each state is calculated separately from an appropriate reference determinant. However, several problems can arise from taking such an approach. First, one would have to impose an adequate reference determinant. How does one choose the electronic configuration that most accurately describes the k^{th} excited-state? Randomly solving for a number of states (one calculation for each state) would be very inefficient. Finally, the states calculated in this manner are not orthogonal making them difficult to interpret.

It is well established that the equation-of-motion coupled cluster (EOM-CC) method can avoid the problems described. In the EOM-CC scheme, the excited-state wavefunctions are obtained by diagonalizing an effective coupled cluster Hamiltonian, $\bar{H}{=}e^{-T}He^{T}$, within a space of n-tuply excited determinants. Within this formalism, the k^{th}-state wave function is obtained by the action of the operator $R(k)$ acting on the ground-state wave function $|\Phi_0\rangle$.

$$|\Phi_k\rangle = R(k)|\Phi_k\rangle \tag{1.51}$$

The operator $R(k)$ can be defined however one chooses, but the most common approach is to define $R(k)$ as a linear excitation operator,

$$R(k) = R_0(k) + R_1(k) + R_2(k) + \cdots \tag{1.52}$$

where $R_0(n)$ is the overlap between the ground- and k^{th}-excited-state, and $R_n(k)$ are all possible n-excitations (n = single, double, triple, ...). The excited-state eigenvalue equation

is now expressed as,

$$\bar{H}R(k)|\Psi_0\rangle = E_T R(k)|\Psi_0\rangle \tag{1.53}$$

where E_T is the total energy of the k^{th} state and $\bar{H}$ is the similarity transformed Hamiltonian, $e^{-T}He^{T}$. Indeed, the ground-state coupled cluster solution is considered a special case given by one root of $\bar{H}$, namely that for which $R = R_0 = 1$.

While solutions to equation (1.53) are certainly possible (discussed in section 3.2), which would involve solving both contracted and uncontracted equations (connected and disconnected diagrams), these equations can be manipulated into a more efficient form. If we multiply the ground-state equation by the linear operator $R(k)$,

$$R(k)\bar{H}|\Psi_0\rangle = R(k)E_0|\Psi_0\rangle, \tag{1.54}$$

and subtract equation (1.54) from equation (1.53).

$$\begin{aligned} \bar{H}R(k)|\Psi_0\rangle - R(k)\bar{H}|\Psi_0\rangle &= E_T R(k)|\Psi_0\rangle - E_0 R(k)|\Psi_0\rangle \\ [\bar{H}, R(k)]|\Psi_0\rangle &= E_{xe}R(k)|\Psi_0\rangle \end{aligned} \tag{1.55}$$

we obtain an excitation energy denoted E_{xe}. Further simplifications can be made by "pulling out" the R_0 terms from the commutator in equation (1.55),

$$\begin{aligned} \bar{H}R_0(k)|\Psi_0\rangle - R_0(k)\bar{H}|\Psi_0\rangle + [\bar{H}, R_n(k)] &= E_{xe}R_n(k)|\Psi_0\rangle \\ \{\bar{H}, R_n(k)\}_c|\Psi_0\rangle &= E_{xe}R_n(k)|\Psi_0\rangle. \end{aligned} \tag{1.56}$$

This is the most common formalism of the equation-of-motion coupled cluster method (EOM-CC). The excited-state wavefunction can now be constructed analogous to the ground-state

equations, where only contracted (diagrammatically connected) elements between the Hamiltonian $\bar{H}$ and vectors $R_n(k)$ are needed. Thus, the necessary equations appear similar to those already derived for the ground-state.

1.4.1 Davidson Method

We now give a brief review of the Davidson method[27] for solving large-scale eigenvalue problems. The method is conceptually similar to the Lanczos algorithm; the basic idea is to build an orthogonal subspace onto which the Hamiltonian is projected. The subspace is initially defined by a basis set of trial vectors (our initial guess will come from diagonalizing the CCS matrix). The basis is then systematically expanded until convergence is met. Although the Davidson method can be generalized for nonsymmetric eigenvalue problems,[28] we focus on solving only the right-hand eigenvector.

We begin by constructing a set of equations which satisfy equation (1.56). Left projection of the EOM-CC equation by R_n^* yields,

$$R_n^* H R_n = R_n^* E R_n \tag{1.57}$$

$$R_n^* \cdot \sigma_n = R_n^* E R_n \tag{1.58}$$

$$G_n = \langle E \rangle \tag{1.59}$$

where we define the projected Hamiltonian matrix G for state n. The vector σ_n is the matrix-vector product HR_n. After the dominant eigenvalues, λ, and eigenvectors, α, of the

Table 1.2: The Davidson-Liu iterative method for solving the lowest few eigenvalues and eigenvectors of real matrices.

1. Select a set of L orthonormal guess vectors (at least one for each root desired) and place them in the set $\{R_n\}$.

2. Use a diagonalization routine to solve the $L \times L$ eigenvalue problem

$$G\alpha^k = \lambda^k \alpha^k, \ k = 1, 2, \ldots, n \tag{1.60}$$

where n is the number of desired roots, and the matrix G is defined by

$$G_{ij} = (R_i, \ HR_j) = (R_i, \ \sigma_j), \ 1 \leq i, j \leq L. \tag{1.61}$$

3. Form the preconditioned residual vector $\{\delta^k\}$, $k = 1, 2, \ldots, n$, defined as

$$\delta^k = \frac{\mathbf{r}^k}{(D - \lambda^k I)} \tag{1.62}$$

where

$$\mathbf{r}^k = \sum_{i=1}^{L} \alpha_i^k (\sigma_i - \lambda^k R_i). \tag{1.63}$$

4. Normalize $\{\delta^k\}$.

5. Schmidt orthonormalize the preconditioned residual vectors against the original set of $\{R_n\}$ vectors and append the results to $\{R_n\}$. This step is repeated for each of the other n-1 remaining $\{\delta^k\}$ vectors, neglecting those whose Schmidt orthonormalized norm is less than some defined threshold.

6. Increase L by n and return to step 2.

G matrix are computed, convergence is determined *via* the residual vector,

$$\mathbf{r} = \alpha(\sigma - \lambda R_n). \tag{1.64}$$

As the subspace becomes more complete the residual vector goes to zero. If the convergence criteria is not met, then it is necessary to expand the basis. For diagonally dominant matrices, the basis is expanded from preconditioning the residual vector,

$$\delta = \frac{\mathbf{r}}{(\lambda I - D)} \tag{1.65}$$

where I is the identity matrix and D is the diagonal elements of the Hamiltonian matrix. The preconditioning step is the essence of the Davidson algorithm. The resulting vector δ is orthonormalized against the original set of R_n trial vectors which is then appended to the original subspace. This procedure is repeated iteratively and the basis will continue to expand until the subspace is complete.

1.5 Efficient Program Implementation

Regardless of whether the computational chemist is theory or applications oriented, a fundamental understanding of computer implementation is essential. When will certain programs fail and what needs to be done to fix such problems? These are just a few of the questions that computational chemists encounter regularly. In this section we focus on some tools utilized to develop high-accuracy coupled cluster models. We address issues for improving the efficiency of these models including symmetry exploitation and spin-factored wave functions. Finally, disk/memory requirements will be discussed.

1.5.1 Direct Product Decomposition

Computers are adept at solving algebraic sets of equations. To take advantage of this, the coupled cluster equations are formulated as matrix-matrix or matrix-vector products. However, despite the incredibly fast pace at which computers are capable of working, it is vital that the program is written in a very efficient manner. Although all of the equations derived thus far are in a spin orbital formalism, implementing the coupled cluster model in this manner is impractical, especially for properties more complex (and more interesting) than a single energy point.

Since the Hamiltonian has the same spatial symmetry as the nuclear framework of the molecule, the irreducible representations of a molecule's symmetry group can be used to represent MO energy levels. Explicit consideration of molecular symmetry in many-body calculations leads to a significant reduction in computation time and storage. Consider, for example, the computation of the T amplitude equations described in section (1.4). We can store the T_1-matrix in terms of i occupied orbitals by a virtual orbitals. The rows and columns of the T_2-matrix consist of compounded ij and ab orbitals, where the *supermatrix* can be viewed as $T_2(ij,ab)$. When utilizing point group symmetry, such as C_{2v}, we do not need to compute the total number of amplitudes. Only the diagonal subblocks or totally symmetric amplitudes have non-zero values. Therefore, we compute those amplitudes which are totally symmetric:

$$\Gamma_{ij} \otimes \Gamma_{ab} \equiv \Gamma_i \otimes \Gamma_j \otimes \Gamma_a \otimes \Gamma_b = A_1. \tag{1.66}$$

	A_1	A_2	B_1	B_2
A_1	X	0	0	0
A_2	0	X	0	0
B_1	0	0	X	0
B_2	0	0	0	X

Figure 1.4: Matrix representation of the totally symmetric amplitudes.

When utilizing point group symmetry, such as C_{2v}, we do not need to compute the total number of amplitudes. Only the diagonal subblocks or totally symmetric amplitudes have non-zero values. Therefore, the only T amplitudes that are computed are those which are totally symmetric. For the R excitation amplitudes, we only compute those symmetry subblocks which equal the direct product of the reference-state and excited-state:

$$\Gamma_{g.s.} \otimes \Gamma_{x.s.} = \Gamma_R. \tag{1.67}$$

Formulating the problem in this manner also allows us to reduce memory/disk requirements since only the diagonal subblocks need to be stored. Furthermore, the number of floating point operations is reduced to include only those of the diagonal subblocks. Scuseria *et al.*[29] reported that by avoiding symmetry forbidden integrals and t_{ij}^{ab} amplitudes, computational times are improved, relative to calculations in which symmetry was ignored, by a factor of h^2 while improving computational storage by a factor of h, where h is the order of the molecular point group. The symmetry simplification of the coupled cluster equations is referred to as the direct product decomposition (DPD) technique.[30]

1.5.2 Spin Factorization

Further simplifications can be made by spin factoring the coupled cluster equations. Using the fact that the spin of the electrons are orthonormal

$$\langle\alpha|\alpha\rangle = 1 \tag{1.68}$$

$$\langle\alpha|\beta\rangle = 0 \tag{1.69}$$

a more efficient set of equations will include only those which are non-zero due to spin integration. In addition, for closed shell models, the total number of unknown amplitudes is found to be reduced by a factor of four using the following relations,

$$t_{i\alpha}^{a\alpha} = t_{i\beta}^{a\beta} = t_i^a \tag{1.70}$$

$$t_{i\alpha j\beta}^{a\alpha b\beta} = t_{i\beta j\alpha}^{a\beta b\alpha} = t_{ij}^{ab} \tag{1.71}$$

Furthermore, using the following relationship, we can spin-adapt the wave function so that only mixed spin, α-β, T_2 amplitudes are computed.

$$t_{ij}^{ab} = t_{ij}^{ab} - t_{ij}^{ba} \tag{1.72}$$

Thus, only the mixed spin amplitudes need to be stored.

How well do production level codes improve efficiency? We demonstrate each effect (DPD and spin adaptation) through CCSD single-point energy calculations of H_2O. As shown in Table (1.3), both of the techniques described can significantly improve computational wall times. These results become particularly apparent for systems with more than a few hundred

Table 1.3: Wall times (reported in seconds) to converge the CCSD amplitude equations. T_0 is the time before utilizing symmetry and spin adaptation. T_{DPD} is the time with symmetry exploitation of the amplitudes. T_{SA} is the time utilizing a spin adapted wave function. T_T is the time utilizing both symmetry and spin adaptation

Basis Set	Number of Orbitals	T_0	T_{DPD}	T_{SA}	T_T
cc-pVDZ	24	11	5	3	2
cc-pVTZ	58	266	41	88	14
cc-pVQZ	115	25291	5024	5692	142

basis functions. For such cases, it is necessary to efficiently solve the coupled cluster equations or else the CCSD model becomes impractical.

The efficiency techniques described in this section form the foundation for writing effective production level codes which have been efficiently implemented within the PSI3 quantum chemical package.[31] Thanks in part to PSI3's many capabilities, including the elaborate DPD library, we were able to develop the high-level coupled cluster models described in Chapter 2.

1.6 Coupled Cluster Diagrams

In this section we will discuss how the the rigorous structure of the coupled cluster equations can be written in a far more efficient manner using simple diagrammatic formalisms. By

example, the algebraic interpretation of the diagram's structures will be illustrated. We will then follow the rules for constructing diagrams to derive the coupled cluster amplitude equations.

We begin by correlating the amplitude equations to diagrams which are symbolic of the types of interactions taking place. Recall that the coupled cluster amplitude equations are formulated by left projection of equation (1.42) by their respective excitation level: $\langle\Phi_i^a|$, $\langle\Phi_{ij}^{ab}|$, $\langle\Phi_{ijk}^{abc}|$, $\cdots$ will give the set of T_1, T_2, T_3, $\cdots$ equations. We note that the right determinant $|\Phi_0\rangle$ of the amplitude equations corresponds to the fermi level; no interactions will occur at or below this level. The diagrammatic structure of the T_1, T_2, and T_3 excitation operators can now be represented by, where the external lines for occupied orbitals i, j, k and

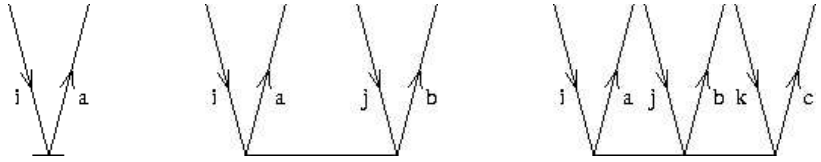

T_i^a T_{ij}^{ab} T_{ijk}^{abc}

virtual orbitals a, b, c connect to an interaction line or vertice. All lines connected to the same vertice are antisymmetric with respect to swapping either the occupied or virtual indices. It is clear that diagrams are particularly useful for identifying which types of determinants they will produce.

Now consider the coupled cluster energy equation,

$$E_{corr} = \langle \Phi_0 | \{ H_N T_1 + H_N T_2 + H_N T_1^2 \}_c | \Phi_0 \rangle. \tag{1.73}$$

No external lines will appear above or below the interaction vertices. Diagrammatically this equation may be illustrated as

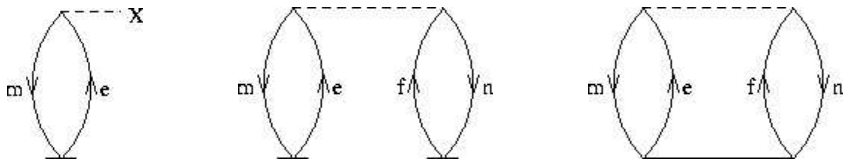

$$\sum_{me} f_{me} t_{me} \qquad \sum_{mnef} \langle mn \| ef \rangle t_m^e t_n^f \qquad \sum_{mnef} \langle mn \| ef \rangle t_{mn}^{ef}$$

Here, the lines are continuous connections between all of the vertices. We now explain the rules for interpreting diagrams.[26]

- Label all directed lines with the appropriate indices.
- Each operator interaction line contributes an integral or amplitude to the matrix element expression. The direction of the lines from the diagram determine which matrix elements are constructed. By the rule the Fock matrix is $\langle out | f | in \rangle$ and the two-electron integrals are labeled by $\langle left\text{-}out \;\; right\text{-}out \;||\; left\text{-}in \;\; right\text{-}in \rangle$.
- Summations are included over all internal indices - that is, all indices associated with lines that begin and end at operator interaction lines and do not extend to infinity above or below the diagram.

- The sign is determined based on the formula $(-1)^{o+l}$ where o is the number of occupied orbitals and l is the number of loops. A loop is a route along a series of directed lines that either returns to its beginning or begins at one external line and ends at another.

- For each pair of "equivalent" lines - that is, lines beginning at the same interaction line and ending at the same interaction line - a prefactor of $\frac{1}{2}$ is multiplied onto the algebraic expression.

- Each pair of unique, external occupied or virtual lines introduces a permutation function, $P(pq)$, to ensure antisymmetry of the final expression.

We now derive the CCSD ground- and excited-state equations utilizing the diagrammatic rules described.

T_1 Equations:

$$\begin{aligned} 0 &= \langle \phi_i^a | f + (fT_1)_c + (fT_1^2)_c + (fT_2)_c \\ &\quad + (VT_1)_c + (VT_2)_c + (VT_1^2)_c + (VT_1T_2)_c + (VT_1^3)_c | \phi_0 \rangle \end{aligned} \tag{1.74}$$

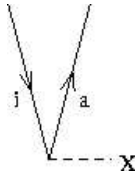

f_{ai}

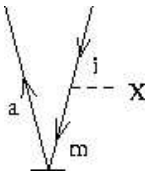

$-\sum_m f_{mi} t_m^a$

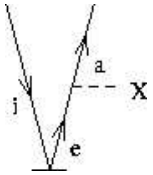

$\sum_e f_{ae} t_i^e$

T_1 Diagrams:

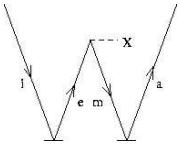

$$-\sum_{me} f_{me} t_i^e t_m^a$$

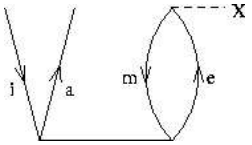

$$\sum_{me} f_{me} t_{im}^{ae}$$

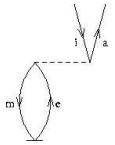

$$\sum_{mnef} \langle ma \| ei \rangle t_m^e$$

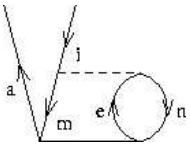

$$-\frac{1}{2} \sum_{mne} \langle mn \| ie \rangle t_{mn}^{ae}$$

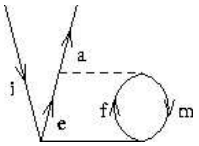

$$\frac{1}{2} \sum_{mef} \langle am \| ef \rangle t_{im}^{ef}$$

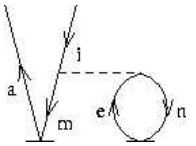

$$-\sum_{mne} \langle mn \| ie \rangle t_m^a t_n^e$$

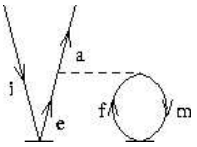

$$\sum_{mef} \langle am \| ef \rangle t_m^f t_i^e$$

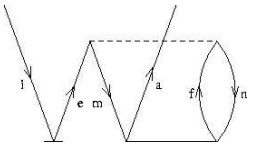

$$-\frac{1}{2} \sum_{mn} \langle mn \| ef \rangle t_i^e t_{mn}^{af}$$

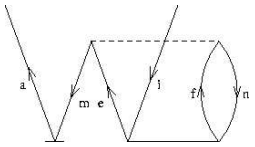

$$-\frac{1}{2} \sum_{mn} \langle mn \| ef \rangle t_m^a t_{in}^{ef}$$

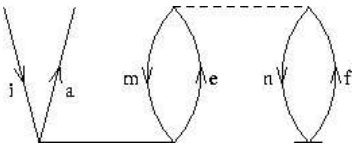

$$\sum_{mn} \langle mn \| ef \rangle t_{im}^{ae} t_n^f$$

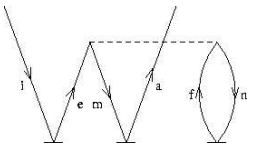

$$\sum_{mn} \langle mn \| ef \rangle t_i^e t_m^a t_n^f$$

T_2-equations:

$$\begin{aligned} 0 &= \langle \phi_{ij}^{ab}|V + (fT_1T_2)_c + (VT_1)_c + (VT_2)_c + (VT_1^2)_c \\ &\quad + (VT_1T_2)_c + (VT_1^3)_c + (VT_1^2T_2)_c + (VT_2^2)_c + (VT_1^4)_c|\phi_0\rangle, \end{aligned} \tag{1.75}$$

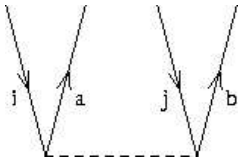

$\langle ab||ij\rangle$

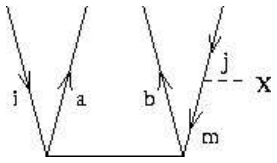

$-P(i,j)\sum_m f_{mj}t_{im}^{ab}$

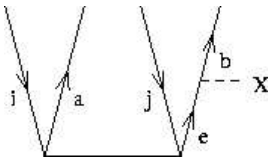

$P(a,b)\sum_e f_{eb}t_{ij}^{ae}$

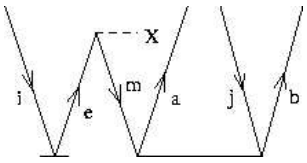

$-P(i,j)\sum_{me} f_{me}t_i^e t_{mj}^{ab}$

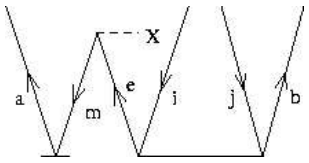

$-P(a,b)\sum_{me} f_{me}t_m^a t_{ij}^{eb}$

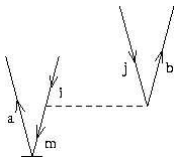

$-P(a,b)\sum_m \langle mb||ij\rangle t_m^a$

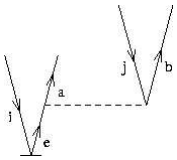

$P(i,j)\sum_e \langle ab||ej\rangle t_i^e$

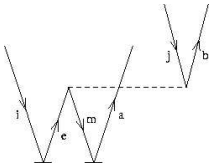

$-P(i,j)P(a,b)\sum_{me}\langle mb||ej\rangle t_i^e t_m^a$

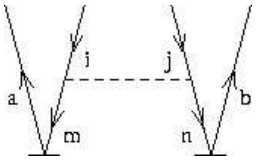

$P(a,b)\frac{1}{2}\sum_{mn}\langle mn||ij\rangle t_m^a t_n^b$

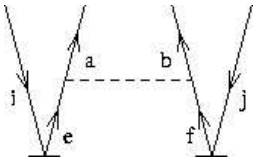

$P(i,j)\frac{1}{2}\sum_{ef}\langle ab||ef\rangle t_i^e t_j^f$

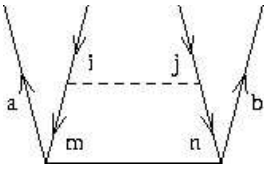

$\frac{1}{2}\sum_{mn}\langle mn||ij\rangle t_{mn}^{ab}$

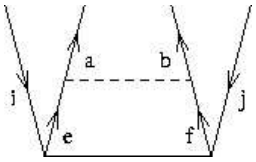

$\frac{1}{2}\sum_{ef}\langle ab||ef\rangle t_{ij}^{ef}$

T_2-equations:

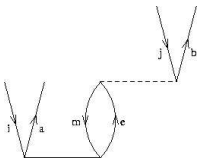

$$P(i,j)P(a,b)\sum_{me}\langle mb\|ej\rangle t_{im}^{ae}$$

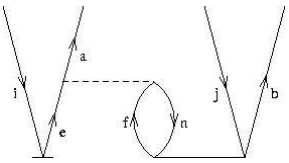

$$P(i,j)P(a,b)\sum_{mef}\langle am\|ef\rangle t_i^e t_{mj}^{fb}$$

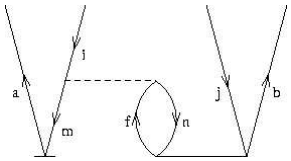

$$-P(i,j)\sum_{e}\langle mn\|je\rangle t_{im}^{ab} t_n^e$$

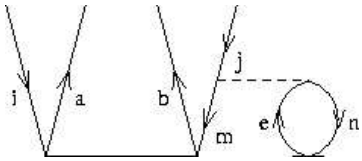

$$-P(a,b)\sum_{mef}\langle bm\|ef\rangle t_{ij}^{ae} t_m^f$$

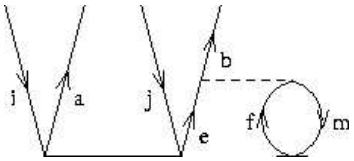

$$-P(i,j)P(a,b)\sum_{mne}\langle mn\|ie\rangle t_m^a t_{nj}^{eb}$$

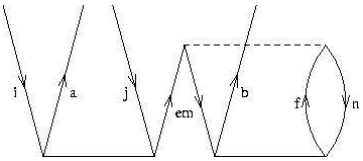

$$-P(a,b)\frac{1}{2}\sum_{mnef}\langle mn\|ef\rangle t_{ij}^{ae} t_{mn}^{bf}$$

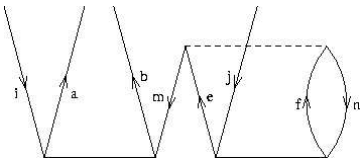

$$-P(i,j)\frac{1}{2}\sum_{mnef}\langle mn\|ef\rangle t_{im}^{ab} t_{jn}^{ef}$$

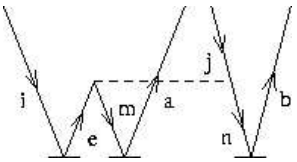

$$P(i,j)P(a,b)\frac{1}{2}\sum_{mne}\langle mn\|ej\rangle t_i^e t_m^a t_n^b$$

T_2-equations:

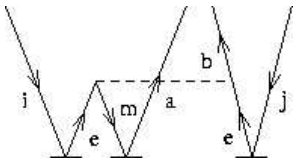

$$-P(i,j)P(a,b)\frac{1}{2}\sum_{mne}\langle mb\|ef\rangle t_i^e t_m^a t_j^e$$

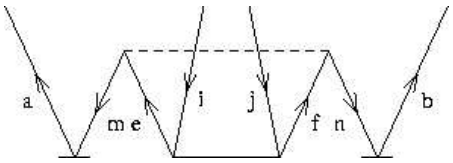

$$P(a,b)\frac{1}{4}\sum_{mnef}\langle mn\|ef\rangle t_m^a t_{ij}^{ef} t_n^b$$

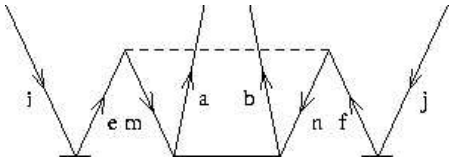

$$P(i,j)\frac{1}{4}\sum_{mnef}\langle mn\|ef\rangle t_i^e t_{mn}^{ab} t_j^f$$

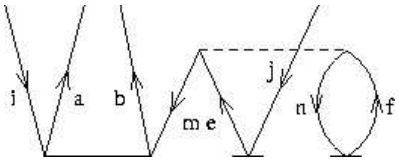

$$-P(i,j)\sum_{mnef}\langle mn\|ef\rangle t_{im}^{ab} t_j^e t_n^f$$

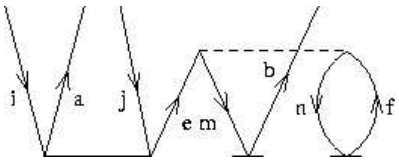

$$-P(a,b)\sum_{mnef}\langle mn\|ef\rangle t_{ij}^{ae} t_m^b t_n^f$$

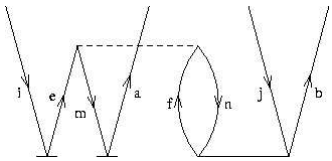

$$-P(i,j)P(a,b)\sum_{e}\langle mn\|ef\rangle t_i^e t_m^a t_{nj}^{fb}$$

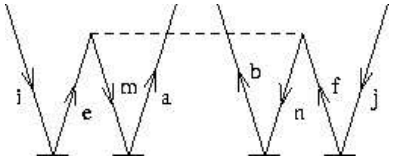

$$P(i,j)P(a,b)\frac{1}{4}\sum_{mnef}\langle mn\|ef\rangle t_i^e t_m^a t_j^f t_n^b$$

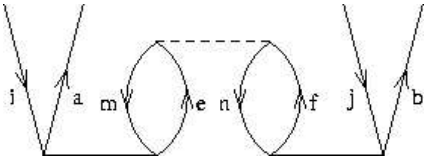

$$P(i,j)P(a,b)\sum_{mnef}\langle mn\|ef\rangle t_{im}^{ae} t_{nj}^{fb}$$

1.6.1 EOM-CCSD Sigma Equations

The derivation of the EOM-CCSD sigma equations involve the similarity transformed intermediates,

$$\begin{aligned}(Fe^{(T_1+T_2)})_c &= \bar{F} \\ (Ve^{(T_1+T_2)})_c &= \bar{W}. \end{aligned} \tag{1.76}$$

σ_1-equations:

$$(\bar{H}R)_i^a = (\bar{F}R_1)_c + (\bar{F}R_2)_c + (\bar{W}R_1)_c + (\bar{W}R_2)_c \tag{1.77}$$

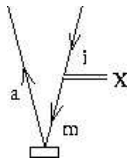

$$-\sum_m \bar{F}_{mi} R_m^a$$

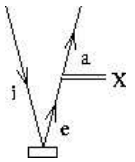

$$\sum_e \bar{F}_{ae} R_i^e$$

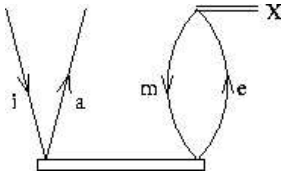

$$\sum_{me} \bar{F}_{me} R_{im}^{ae}$$

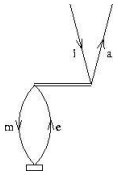

$$\sum_{me} \bar{W}_{maei} R_m^e$$

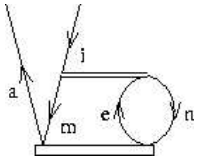

$$-\frac{1}{2}\sum_{mne} \bar{W}_{mnie} R_{mn}^{ae}$$

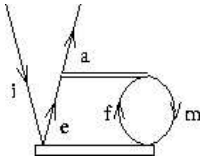

$$\frac{1}{2}\sum_{efm} \bar{W}_{amef} R_{im}^{ef}$$

σ_2-equations:

$$(\bar{H}R)_{ij}^{ab} = (\bar{W}R_1)_c + (\hat{W}R_1)_c + (\bar{F}R_2)_c + (\bar{W}R_2)_c + (\hat{W}R_2)_c \tag{1.78}$$

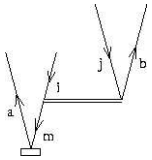

$$-P(a/b)\sum_m \bar{W}_{mbij}R_m^a$$

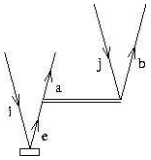

$$P(i/j)\sum_e \bar{W}_{abej}R_i^e$$

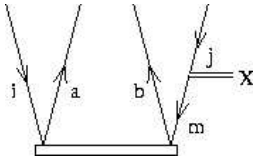

$$-P(i/j)\sum_m \bar{F}_{mj}R_{im}^{ab}$$

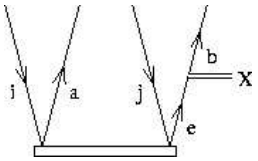

$$P(a/b)\sum_e \bar{F}_{be}R_{ij}^{ae}$$

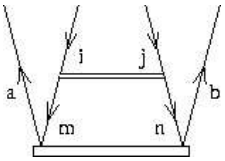

$$\frac{1}{2}\sum_{mn} \bar{W}_{mnij}R_{mn}^{ab}$$

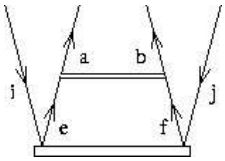

$$\frac{1}{2}\sum_{ef} \bar{W}_{abef}R_{ij}^{ef}$$

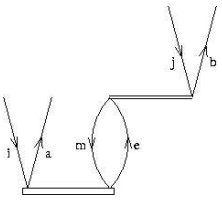

$$P(i/j)P(a/b)\sum_{me} \bar{W}_{mbej}R_{im}^{ae}$$

σ_2-equations:

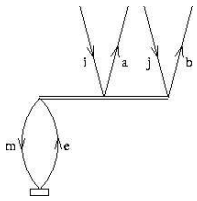

$$\sum_{me} \hat{W}_{mabeij} R^e_m$$

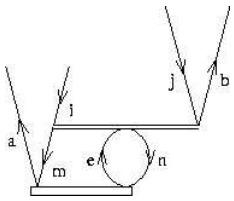

$$-P(a/b)\frac{1}{2}\sum_{me} \hat{W}_{mnbiej} R^{ae}_{mn}$$

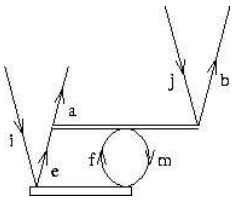

$$P(a/b)\frac{1}{2}\sum_{me} \hat{W}_{imbefj} R^{ef}_{im}$$

The three-body intermediates $\hat{W}$ are defined in Stanton's EOM article.[32]

Chapter 2

Approximate Triples Corrections

> "Because of recent improvements in the accuracy of theoretical predictions based on large scale ab initio quantum mechanical calculations, meaningful comparisons between theoretical and experimental findings have become possible.[33]"
>
> -Yuan T. Lee

Many studies have shown that the accuracy of the coupled cluster model depends on extending the singles and doubles truncated wave function to include higher excitation levels. For example, the singles and doubles truncation of the equation-of-motion coupled cluster method (EOM-CCSD) is known to generally provide reliable accuracy (on the order of 0.2 eV) for transition energies of predominantly one-electron excitations relative to the reference state. However, substantially worse results are found with states described by excitation of two-electrons. Recall that the double-excitation amplitudes are the primary contributor to

electron correlation; the single-excitations are linked to orbital relaxation effects. If the reference is the coupled cluster ground-state (although it doesn't have to be), then for states described by double-replacement excitations there is essentially no electron correlation in the wave function. For such transitions, the EOM-CCSD model breaks down because of the lack of electron correlation.

In order to overcome these problems, at least connected triple excitations should be included in the truncated wave function. Such an approach has shown some ability to recover static correlation contributions and is found to be very successful in modeling two-electron transitions. Unfortunately, the full inclusion of triples is often far too expensive to be computationally practical. For example, CCSD scales as N^6, where N is the number of orbitals, while CCSDT scales as N^8 and requires the storage of the N^6 triples amplitudes. Accordingly, numerous research efforts have focused on the development of methods where the triples are treated in an approximate fashion.

The focus of this chapter is to review the construction of approximate triples corrective schemes. There are two primary strategies to reduce the computational effort to N^7 and bypass the necessity to store the triple excitation amplitudes. The first approach is to approximate the full CCSDT amplitude equations by adding the lowest-order perturbation energy contributions from the connected triples to the CCSD energy. The CCSD(T) method is the most popular approach for incorporating the effects of the T_3 operator in the coupled cluster model. The (T) correction scales as a non-iterative N^7 calculation and reduces the CCSD error by five to ten times while recovering about 70 percent of the full T effects.[34]

The second approach is to remove terms from the full CCSDT equations which at least scale larger than N^7. The iterative CCSDT-n (n=1,2,3) and CC3 methods approximate the full triples equation and directly couple their effects to the singles and doubles equation. Compared to CCSD(T), these iterative methods can have some advantages for modeling time-dependent properties.[35] However, for the calculation of energies and static properties, the non-iterative CCSD(T) is the method of choice.[35]

2.1 Perturbative Energy Correction

The connection between coupled cluster theory and many-body perturbation theory allows us to construct finite-order perturbation theory energy and wave function corrections to the coupled cluster equations. We illustrate this connection through the derivation of the popular CCSD(T) model. Furthermore, the main concepts discussed will be utilized to develop two excited-state models: the EOM-CCSD(T) and EOM-CCSD($\tilde{\mathrm{T}}$) methods.

2.1.1 Ground-State Equations

As described in section (1.3.1), the electronic Hamiltonian can be partitioned into two terms, where the zeroth-order component is taken to be the Fock operator and the remaining two-electron operator (or fluctuation potential) is the perturbation,

$$H_N = H_N^{(0)} + H_N^{(1)} = F_N + V_N \tag{2.1}$$

Since the exact wave function can be decomposed by orders of perturbation theory, we can thus make an analogous decomposition of the coupled cluster operator T_n.

$$T_n = T_n^{(1)} + T_n^{(2)} + T_n^{(3)} + T_n^{(4)} + T_n^{(5)} + \cdots \tag{2.2}$$

Certain terms may naturally be zero, depending on the choice of molecular orbital basis. For example, in Møller-Plesset theory, the only first-order component is T_2,

$$\begin{aligned} 0 &= \langle \Phi_{ij}^{ab} | \{ H_N e^T \}_c^{(1)} | \Phi_0 \rangle \\ &= \langle \Phi_{ij}^{ab} | \{ F_N T_2^{(1)} + V_N | \Phi_0 \rangle \end{aligned} \tag{2.3}$$

which may be rewritten as

$$(f_{ii} + f_{jj} - f_{aa} - f_{bb}) t_{ij}^{ab(1)} = \langle ij \| ab \rangle. \tag{2.4}$$

Diagrammatically this is illustrated as,

$$t_{ij}^{ab(1)} = \frac{\langle ab || ij \rangle}{D_{ij}^{ab}} = \tag{2.5}$$

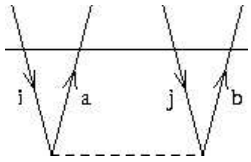

The extra horizontal line denotes the the difference in energies between occupied orbitals i, j and virtual orbitals a, b (also denoted D_{ij}^{ab}).

Contributions to T_1, T_3 and T_4 first appear in the second-order wavefunction. While CCSD includes second- and third-order energy contributions, it lacks the fourth-order contribution. Therefore, it seems natural that this should be our first pertubational improvement to the

CCSD wavefunction,

$$E^{(4)} = \langle\Phi_0|\{H_N e^T\}_c^{(4)}|\Phi_0\rangle = \langle\Phi_0|\{V_N T_2^{(3)}\}_c|\Phi_0\rangle = \tag{2.6}$$

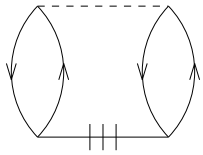

where equation (2.6) includes the only term that is non-zero. We must now solve for the unknown $T_2^{(3)}$.

$$\begin{aligned} 0 &= \langle\Phi_{ij}^{ab}|\{H_N e^T\}_c^{(3)}|\Phi_0\rangle \\ &= \langle\Phi_{ij}^{ab}|\{F_N T_2^{(3)} + V_N T_1^{(2)} + V_N T_2^{(2)} + V_N T_3^{(2)} + \frac{1}{2} V_N (T_2^{(1)})^2\}_c|\Phi_0\rangle \end{aligned} \tag{2.7}$$

Since the CCSD equations already include contributions from first- and second-order T_1 and T_2, we only need to construct $V_N T_3^{(2)}$,

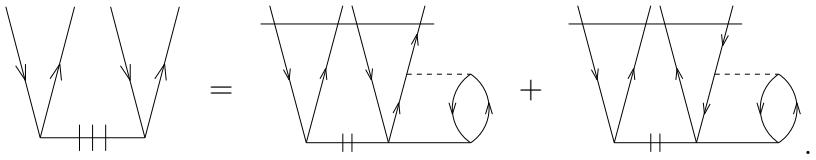

(2.8)

The order is indicated by the extra hash marks on the corresponding interaction line. The $T_3^{(2)}$ amplitudes are determined from the second-order T_3 amplitude equation:

$$\begin{aligned} 0 &= \langle\Phi_{ijk}^{abc}|\{H_N e^T\}_c^{(2)}|\Phi_0\rangle \\ &= \langle\Phi_{ijk}^{abc}|\{V_N T_2^{(1)} + F_N T_3^{(2)}\}_c|\Phi_0\rangle \end{aligned} \tag{2.9}$$

which may be written using the same diagrammatic notation described above

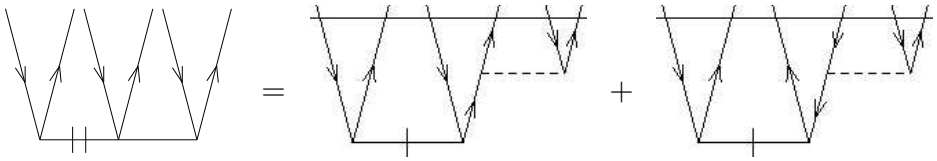

(2.10)

Equation (2.10) provides us with a perturbative means for including the effects of triple excitations in the coupled cluster energy. We now have the necessary tools to solve the fourth-order energy correction that we desired; the first-order $T_2^{(1)}$ amplitudes, computed from equation (2.3), are used to obtain the $T_3^{(2)}$ amplitudes; the $T_3^{(2)}$ amplitudes are then used to solve the third-order $T_2^{(3)}$ amplitudes, equation (2.8). The sum of all these contributions to the fourth-order energy can now be interpreted as,

$$E^{(4)} = \quad = \frac{1}{36} \sum_{ijkabc} t_{ijk}^{abc} D_{ijk}^{abc} t_{ijk}^{abc}. \tag{2.11}$$

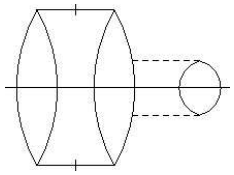

Using the energy corrections described, we would expect an improvement in the CCSD energy. However, the fourth-order perturbational correction overestimates the triples effects. The problem is that there is an improper balance between the connection of the perturbational correction to the single and double excitations. In order to correct this, additional terms beyond fourth-order must be included. While all fifth-order contributions have been considered, Raghavachari *et al.* determined that folowing fifth-order correction should also be included.[36]

$$E^{(5)} = \frac{1}{4} \sum_{ijkabc} \langle jk \| bc \rangle t_i^a t_{ijk}^{abc} \tag{2.12}$$

This fifth-order term can be derived analogously to the fourth-order expression. The combination of the fourth-order term, equation (2.11), and fifth-order, equation (2.12), is known as the CCSD(T) model and is the most popular and successful of the perturbation-based corrections.

Table 2.1: CCSD(T) contributions to the CCSD excited-state amplitude equations. $\tilde{V} = (VT_2)_c + (VT_1T_2)_c + (VT_2^2/2)_c + (VT_1^2T_2/2)_c + (VT_1T_2^2/2)_c + (VT_1^3T_2/2)_c/3!$

Method	$(D_{ijk}^{abc} + \omega_{ccsd})R_{ijk}^{abc}$	$(D_{ijk}^{abc} + \omega_{ccsd})L_{ijk}^{abc}$
EOM-CCSD(T)	$(VR_2)_c + (VR_1)_c$	$(VL_1)_c + (VL_2)_c$
EOM-CCSD($\tilde{\text{T}}$) [1]	$(\tilde{V}R_2)_c + (\tilde{V}R_1)_c$	$(L_2\tilde{V})_c + (L_1\tilde{V})_c$

2.1.2 Excited-State Equations

The goal of the EOM-CC method is to establish a similar reliability to the ground-state CCSD(T) method, which is a sufficiently good approximation to CCSDT. Finite-order energy corrections can also be made to the EOM-CCSD model through solutions of the expectation value of the similarity transformed Hamiltonian $\bar{H}$,

$$\omega = \langle L|\bar{H}|R\rangle. \tag{2.13}$$

We note that the similarity transformed Hamiltonian is not Hermitian and therefore each root of $\bar{H}$ is associated with the two distinct eigenvectors R and L. The left-hand solutions can be solved in the same Davidson manner as the right-hand solutions. Unlike the right-hand states, however, there is no connectivity requirement between the left-hand states and the Hamiltonian.

After solving the EOM-CCSD R and L equations, we need the remaining terms included in

equation (2.13). For truncated triples,

$$\omega = \omega_{ccsd} + \langle L_1|V|R_3\rangle. + \langle L_2|(f+V)|R_3\rangle + \langle L_3|V|R_2\rangle + \langle L_3|f|R_3\rangle. \quad (2.14)$$

We thus need to solve for the L_3 and R_3 terms. However, unlike the T_3 amplitudes which are directly generated from T_2, the excited-state triples are solved in a slightly different manner: the R_3 and L_3 amplitudes are constructed from the equations in Table (2.1) which include the EOM-CCSD eigenvalue ω. The resulting R_3 and L_3 amplitudes are then used in equation (2.14) to generate the noniterative triples correction to the EOM-CCSD excitation energy.

2.2 Iterative Triples Correction

The CCSD(T) method described in the last section is only an energy correction. Therefore, the single- and double-excitation amplitudes do not "feel" the response of the triple-excitation amplitudes. This response is important for frequency dependent molecular properties. Another approach is to couple the triples into the singles and doubles equations. With most iterative methods of this type, the singles and doubles equations are exact with respect to the full CCSDT method, and approximations are made in the construction of the T_3 amplitude equations. We note that by approximating the triples equation, there is no associated wave function so the exact form of $\bar{H}$ is not clear. In other words, the effective Hamiltonian can not be explicitly defined like with CCSDT: $\bar{H}=(He^{T_1+T_2+T_3})_c$.

Table 2.2: Triples contributions to the CCSD ground-state amplitude equations.

Method	$\langle\phi_i^a\|\bar{H}\|\phi_0\rangle$	$\langle\phi_{ij}^{ab}\|\bar{H}\|\phi_0\rangle$	$\langle\phi_{ijk}^{abc}\|\bar{H}\|\phi_0\rangle$
CCSDT-1b	$(VT_3)_c$	$(HT_3)_c + (VT_1T_3)_c$	$(fT_3)_c + (VT_2)_c$
CCSDT-2	$\vdots$	$\vdots$	$(fT_3)_c + (VT_2)_c + (VT_2T_2)c$
CCSDT-3	$\vdots$	$\vdots$	$(fT_3)_c + (VT_2)_c + (VT_1T_2)c$
			$+(VT_1T_1T_2)_c + (VT_1T_1T_1T_2)_c$
			$+(VT_2T_2)_c + (VT_1T_2T_2)c$
CC3	$\vdots$	$\vdots$	$(fT_3)_c + (VT_2)_c + (VT_1T_2)c$
			$+(VT_1T_1T_2)_c + (VT_1T_1T_1T_2)_c$

2.2.1 CCSDT-n Methods

Table 2.1 includes the approximate triples equations for the CCSDT-n (n=1,2,3) methods of Bartlett *et al.*[37,38] The CCSDT-1 method is perhaps the simplest and most economical technique for incorporating connected triples in the CCSD wave function. Note that the T_3 equation defining the CCSDT-1 method is the same as that in the the (T) correction. For the CCSDT-3 method, all CCSDT terms are included which can be evaluated with N^7 scaling: the target T_3 amplitudes retain all possible T_1 and T_2 terms but eliminates contributions containing T_3.

The EOM-CCSDT-n models adopt an analogous strategy to the ground-state where the singles and doubles amplitudes are exact with respect to EOM-CCSDT while the triples

Table 2.3: Triples contributions to the EOM-CCSD excited-state σ-equations. $\bar{W}$=$e^{-(T_1+T_2)}Ve^{(T_1+T_2)}$, $\hat{W}_{T-3}$=$(fT_3)_c + (VT_2)_c + (VT_1T_2)_c$+ $(VT_1T_1T_2)_c + (VT_1T_1T_1T_2)_c$+ $(VT_2T_2)_c + (VT_1T_2T_2)_c$, $\hat{W}_{CC3}$=$(fT_3)_c + (VT_2)_c + (VT_1T_2)_c$+ $(VT_1T_1T_2)_c + (VT_1T_1T_1T_2)_c$

Method	$(\bar{H}R)_i^a$	$(\bar{H}R)_{ij}^{ab}$	$(\bar{H}R)_{ijk}^{abc}$
CCSDT-1	$(\bar{W}R_3)_c$	$((f+\bar{W})R_3)_c + (\bar{W}T_3R_1)_c$	$(fR_3)_c + (VR_2)_c$
CCSDT-3	$\vdots$	$\vdots$	$(fR_3)_c + (\hat{W}_{T-3}R_1)_c + (\hat{W}_{T-3}R_2)_c$
CC3	$\vdots$	$\vdots$	$(fR_3)_c + (\hat{W}_{CC3}R_1)_c + (\hat{W}_{CC3}R_2)_c$

are approximated in some manner. A benchmark study of the EOM-CCSDT-1 method[39] revealed substantial improvement for two-electron transitions over the EOM-CCSD method, but not as close to experiment as EOM-CCSDT.[40]

The method was found to be no better than EOM-CCSD for one-electron excitations, though this was thought to be insignificant since a number of prior studies had demonstrated EOM-CCSD's success with these types of transitions.[32] However, for certain one-electron valence transitions Bartlett *et al.* reported some suprising failures with the EOM-CCSDT-1 model, suggesting that the triple excitation approximation needs to be improved.[41] It can be seen from Table (2.3) that the EOM-CCSDT-1 method has limited coupling between the triple amplitudes and the single and double amplitudes. The singles do not appear in the triples equation so their effect on one-electron transitions is very little.

At the EOM-CCSDT-3 level, all R-terms in the EOM-CCSDT method are retained except

the costly R_3 into R_3 terms.[41] Compared to EOM-CCSDT-1, the additional terms included in the EOM-CCSDT-3 method introduce important corrections for both singly and doubly excited states. These additional terms appear in higher orders of perturbation theory and therefore may produce more accurate results. Indeed, the EOM-CCSDT-3 method is generally accepted as the most reliable of the EOM-CCSDT-n methods, at least for closed-shell species.

2.2.2 CC3

The CC3 model[2–4] is similar in spirit to the CCSDT-n models where various contributions from the full triples equation are retained. However, such approximations may become unbalanced if the terms to be included are not carefully selected according to perturbation theory. We observed this in the last section with the development of the CCSD(T) model; the fifth-order term was included to properly balance the fourth-order energy correction.

The CC3 method was developed from a perturbational analysis of the Hartree-Fock wave function. Based on Møller-Plesset theory, the singles first occur in the second-order wave function and the fourth-order energy. It thus appears that the singles are much less important than the doubles, which occur in the first-order wave function and second-order energy. However, it is well established that the singles play a unique role as approximate orbital relaxation parameters. When an external perturbation is applied to the system, the singles become first-order in the external perturbation and zeroth-order in the fluctuation potential.

The singles' unique role in response-type properties suggests that no approximations should be made in their treatment. The CC3 method thus treats the singles, doubles and triples as first appearing in the zeroth-, first-, and second-order wave function, respectively. This leads us to the introduction of the modified one- and two-electron Hamiltonian,

$$\hat{H} = e^{-T_1} H e^{T_1}. \tag{2.15}$$

The CCSDT triples equation may now be written as,

$$0 = \langle \phi_{ijk}^{abc} | (FT_3)_c + (\hat{V}T_2)_c + (\hat{V}T_2T_2)_c + (\hat{V}T_3)_c + (VT_2T_3)_c | \phi_0 \rangle. \tag{2.16}$$

By including the first two terms in equation (2.16) the connected triples are ensured to be correct through second-order in perturbation theory. The third term is not included since it is third order and the fourth and fifth terms are not included as they are third and fourth order and scale as N^8. We note that the inclusion of all singles does not give an unbalanced triples equation because of their unique role as approximate orbital relaxation parameters.

2.3 CC3 Diagrams

We now conclude with a diagrammatic derivation of the ground- and excited-state CC3 equations which are illustrated in Figures (2.1) and (2.2). The CC3 model is utilized in Chapters 4 and 5 to predict excitation energies for a few open-shell molecules. While the computational aspects of the CC3 code are given in Chapter 4, we note that the diagrammatic structure of the ground- and excited-state T_3 and R_3 equations are very similar (this becomes

particularly clear if one explicitly writes out all of the contributing terms which are implicitly included in the T_1 integral transformation). Therefore, we have written a generalized triples function in which the ground- and excited-state amplitudes are determined based on one's choice of input parameters. This function computes all possible A, B, C virtual orbital combinations for fixed I, J, K occupied orbital indices. Thus, the triples are computed *on-the-fly* as they are needed thus reducing the computational storage costs to N^3 orbitals.

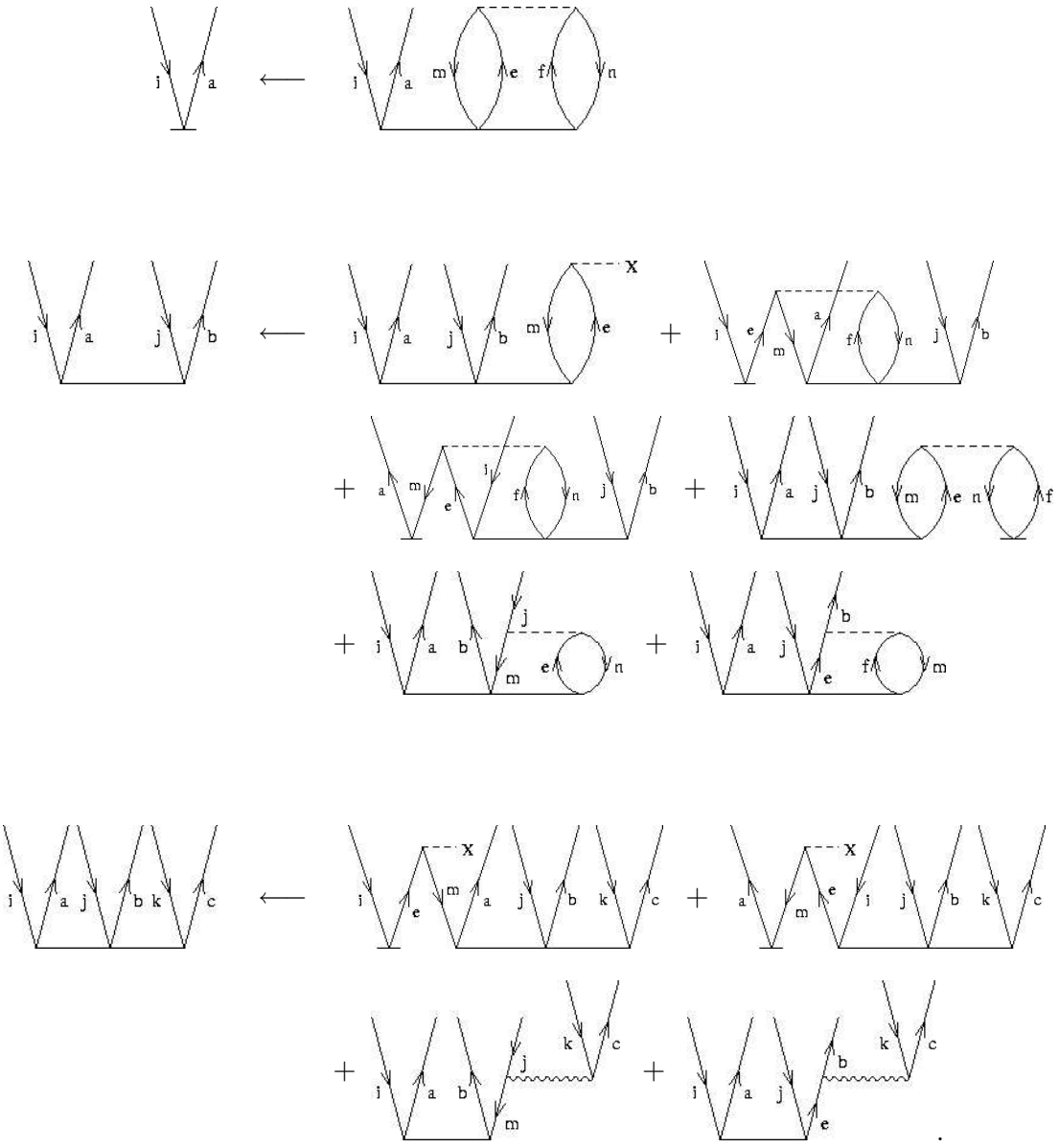

Figure 2.1: Ground-state triples contributions to the CC3 amplitude equations. The squiggly interaction lines refer to the T_1-transformed intermediates, defined by equation (2.15).

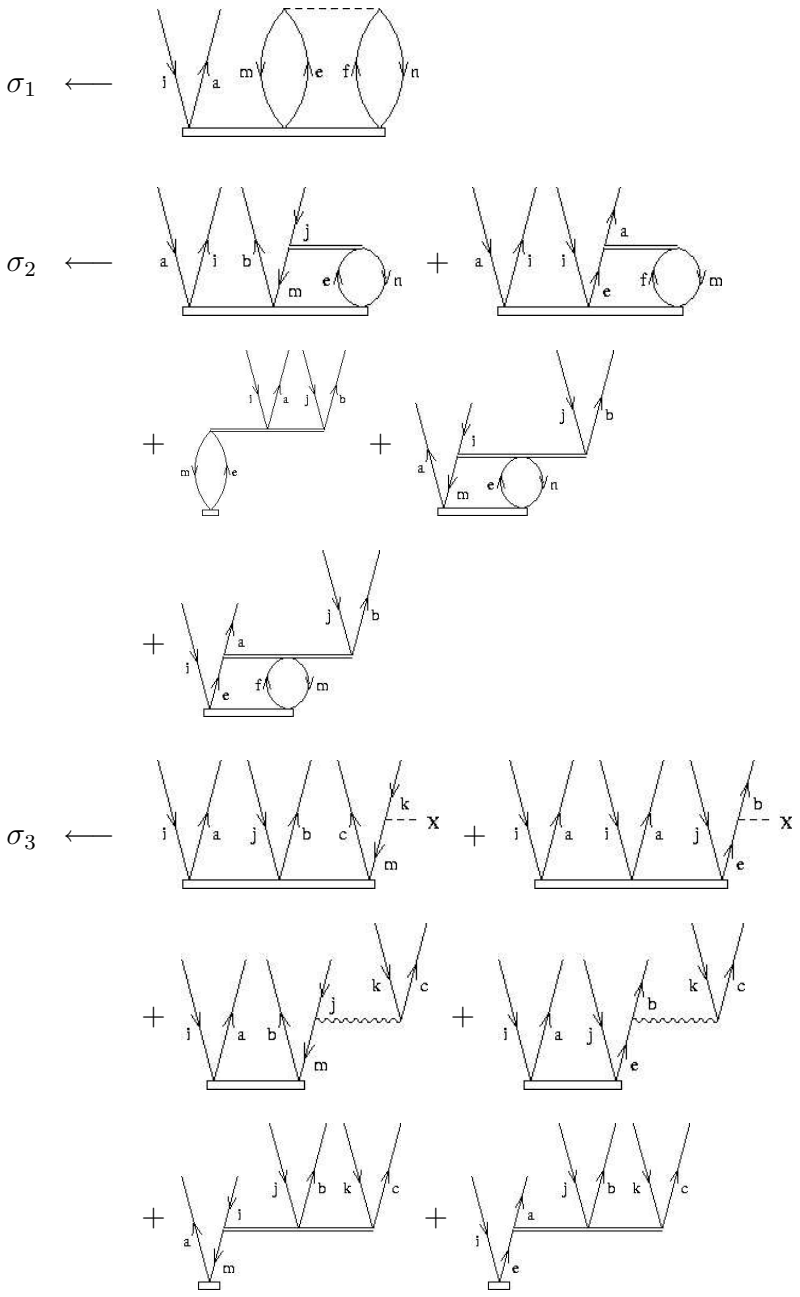

Figure 2.2: Excited-state triples contributions to the CC3 sigma equations. The three-body terms are given in literature by Christiansen, Koch, Jørgensen and co-workers.[2–4]

Chapter 3

The Structures of *m*-Benzyne and Tetrafluoro-*m*-Benzyne

3.1 Introduction

1,3-Didehydrobenzene (commonly known as *m*-benzyne, see Fig. 3.1) and its derivatives provide excellent examples of the often symbiotic relationship between theory and experiment. *m*-Benzynes are stable only at low temperatures and can be characterized by matrix isolation infrared spectroscopy,[6–8,42–45] and quantum chemical calculations can reproduce the measured spectrum provided they also correctly describe the molecule's geometry and electronic structure.[5,6,46–53] Hence, agreement between measured and calculated infrared spectra is synonymous with identification and structural characterization. Although this strategy of

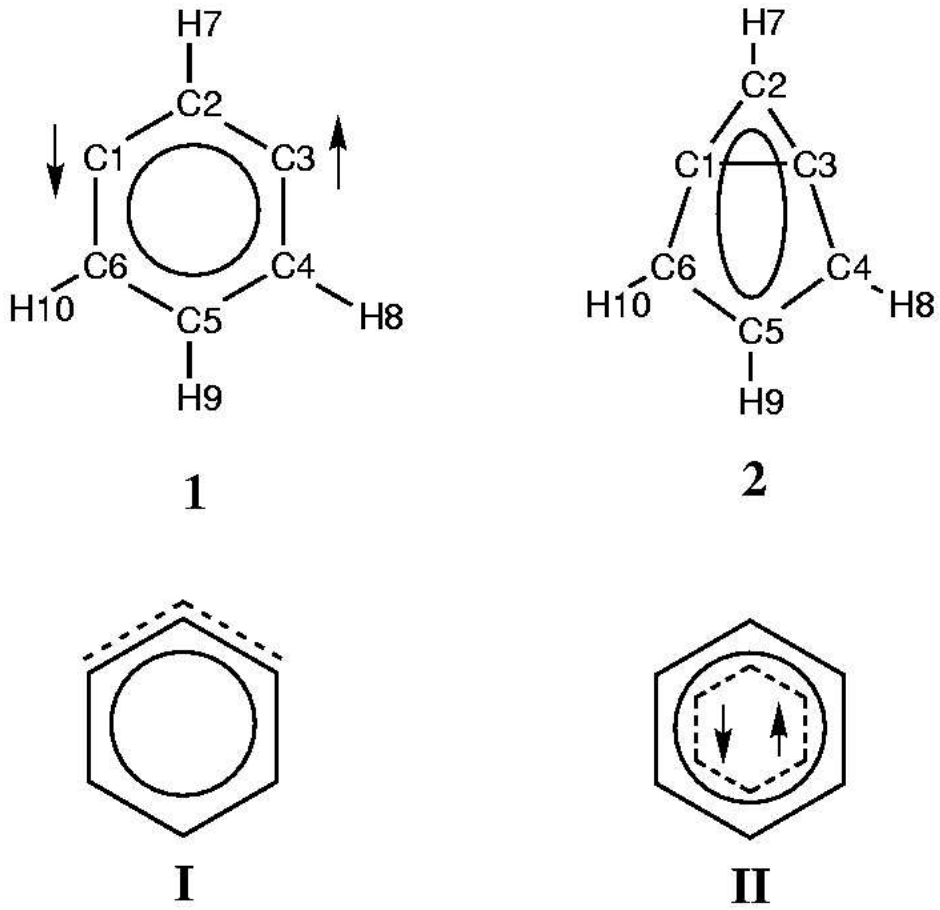

Figure 3.1: Possible structural forms of *m*-benzyne: a monocyclic singlet biradical (**1**) vs. a bicyclic closed-shell singlet (**2**); the σ-allylic structure of Winkler and Sander[5] (**I**) vs. a σ-delocalized structure (**II**). In structure **2**, the ring denotes the π system, which remains essentially intact (relative to benzene) after the formation of the C1−C3 bond. In structure **I**, the dotted line indicates the presence of σ-through-bond coupling between C1−C3 and C1−C2/C2−C3. For structure **II**, the circle indicates the delocalized π system, the dashed hexagon through-bond delocalization, and the coupled arrows a strong degree of spin coupling leaving little, but still finite biradical character.

combining theory and experiment promises useful insight into the electronic structure of labile compounds not amenable to other structural investigations, it is easily hampered by complicating factors that may make the comparison problematic. These may have to do with the experimental conditions (e.g., low resolution of the measured spectra, limited detection range, presence of other molecules in the matrix, etc.) or the limitations of the theoretical description (e.g., multireference effects, basis set incompleteness, etc.). (For a recent review of many of the issues hampering theoretical descriptions of benzyne diradicals.[54]

Marquardt, Sander, and Kraka carried out the photolytic destruction of [2,2]meta-paracyclophane-2,9-dione trapped in an argon matrix at 10 K and hypothesized that *m*-benzyne was one of the products.[6] Theoretical calculations using coupled cluster theory supported this conclusion: the coupled cluster singles and doubles method with perturbative triples [CCSD(T)][36] and the 6-31G(*d*,*p*) basis set[55] predicts a monocyclic structure (structure **1** of Fig. 3.1) whose harmonic vibrational spectrum shows good agreement with the experimental infrared difference spectrum.[6] Kraka and Cremer, using the same level of theory, predicted a C1−C3 bond length of ca. 2.0 Å and a relatively weak biradical character of just 20%.[46,47] These investigations were later repeated by generating *m*-benzyne from other precursors, and in each case the same infrared spectrum was observed.[45]

Several authors have also performed density-functional theory (DFT)[56] and wave-function-based calculations to explore the potential energy surface (PES) along the *m*-benzyne C1−C3 distance.[5,50] At smaller values of r(C1−C3) a second structure, bicyclo[3.1.0]hexatriene (structure **2** of Fig. 3.1) may be located, which, despite its high ring strain resulting from

the existence of a cyclopropenyl unit and two inverted carbon atoms (C1 and C3), is remarkably stable relative to the open form. However, whether the monocyclic or bicyclic structure is most stable depends heavily on the type of method used, and the choice of density functional, wave function, basis set, correlation correction, etc. can have a dramatic effect on the shape of the PES.[5,50] Among density functionals, in particular, the RB3LYP functional[57,58] predicts the bicyclic structure to be the most stable, whereas the RBLYP functional[58,59] prefers the monocyclic structure, and an extensive discussion exists in the literature over the most appropriate choice of method for biradicals.[50,60–67] Wenk and Sander recently reported the generation of tetrafluoro-*m*-benzyne in solid neon at 3 K identified by its corresponding infrared difference spectrum.[7,8] Just as for the parent *m*-benzyne, density functional calculations give widely varying results depending on the choice of functional. Based upon their previous studies of *m*-benzyne, Wenk and Sander concluded that the RB3LYP functional overestimates the interaction between the radical centers. They therefore preferred the RBLYP functional, which predicts a monocyclic structure.

However, Hess has recently disputed the conclusions of these investigations,[51] and has suggested that still higher levels of theory should be applied to finally lay to rest the question of *m*-benzyne's structure. Indeed, the variability of computed results from coupled cluster theory with respect to the choice of reference determinant, an important aspect for related compounds such as 1,4-didehydrobenzene (also known as *p*-benzyne),[18] has not yet been examined for *m*-benzyne or tetrafluoro-*m*-benzyne. Furthermore, calculated infrared spectra have been exclusively based on the harmonic approximation combined with various

scaling procedures to simulate the true fundamental infrared vibrational frequencies of the compound.[6,45,48,50] Although this approach is common in quantum chemistry,[68] it makes spectra comparison more a qualitative rather than the needed quantitative exercise.

Several other questions must be answered in connection with the *m*-benzyne (and tetrafluoro-*m*-benzyne) problem: (1) What level of theory is required to obtain the most reliable description of the two *m*-benzyne forms, or, equivalently, how can one obtain a reliable description of the PES along the C1−C3 distance? (2) What is the shape of this PES profile: a double-well, a simple single-well, a strongly asymmetric single-well, or a broad, flat single-well embedding both *m*-benzyne forms and leading to a large amplitude vibration? (3) Can one assess the answers to these two questions *via* a comparison of measured and calculated infrared vibrational spectra of *m*-benzyne?

Some of these questions have been investigated in the past. For example, the most extensive study of *m*-benzyne to date is that of Winkler and Sander,[5] who used both DFT and wave-function-based methods to investigate the PES along the C1−C3 distance. They found that pure functionals based on the generalized gradient approximation (GGA) such as BLYP were superior to hybrid functionals such as B3LYP for *m*-benzyne because they produced energy profiles that more closely mimicked those from higher level coupled cluster theory. However, Kraka, Cremer, and co-workers have shown that this is due to the fact that BLYP includes non-specific, non-dynamical correlation effects *via* the semilocal exchange functional.[60–62,64–67] In this way the stability of the restricted BLYP solution is artificially increased and an unrestricted BLYP solution suppressed so that zero biradical

character is enforced for any *m*-benzyne form. B3LYP, which contains only a reduced amount of non-dynamical electron correlation, has an unrestricted solution in the case of *m*-benzyne that is higher in energy than the restricted solution for the bicyclic form.

Standard DFT with the approximate exchange-correlation functionals in use today fails to describe the multiconfigurational character of *m*-benzyne. The use of BLYP and other GGA functionals in a sense disguises the true problem by predicting a perfect coupling of the single electrons (*via* peripheral delocalization or an unlikely long CC bond close to 2 Å). Accordingly, the reactivity of a typical closed shell system rather than a molecule with some biradical character is predicted. More reliable results can only be obtained if a two-configurational approach such as the restricted ensemble Kohn-Sham (REKS) approach is used with a hybrid functional to exclude at least partly the non-dynamic correlation introduced through the exchange functional.[67] But even a two-configurational DFT approach has to be verified with a method that works without any assumptions and approximations and is known to provide reliable results in the case of biradicals. Clearly coupled cluster is such a method.

The objective of the present work is to reconsider the ability of various single-determinant-reference coupled cluster methods[26,69] in the prediction of the structure of *m*-benzyne and tetrafluoro-*m*-benzyne. We have examined the influence of the reference molecular orbitals (spin-restricted, spin-unrestricted, or Brueckner) on the predicted structure, as well as basis-set effects and higher levels of dynamic electron correlation. We have computed energy profiles of both molecules using structural optimizations at coupled cluster levels of theory with

varying basis sets. In addition, we have considered the potential importance of anharmonicity on the vibrational spectrum of *m*-benzyne by computing the fundamental vibrational transition wavenumbers. These results provide, among other things, reliable reference data for comparison to more approximate methods, such as DFT.

3.2 Computational Approach

We have investigated the structures of *m*-benzyne and tetrafluoro-*m*-benzyne at the CCSD,[70,71] CCSD(T),[72,73] and full CCSDT levels of theory.[74,75] In order to identify potential problems associated with the underlying molecular orbital definitions, we utilized three types of reference determinants with the CC methods: spin-restricted Hartree-Fock (RHF), spin-unrestricted Hartree-Fock (UHF), and Brueckner orbitals.[76,77] Two basis sets were used in this study: the Pople-type split-valence 6-31G(*d*,*p*) basis set,[55] and the larger correlation-consistent triple-zeta basis set (cc-pVTZ) developed by Dunning,[78] which corresponds to a (10s5p2d1f/5s2p1d)/[4s3p2d1f/3s2p1d] basis.

Optimized geometries were obtained using analytic energy gradients at the CCSD and CCSD(T) levels of theory with the RHF[79–82] and UHF[83] reference determinants, as well as at the CCD level with Brueckner orbitals.[77] Finite-differences of energies were used to obtain gradients at the full CCSDT and B-CCD(T) levels. Energy profiles of *m*-benzyne and tetrafluoro-*m*-benzyne were obtained from optimized structures with constrained C1−C3 distances.

Harmonic vibrational frequencies were determined using analytic energy second derivatives at the CCSD and CCSD(T) levels of theory with the RHF and UHF reference functions,[84–86] numerical differentiation of analytic gradients at the B-CCD level,[77] and numerical differentiation of energies at the B-CCD(T) level. Infrared absorption intensities were computed for all methods for which at least analytic energy gradients were available. RHF-CCSD(T) fundamental vibrational frequencies of *m*-benzyne were determined using second-order vibrational perturbation theory with cubic and semidiagonal quartic force constants computed *via* finite differences of analytic second derivatives using the method described by Stanton, Lopreore, and Gauss.[87]

T_1 and T_2 excitation amplitudes were monitored as diagnostics of the quality of the coupled cluster wave functions. All electrons were correlated at the CCSD and CCSD(T) levels of theory, and the 1*s* core electrons on carbon and fluorine were frozen at the full CCSDT level. All calculations were performed using the ACESII program system.[88]

3.3 Results and Discussion: *m*-Benzyne

Table 3.1 summarizes coupled cluster predictions of the structure of *m*-benzyne. With the CCSD/6-31G(*d*,*p*) method, all three reference determinants — RHF, UHF, and Brueckner — predict a bicyclic structure as the global minimum on the PES, with a C1−C3 distance of 1.56 Å. (At this geometry, there is no true UHF wave function, i.e., the RHF determinant is stable to spin-symmetry breaking. Thus, the RHF-CCSD and UHF-CCSD structures given

Table 3.1: Optimized geometrical parameters of *m*-benzyne (bond distances in Å, angles in degrees, and energies in E_h).

	6-31G(*d*,*p*)						cc-pVTZ		
	CCSD			CCSD(T)			CCSDT	CCSD	CCSD(T)
	RHF	UHF	Brueckner	RHF	UHF	Brueckner	RHF	RHF	RHF
$r(C_1-C_3)$	1.563	1.563	1.561	2.106	2.088	2.105	2.093	1.551	2.026
$r(C_2-C_3)$	1.351	1.351	1.351	1.377	1.372	1.377	1.376	1.343	1.364
$r(C_3-C_4)$	1.384	1.384	1.384	1.383	1.379	1.383	1.384	1.376	1.372
$r(C_4-C_5)$	1.411	1.411	1.411	1.405	1.401	1.405	1.406	1.404	1.398
$r(C_2-H)$	1.080	1.080	1.080	1.078	1.078	1.078	1.079	1.074	1.072
$r(C_4-H)$	1.077	1.077	1.077	1.082	1.082	1.082	1.083	1.071	1.076
$r(C_5-H)$	1.083	1.083	1.083	1.086	1.086	1.086	1.087	1.078	1.080
$\theta(C_1-C_2-C_3)$	70.7	70.7	70.6	99.8	99.1	99.7	99.0	70.5	95.9
$\theta(C_3-C_4-C_5)$	107.7	107.7	107.7	117.3	117.0	117.3	117.1	107.7	116.7
$\theta(C_4-C_5-C_6)$	111.9	111.9	111.9	114.5	114.5	114.5	114.3	111.7	113.4
$\theta(C_3-C_4-H)$	126.3	126.3	126.3	120.5	120.6	120.6	120.6	126.3	120.7
Energy	-230.221066	-230.221066	-230.219548	-230.268076	-230.266229	-230.268097	-230.237040	-230.490523	-230.550092

in Table 3.1 are identical.) However, triple excitations produce a dramatic change in *m*-benzyne's predicted structure: the CCSD(T)/6-31G(*d*,*p*) level of theory predicts a monocyclic structure as the global minimum, with C1−C3 distances of 2.11, 2.09, and 2.11 Å, respectively, with the RHF, UHF, and Brueckner reference determinants. This qualitative difference continues at the full RHF-CCSDT level of theory, which gives a C1−C3 distance of 2.09 Å. We observed similar trends using the larger cc-pVTZ basis set, as reported for the RHF-CCSD and RHF-CCSD(T) levels of theory in Table 3.1. If we consider the fact that the larger cc-pVTZ basis set reduces the C1−C3 distance by 0.08 Å, we predict that a value of ca. 2.013 Å would be obtained at the CCSDT/cc-pVTZ level of theory.

3.3.1 Electronic Structure of *m*-Benzyne

Fig. 3.2(a) presents the RHF-CCSD and RHF-CCSD(T) energy profiles of *m*-benzyne (relative to the minimum at the given level of theory) as a function of the C1−C3 distance, where all other geometrical parameters were optimized. These diagrams illustrate clearly the difference in predicted structures, with the CCSD minimum at 1.56 Å and the CCSD(T) minimum at 2.11 Å, and with a noticeable "shoulder" on both profiles.

CCSD provides an accurate account of pair correlation in the singles and double space, and it should therefore correctly describe the degree of through-space pairing between the single electrons at C1 and C3. However, it includes only disconnected three-electron correlation effects so that through-bond interactions of the single electrons are underestimated.[89,90]

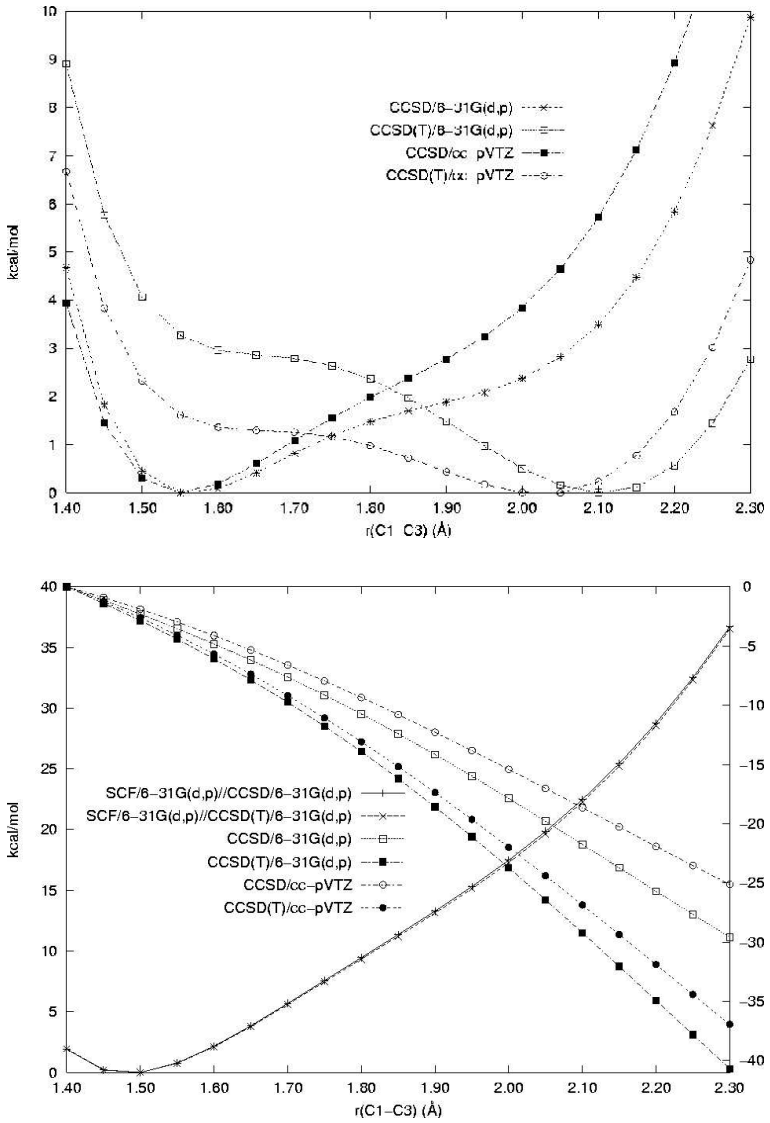

Figure 3.2: RHF-CCSD and RHF-CCSD(T) C1−C3 energy profiles for *m*-benzyne using a 6-31G(*d*,*p*) basis set. Structural parameters were optimized for fixed C1−C3 distances. Energies are reported relative to the global minimum on the respective PES. (a) Total energies; (b) SCF energies (left-hand *y*-axis) and change in correlation energy with respect to the C1−C3 distance, relative to the correlation energy at $r(\mathrm{C1{-}C3}) = 1.40$ Å (right-hand *y*-axis).

Accordingly, it exaggerates the importance of forming a C1−C3 bond and wrongly predicts the existence of a bicyclic form. Both basis sets used [6-31G(d,p) and cc-pVTZ] predict an asymmetric PES with a shoulder at the position of the open form. The larger basis set stabilizes the bicyclic form stronger relative to the open form (4-5 kcal/mol higher in energy) than the smaller basis set (2-3 kcal/mol).

CCSD(T), on the other hand, gives a more balanced account of both pairwise and connected three-electron correlation effects so that the stabilization of the open form by through-bond delocalization is correctly assessed. This is confirmed by Fig. 3.2(b), which gives the SCF (left-hand y-axis) and correlation contributions (right-hand y-axis) to the total energies. We note that the SCF energy profiles are identical, indicating that the differing shapes of the CCSD and CCSD(T) surfaces are due entirely to electron correlation effects. The shapes of the CCSD and CCSD(T) correlation energy curves in Fig. 3.2(b) are similar, but the steeper slope of the latter leads to a shift in the minimum to a larger C1−C3 distance shown in the total energy profile given in Fig. 3.2(a). There is also a clear change in the CCSD(T) PES when using the larger cc-pVTZ basis set. The shoulder at the position of the bicyclic form is lowered significantly from 3.2 to 1.6 kcal/mol, which leads to a shift of the minimum from 2.11 to 2.05 Å [Fig. 3.2(a)]. Clearly, the correct PES profile along the C1−C3 distance corresponds to an asymmetric, single-minimum potential. This result is confirmed by UHF- and Brueckner-CCSD(T) calculations that do not significantly change the shape of the PES profile.

3.3.2 Biradical Character of *m*-Benzyne

What is the biradical character of the reference wave function in the two most important regions of the energy profiles described above — the bicyclic region for which CCSD predicts a minimum and the monocyclic region preferred by CCSD(T)? One measurement of such multireference character is the size of the T_2 cluster amplitudes. For short C1−C3 distances, the maximum T_2 RHF-CCSD amplitude is 0.09. (As noted earlier, UHF-CCSD gives identical results in this case because the RHF wave function is spin-stable.) For longer C1−C3 distances, on the other hand, the maximum RHF-CCSD T_2 amplitude increases to 0.24 (corresponding to a HOMO-LUMO double excitation) clearly indicating greater biradical character in the reference function. (UHF-CCSD gives nearly identical values.) As a second measure of biradical character in the wave function, we have also computed natural orbital occupation numbers (NOON). For the RHF-CCSD wave function in the short C1−C3 region (i.e., the bicyclic structure), the HOMO and LUMO NOON values are 1.92 and 0.07, respectively, while in the long C1−C3 region (i.e., the monocyclic structure) the values are 1.75 and 0.24, in agreement with the results obtained by Kraka and Cremer.[46,47] Again, we see that the biradical character increases with the C1−C3 distance, as expected, though, its magnitude is significantly smaller than for *p*-benzyne, with HOMO and LUMO NOON values of 1.18 and 0.82, respectively.[18]

We note also that Winkler and Sander concluded *via* a natural bond-orbital analysis that *m*-benzyne's monocyclic structure should not be described as a biradical but rather a σ-allylic structure (Fig. 3.1, structure I)[5] referring to the fact that the two single electrons

can delocalize from the a_1-symmetrical C1−C3 bonding orbital into the antibonding C2−H7 orbital. The same authors show, however, that this delocalization effect is much stronger in the case of the bicyclic compound and that significant contributions arise from the through-bond interactions involving σ-bonds C1−C2, C2−C3, C4−C5, and C5−C6. Hence, structure II of Fig. 3.1 may provide a more realistic description of the electronic situation, which is characterized by increased pairing of the single electrons caused by their delocalization through the whole σ-framework of the ring. Representation II is also to be preferred as it illustrates explicitly the partial biradical character and does not conflict with the fact that a partial allene structure (formula I) should cause a widening of the C1−C2−C3 angle (relative to benzene), where the opposite is actually the case.

The reduced biradical character of *m*-benzyne is the reason that the molecule has a relatively low tendency to abstract hydrogen atoms.[91] Instead it undergoes reactions with nucleophiles, which of course does not imply a preference for the bicyclic versus the monocyclic form, because a monocyclic structure with delocalized single electrons is easily polarizable and can react either as an electrophile or as a nucleophile.

3.3.3 The Infrared Spectrum of *m*-Benzyne

Marquardt *et al.* reported *m*-benzyne's infrared (IR) difference spectrum from the isolated photolytic decomposition of [2,2]meta-paracyclophane-2,9-dione in solid argon at 10 K.[6,44] Table 3.2 includes experimental IR vibrational data reported by Sander, and theoretical

Table 3.2: Computed harmonic vibrational frequencies (in cm^{-1}) for *m*-benzyne determined using the 6-31G(*d*,*p*) basis set. Normalized infrared absorption intensities (in km/mol) are given in parentheses.

	CCSD			CCSD(T)			Argon, 10 K[6]
	RHF	UHF	Brueckner	RHF	UHF	Brueckner	
$\omega_1(a_1)$	522.3 (0.76)	522.3 (0.76)	533.3 (0.76)	386.4 (0.05)	371.7 (0.07)	389.7	
$\omega_2(a_1)$	839.9 (0.00)	839.9 (0.00)	840.8 (0.00)	848.7 (0.01)	849.1 (0.01)	849.6	
$\omega_3(a_1)$	1094.0 (0.00)	1094.0 (0.00)	1095.6 (0.00)	1051.8 (0.00)	1078.7 (0.01)	1055.0	
$\omega_4(a_1)$	1115.8 (0.00)	1115.8 (0.00)	1117.6 (0.00)	1118.4 (0.00)	1130.6 (0.01)	1115.4	
$\omega_5(a_1)$	1466.2 (0.14)	1466.2 (0.14)	1468.4 (0.14)	1454.2 (0.14)	1471.8 (0.16)	1451.5	1402 (0.15)
$\omega_6(a_1)$	1882.2 (0.03)	1882.2 (0.03)	1885.9 (0.03)	1706.6 (0.01)	1757.3 (0.03)	1707.5	
$\omega_7(a_1)$	3247.0 (0.22)	3247.0 (0.22)	3249.4 (0.21)	3210.1 (0.22)	3210.1 (0.24)	3201.8	3037 (0.05)
$\omega_8(a_1)$	3270.7 (0.16)	3270.7 (0.16)	3272.1 (0.15)	3255.5 (0.07)	3258.0 (0.07)	3270.7	
$\omega_9(a_1)$	3306.2 (0.11)	3306.2 (0.11)	3308.0 (0.11)	3289.2 (0.05)	3289.3 (0.05)	3296.8	
$\omega_{10}(a_2)$	611.4 (0.00)	611.4 (0.00)	612.0 (0.00)	496.6 (0.00)	517.4 (0.00)	494.8	
$\omega_{11}(a_2)$	808.5 (0.00)	808.6 (0.00)	809.4 (0.00)	824.6 (0.00)	843.0 (0.00)	826.2	
$\omega_{12}(b_1)$	576.4 (1.00)	576.4 (1.00)	577.7 (1.00)	544.5 (1.00)	553.5 (1.00)	549.9	547 (1.00)
$\omega_{13}(b_1)$	923.9 (0.02)	923.9 (0.02)	925.4 (0.02)	974.8 (0.28)	986.7 (0.30)	982.7	936 (0.25)
$\omega_{14}(b_1)$	1093.3 (0.28)	1093.3 (0.28)	1094.3 (0.28)	1151.6 (0.00)	1152.8 (0.00)	1139.2	
$\omega_{15}(b_1)$	1201.0 (0.00)	1201.0 (0.00)	1202.0 (0.00)	1284.4 (0.00)	1285.5 (0.01)	1273.8	
$\omega_{16}(b_1)$	1335.7 (0.17)	1335.7 (0.17)	1337.1 (0.17)	1336.3 (0.00)	1331.8 (0.00)	1298.0	
$\omega_{17}(b_1)$	1390.6 (0.24)	1390.6 (0.24)	1392.0 (0.24)	1419.9 (0.00)	1412.9 (0.00)	1420.8	
$\omega_{18}(b_1)$	1606.8 (0.18)	1606.8 (0.18)	1609.7 (0.18)	1543.9 (0.18)	1578.5 (0.14)	1537.1	1486 (0.15)
$\omega_{19}(b_1)$	3301.8 (0.20)	3301.8 (0.20)	3303.6 (0.20)	3250.5 (0.12)	3253.2 (0.12)	3241.0	
$\omega_{20}(b_2)$	297.4 (0.15)	297.4 (0.15)	297.3 (0.15)	366.6 (0.04)	379.3 (0.04)	366.7	
$\omega_{21}(b_2)$	564.3 (0.00)	564.3 (0.00)	564.3 (0.00)	478.7 (0.03)	509.4 (0.04)	482.6	
$\omega_{22}(b_2)$	779.8 (0.28)	779.8 (0.28)	781.8 (0.28)	743.5 (0.54)	766.3 (0.60)	743.7	751 (0.45)
$\omega_{23}(b_2)$	811.0 (0.61)	811.0 (0.61)	811.7 (0.60)	818.2 (0.10)	837.4 (0.12)	820.3	824 (0.20)
$\omega_{24}(b_2)$	973.0 (0.01)	973.0 (0.01)	973.3 (0.01)	917.7 (0.00)	951.5 (0.00)	917.8	

vibrational frequencies determined by CCSD/ and CCSD(T)/6-31G(*d*,*p*). The latter are in agreement with those given by Marquardt *et al.*[6,45] Among the totally symmetric modes, only three directly affect the C1−C3 distance: ω_1 (C1−C2−C3 bending), ω_2 (out-of-phase breathing of C1−C2−C3 and C4−C5−C6), and ω_5 (C1−C2/C3−C2 symmetric stretching). However, only ω_5 is computed to have any significant intensity. Again we find that for both CCSD and CCSD(T) methods the computed IR frequencies are invariant with respect to choice of reference determinant. This is in contrast to *p*-benzyne for which Crawford *et al.* found that the RHF reference wave function suffered from MO instabilities, leading to dramatic shifts in the computed vibrational frequencies.[18] Figures 3.3(a) and 3.3(b) are comparisons of the experimental IR vibrational spectrum vs. those determined by theory in the 500-1600 cm^{-1} range. The CCSD spectrum shown in Fig. 3.3(a) includes nine absorption peaks within this range, three of which can not be matched to any of the peaks in the experimental difference spectrum. Furthermore, the CCSD b_1 vibrational mode at 1093 cm^{-1} does not reasonably fit with any of the experimental absorption peaks.

The CCSD(T) infrared spectrum [Fig. 3.3(b)], on the other hand, accounts for all the experimental absorption peaks within this range and correctly reproduces the relative intensities as well. Due to the somewhat anharmonic nature of the PES (*vide supra*), we also calculated CCSD(T) fundamental frequencies as reported in Table 3.3. Most of the shifts are small (less than 50 cm^{-1}) and most are negative, except for the 545, 743, and 818 cm^{-1} harmonic frequencies, which lie slightly below the corresponding experimental fundamentals at 547, 751 and 824 cm^{-1}, respectively. In nearly every case, the computed fundamentals align superbly

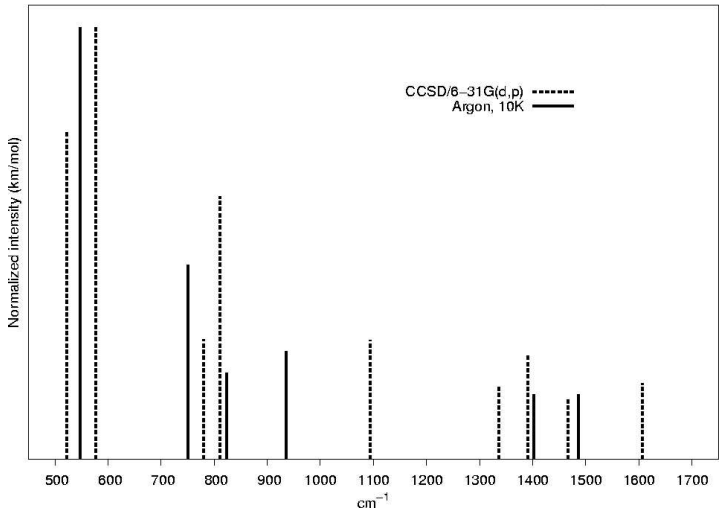

(a)

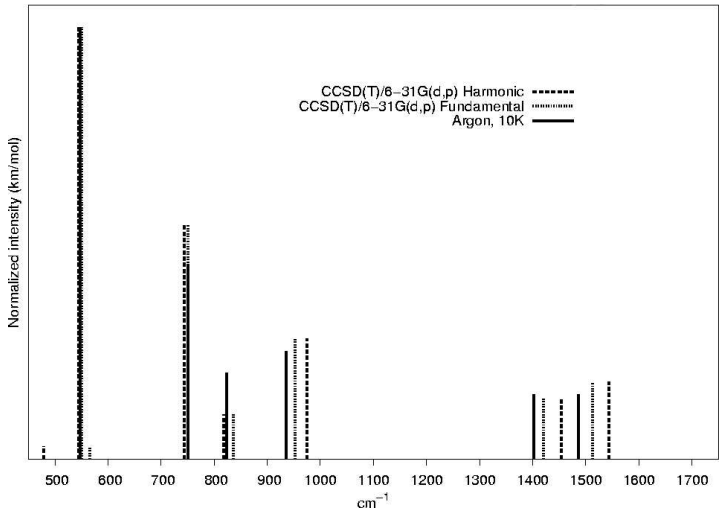

(b)

Figure 3.3: RHF-CCSD and CCSD(T) infrared vibrational spectra for *m*-benzyne using a 6-31G(*d*,*p*) basis. The experimental infrared difference spectrum reported by Marquardt *et al.*[6] is compared to **(a)** the CCSD harmonic infrared spectrum and **(b)** the CCSD(T) harmonic and fundamental infrared spectra.

Table 3.3: Anharmonicities and fundamental vibrational frequencies (cm^{-1}) of *m*-benzyne computed at the RHF-CCSD(T)/6-31G(*d*,*p*) level of theory.

	Anharmonicity	Fundamental	Argon, 10 K.[6]
$\omega_1(a_1)$	-20.3	366.1	
$\omega_2(a_1)$	0.9	849.6	
$\omega_3(a_1)$	-9.3	1042.5	
$\omega_4(a_1)$	-21.8	1096.5	
$\omega_5(a_1)$	-33.6	1420.6	1402 (0.15)
$\omega_6(a_1)$	-46.5	1660.1	
$\omega_7(a_1)$	-133.3	3076.9	3037 (0.05)
$\omega_8(a_1)$	-138.2	3117.3	
$\omega_9(a_1)$	-146.1	3143.0	
$\omega_{10}(a_2)$	1.9	498.5	
$\omega_{11}(a_2)$	5.2	829.8	
$\omega_{12}(b_1)$	5.5	550.0	547 (1.00)
$\omega_{13}(b_1)$	-22.8	951.9	936 (0.25)
$\omega_{14}(b_1)$	-24.6	1127.1	
$\omega_{15}(b_1)$	-19.8	1264.6	
$\omega_{16}(b_1)$	-37.3	1299.0	
$\omega_{17}(b_1)$	-40.5	1379.4	
$\omega_{18}(b_1)$	-30.9	1513.0	1486 (0.15)
$\omega_{19}(b_1)$	-155.1	3095.5	
$\omega_{20}(b_2)$	0.6	367.1	
$\omega_{21}(b_2)$	86.8	565.6	
$\omega_{22}(b_2)$	6.9	750.4	751 (0.45)
$\omega_{23}(b_2)$	17.9	836.0	824 (0.20)
$\omega_{24}(b_2)$	32.9	950.6	

with the experimental infrared absorption peaks, as illustrated in Fig.3.3(b). Thus, based on the above evidence, we agree with Marquardt *et al.*,[6] Kraka *et al.*,,[50] and Sander *et al.*[45] that the infrared spectrum clearly identifies the monocyclic structure of *m*-benzyne.

3.4 Results and Discussion: Tetrafluoro-*m*-Benzyne

Table 3.4 summarizes coupled cluster predictions of the structure of tetrafluoro-*m*-benzyne. At the CCSD/6-31G(*d*,*p*) level of theory, all three reference functions predict a nominally bicyclic structure, with C1−C3 distances (in Å) of 1.621 (RHF), 1.600 (UHF), and 1.617 (Brueckner), though we note that (1) the agreement among the orbital choices is significantly poorer for C_6F_4 than for *m*-benzyne and (2) the C1−C3 distance in C_6F_4 is 0.04-0.05 Å longer than in *m*-benzyne (cf. Table 3.1). Again, triple excitations lead to a widening in the C1−C3 distance, ranging from 0.08-0.12 Å, depending on the choice of reference, but much smaller than that observed for *m*-benzyne, for which the C1−C3 distance shifts by more than 0.5 Å between CCSD and CCSD(T).

Clearly, the steric repulsion of the substituents F8, F9, and F10 is sufficient to overcome all electronic factors that favor a C1−C3 distance of 2 Å or larger. Indeed, it is likely that this distance would be even shorter if the substituent F7 at C2 did not destabilize the C1−C3 interactions. We rationalize these results as follows: (a) The inductive effect of fluorine withdraws electron density out of the C1−C3 region into the σ^*(C2−F7) orbital; (b) At the same time, the in-plane lone-pair of F7 can donate density into the C1−C3 antibonding

Table 3.4: Optimized geometrical parameters of tetrafluoro-*m*-benzyne (bond distances in Å, angles in degrees, and energies in E_h) computed with the 6-31G(*d*,*p*) basis set.

	CCSD			CCSD(T)			CCSD(T)[1]
	RHF	UHF	Brueckner	RHF	UHF	Brueckner	RHF
$r(C_1-C_3)$	1.621	1.600	1.617	1.744	1.680	1.753	1.981
$r(C_2-C_3)$	1.334	1.334	1.335	1.338	1.337	1.339	1.348
$r(C_3-C_4)$	1.367	1.364	1.368	1.370	1.367	1.371	1.375
$r(C_4-C_5)$	1.404	1.400	1.405	1.405	1.403	1.406	1.401
$r(C_2-F)$	1.317	1.317	1.318	1.325	1.324	1.326	1.330
$r(C_4-F)$	1.341	1.342	1.342	1.344	1.345	1.345	1.344
$r(C_5-F)$	1.329	1.329	1.330	1.333	1.332	1.334	1.336
$\theta(C_1-C_2-C_3)$	74.8	74.8	74.6	81.3	77.9	81.8	94.5
$\theta(C_3-C_4-C_5)$	109.1	109.1	109.0	111.6	110.2	111.8	115.7
$\theta(C_4-C_5-C_6)$	111.8	111.8	111.8	112.0	112.1	112.1	113.5
$\theta(C_3-C_4-F)$	127.0	127.3	127.1	125.3	126.2	125.2	122.7
Energy	-626.231418	-626.230941	-626.192360	-626.290841	-626.289857	-626.292003	-626.290948

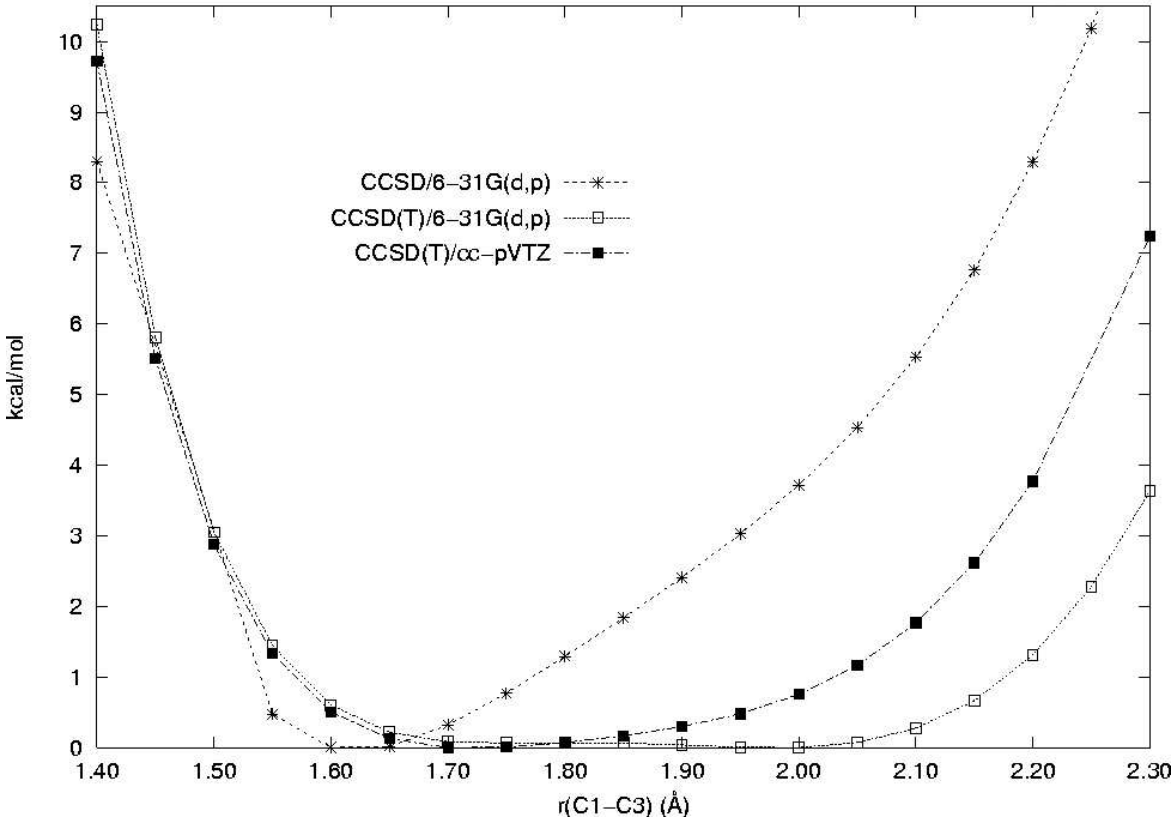

Figure 3.4: RHF-CCSD and RHF-CCSD(T) C1−C3 energy profiles for tetrafluoro-*m*-benzyne using the 6-31G(*d*,*p*) and cc-pVTZ basis sets. Structural parameters were optimized for fixed C1−C3 distances at the RHF-CCSD(T)/6-31G(*d*,*p*) level of theory. Energies are reported relative to the global minimum on the respective PES.

orbital, thus hindering the formation of a shorter C1−C3 bond; (c) The π-donor capacity of F7 also stabilizes the bicyclic structure because it supports a resonance structure in which the *pi* system of the *m*-benzyen splits into an aromatic allyl anion unit and a non-aromatic (as opposed to anti-aromatic) cyclopropenylium cation. (We also note that the π-donor effects of F8, F9, and F10 serve to somewhat offset the effect of F7 and destabilize the bicyclic form.)

Fig. 3.4 presents RHF-CCSD/ and RHF-CCSD(T)/6-31G(*d*,*p*) energy profiles of tetrafluoro-*m*-benzyne (relative to the minimum-energy structure at each level of theory) as a function of the C1−C3 distance, where all geometrical parameters were optimized. As for *m*-benzyne [cf. Fig. 3.2(a)], the CCSD level clearly favors the bicyclic structure with only a slight "shoulder" as the C1−C3 distance increases. However, the CCSD(T) level produces a very flat PES, with a minuscule barrier of only 0.07 kcal/mol separating the inner minimum at C1−C3 = 1.744 Å and and an outer minimum at C1−C3 = 1.981 Å, similar to that found for *m*-benzyne. Although this result could support the hypothesis that the true structure is characterized by a large amplitude vibration encompassing open and bicyclic forms as extreme cases, the 6-31G(*d*,*p*) basis is clearly too small to provide an accurate description. The shape of the PES is significantly basis-set dependent, as shown in Fig. 3.4, which also plots RHF-CCSD(T)/cc-pVTZ energies computed at the same RHF-CCSD(T)/6-31G(*d*,*p*) constrained structures. With the larger basis set, the outer minimum disappears, leaving only a single minimum with a C1−C3 distance at approximately 1.75 Å, comparable to the RHF-CCSD(T) inner minimum with the 6-31G(*d*,*p*) basis set. Clearly, the minimum energy

structure of tetrafluoro-*m*-benzyne corresponds more to that of a bicyclo[3.1.0]hexatriene than to that of a monocyclic structure considering the fact that C−C distances of 1.75 Å should still provide some weak bonding. In addition, we note that this distance if significantly shorter than that given by BLYP/6-311++G(*d*,*p*) (1.909 Å).[7]

3.4.1 The Infrared Spectrum of Tetrafluoro-*m*-Benzyne

Wenk and Sander used UV photolysis of 1,3-diiodo-2,4,5,6-tetrafluorobenzene in solid neon at 3 K and recorded an infrared difference spectrum that they subsequently assigned to tetrafluoro-*m*-benzyne based in part on DFT calculations.[7,8] Table 3.5 compares the experimental results of Wenk and Sander to the CCSD/ and CCSD(T)/6-31G(*d*,*p*) harmonic vibrational frequencies associated with the optimized structures given in Table 3.4. Among the totally symmetric modes, ω_1 (C1−C2−C3 bending), ω_4 (ring breathing), and ω_5 (C1−C2/C3−C2 symmetric stretching) directly affect the C1−C3 distance, but only ω_5 is computed to have significant intensity. (It is also worth noting that the relative intensity of ω_5 is significantly higher than in the parent *m*-benzyne, for which the mode has a similar C−C stretching structure.) The computed infrared frequencies vary little with respect to the choice of reference determinant (at most 50 cm^{-1}), though the variation is somewhat larger than for *m*-benzyne. Figs. 3.5(a), 3.5(b), and 3.5(c) are comparisons of the experimental IR vibrational spectrum vs. those determined by theory in the 400-2100 cm^{-1} range for the RHF-CCSD, inner-RHF-CCSD(T), and outer-RHF-CCSD(T) structures, respectively.

Table 3.5: Computed harmonic vibrational frequencies (in cm^{-1}) for tetrafluoro-*m*-benzyne determined using the 6-31G(*d*,*p*) basis set. Normalized infrared absorption intensities (in km/mol) are given in parentheses.

	CCSD			CCSD(T)		CCSD(T)[2]	Neon, 3K[3]
	RHF	UHF	Brueckner	RHF	UHF	RHF	
$\omega_1(a_1)$	288.1 (0.00)	289.6 (0.00)	289.9 (0.00)	124.7 (0.00)	241.8 (0.04)	151.9 (0.01)	
$\omega_2(a_1)$	439.5 (0.09)	467.1 (0.09)	447.9 (0.09)	307.2 (0.02)	323.3 (0.05)	316.6 (0.01)	
$\omega_3(a_1)$	530.5 (0.01)	530.6 (0.01)	531.1 (0.01)	515.9 (0.00)	518.0 (0.00)	524.6 (0.00)	
$\omega_4(a_1)$	666.3 (0.02)	678.3 (0.02)	668.3 (0.02)	626.6 (0.00)	642.9 (0.01)	629.8 (0.00)	
$\omega_5(a_1)$	980.6 (1.00)	990.2 (0.96)	979.7 (1.00)	954.6 (0.81)	961.4 (0.84)	966.4 (0.57)	952.3 (1.00)
$\omega_6(a_1)$	1265.5 (0.02)	1272.7 (0.02)	1263.7 (0.02)	1238.3 (0.01)	1246.7 (0.01)	1229.0 (0.01)	
$\omega_7(a_1)$	1537.3 (0.16)	1553.9 (0.18)	1534.3 (0.15)	1508.1 (0.07)	1526.4 (0.12)	1498.0 (0.01)	
$\omega_8(a_1)$	1617.7 (0.95)	1635.0 (1.00)	1614.9 (0.93)	1586.4 (1.00)	1605.9 (1.00)	1579.0 (1.00)	1534.2 (0.92)
$\omega_9(a_1)$	2031.1 (0.96)	2079.2 (0.73)	2028.4 (0.94)	1961.9 (0.99)	2018.8 (0.82)	1864.1 (0.71)	1817.7 (0.15)
$\omega_{10}(a_2)$	385.7 (0.00)	398.1 (0.00)	388.7 (0.00)	365.6 (0.00)	382.7 (0.00)	337.3 (0.00)	
$\omega_{11}(a_2)$	564.2 (0.00)	598.2 (0.00)	567.4 (0.00)	529.7 (0.00)	562.9 (0.00)	524.6 (0.00)	
$\omega_{12}(b_1)$	242.1 (0.00)	242.0 (0.00)	243.4 (0.00)	244.8 (0.00)	242.8 (0.00)	252.8 (0.00)	
$\omega_{13}(b_1)$	281.5 (0.00)	283.4 (0.00)	282.6 (0.00)	283.0 (0.00)	281.9 (0.00)	298.9 (0.00)	
$\omega_{14}(b_1)$	584.4 (0.04)	595.3 (0.03)	586.3 (0.04)	540.1 (0.06)	562.0 (0.04)	503.6 (0.05)	511.6 (0.07)
$\omega_{15}(b_1)$	645.9 (0.08)	649.0 (0.08)	647.4 (0.08)	640.6 (0.05)	640.6 (0.06)	651.6 (0.02)	649.1 (0.05)
$\omega_{16}(b_1)$	989.7 (0.75)	994.3 (0.72)	988.6 (0.75)	987.4 (0.68)	986.9 (0.68)	1020.2 (0.58)	981.3 (0.44)
$\omega_{17}(b_1)$	1291.9 (0.29)	1295.7 (0.27)	1289.0 (0.29)	1291.6 (0.28)	1298.7 (0.30)	1326.5 (0.23)	1268.5 (0.19)
$\omega_{18}(b_1)$	1412.2 (0.02)	1390.4 (0.07)	1408.2 (0.02)	1443.3 (0.02)	1412.1 (0.02)	1434.2 (0.01)	1497 (0.19)
$\omega_{19}(b_1)$	1715.0 (0.83)	1765.8 (0.57)	1712.1 (0.81)	1679.9 (0.80)	1722.3 (0.66)	1653.3 (0.64)	1605.4 (0.93)
$\omega_{20}(b_2)$	116.7 (0.00)	121.0 (0.00)	120.6 (0.00)	116.4 (0.00)	118.7 (0.00)	121.8 (0.00)	
$\omega_{21}(b_2)$	176.2 (0.00)	184.8 (0.01)	179.4 (0.00)	170.3 (0.00)	178.8 (0.00)	162.9 (0.00)	
$\omega_{22}(b_2)$	431.2 (0.00)	444.6 (0.00)	434.1 (0.00)	424.8 (0.00)	436.5 (0.00)	381.4 (0.04)	
$\omega_{23}(b_2)$	504.5 (0.03)	554.1 (0.03)	509.1 (0.03)	448.1 (0.03)	505.7 (0.03)	425.3 (0.00)	488.2 (0.05)
$\omega_{24}(b_2)$	623.3 (0.00)	666.7 (0.01)	626.6 (0.00)	581.0 (0.00)	623.4 (0.00)	563.8 (0.00)	

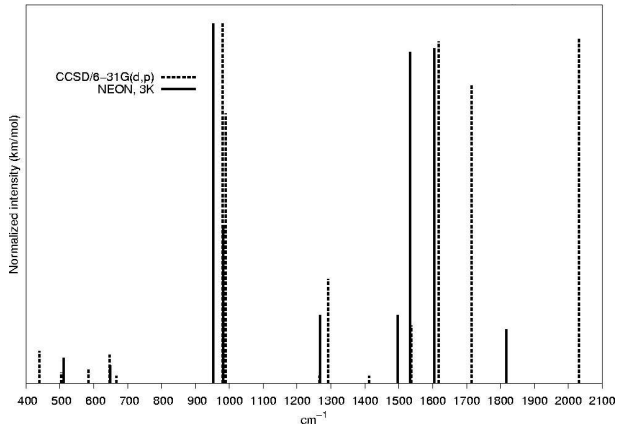

(a)

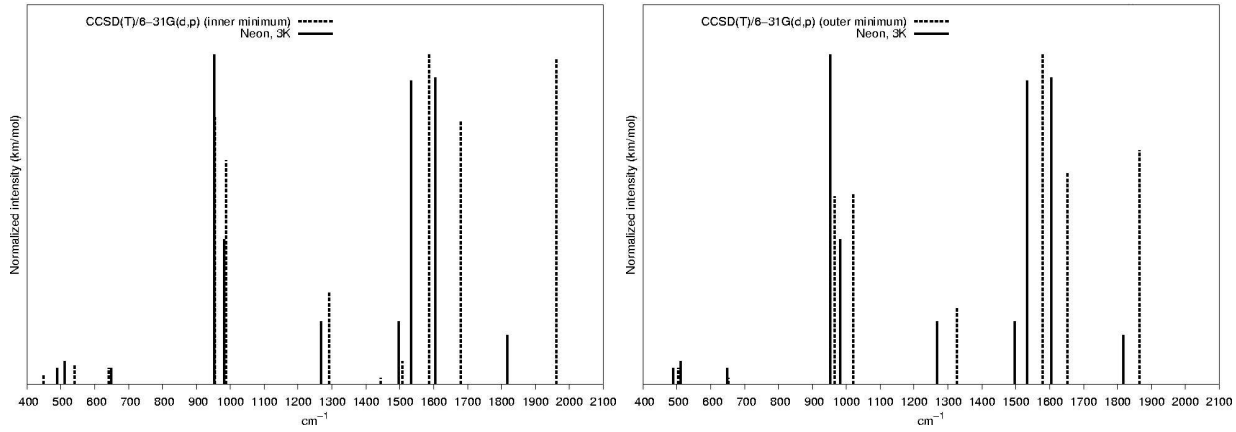

(b) **(c)**

Figure 3.5: RHF-CCSD and RHF-CCSD(T) harmonic vibrational spectra for tetrafluoro-*m*-benzyne using a 6-31G(*d*,*p*) basis. The experimental infrared difference spectrum reported by Wenk and Sander[7,8] is compared to (**a**) the CCSD spectrum, (**b**) the CCSD(T) spectrum for the "inner" minimum, and (**c**) the CCSD(T) spectrum for the "outer" minimum.

The CCSD frequencies compare reasonably well, except for one additional low-frequency line in the 400-700 cm^{-1} range and two low-intensity lines between 1200 and 1400 cm^{-1}. In addition, the intensity of the line at 2031 cm^{-1} is much too large, assuming it should compare to the experimental line at 1818 cm^{-1}. The CCSD(T) data compare somewhat better with experiment, apart from the low-intensity line at 1443 cm^{-1} for the inner minimum [Fig. 3.5(b)] and a missing low-frequency, low-intensity line near 500 cm^{-1} for the outer minimum [Fig. 3.5(c)]. The highest-frequency line compares better to experiment in position for both sets of CCSD(T) data, but are too high in intensity, just as for CCSD.

If one considers the substantial basis-set dependence of the structures in Table 3.4 and the CCSD(T) energy profile in Fig. 3.4, as well as the need for anharmonicity corrections in the high-frequency range (cf. Table 3.3 for the parent molecule), then the accuracy of the CCSD(T)/6-31G(*d*,*p*) level of theory cannot be considered the final authority on the structure of tetrafluoro-*m*-benzyne. Indeed, additional CCSD(T)/cc-pVTZ data, which were not feasible in the present work due to computational limitations, will be necessary to finally resolve this issue. However, there are three reasons that suggest that the experimental spectrum supports a bicyclic rather than monocyclic form:

1. For the CCSD(T) spectrum calculated at C1−C3 = 1.744 Å all measured infrared bands can be assigned. It is more than likely that the "extra" low-intensity lines suggested by theory cannot be resolved in the experimental spectrum. In addition, the infrared band at 1500 cm^{-1} (which is missing in the CCSD(T) spectrum calculated for C1−C3 = 1.981 Å) *must* belong to the difference infrared spectrum of tetrafluoro-*m*-

benzyne.

2. Basis set and anharmonicity corrections are often simulated by using a scaling factor of 0.96 for CCSD(T)/6-31G(*d*,*p*) frequencies,[6,48] a particularly useful technique in the high-frequency range to approach experimental values from above. In the case of the CCSD(T) spectrum calculated for C1−C3 = 1.744 Å this would lead to an improvement between theory and experiment for the bands between 1500 and 1830 cm^{-1}, but not in the case of the CCSD(T) spectrum calculated for C1−C3 = 1.981 Å.

3. For the bicyclic structure, the band ω_5, which is the only totally symmetric band that leads to a reduction of the C1−C3 distrance, is one of the most intense transitions according CCSD(T) calculations at C1−C3 = 1.744 Å, but is significantly reduced in intensity at C1−C3 = 1.981 Å. In the experimental spectrum this is indeed the most intense band (cf. Table 3.5).

We conclude that the infrared spectrum does indeed suggest a bicyclic structure with a relatively long C1−C3 bond of approximately 1.75 Å. It is beyond the computational possibilities presently available to determine if measured infrared spectrum confirms a large amplitude vibration involving ω_5.

3.4.2 Biradical Character of Tetrafluoro-*m*-Benzyne

The biradical character of the tetrafluoro-*m*-benzyne structures, as estimated by the magnitudes of the T_1 and T_2 cluster amplitudes, is rather small. For the CCSD/6-31G(*d*,*p*)

structure T_1(max) = 0.03 and T_2(max) = 0.08. (UHF-CCSD gives a similar maximum T_2, and a somewhat larger maximum T_1 of 0.08.) For the RHF-CCSD(T)/6-31G(*d*,*p*) structure with C1-C3 = 1.75 Å, these values are similar: T_1(max) = 0.03 and T_2(max) = 0.11. The HOMO and LUMO NOON values for each structure are comparable: CCSD = 1.92/0.07, CCSD(T) = 1.89/0.09. Hence, tetrafluoro-*m*-benzyne is best described as a bicyclic structure with an elongated C1−C3 bond.

In addition, the calculated singlet-triplet (S-T) splitting of tetrafluoro-*m*-benzyne is in line with the above description. At CCSD(T)/6-31G(*d*,*p*), we obtain a value of 26.8 kcal/mol (in favor of the singlet), which is 7 kcal/mol larger than that calculated for *m*-benzyne (20 kcal/mol compared to an experimental value of of 21 kcal/mol[92]). An increase in the S-T splitting suggests that in the S state the single electrons are more strongly coupled either by through-space or through-bond coupling, which in the latter case implies a shorter 1,3-distance.

We note that bicyclic *m*-benzyne structures have also been discussed by Cramer and co-workers[93–95] for various aza-derivatives of *m*-benzyne, though no experimental evidence is yet available for the molecules investigated.

3.5 Conclusions

The structure of *m*-benzyne was characterized by CCSD, CCSD(T), and CCSDT methods. Basis set effects are small in this case, as indicated by strong similarities in computed ge-

ometries with 6-31G(*d*,*p*) and cc-pVTZ basis sets. However, the level of dynamic electron correlation included in the theoretical model is paramount: while the CCSD methods predicts a bicyclic structure with a C1−C3 distance of 1.56 Å to be the most stable isomer of *m*-benzyne, the CCSD(T) method predicts a monocyclic structure with a C1−C3 distance of approximately 2.1 Å. These results may be understood in terms of three-electron through-bond delocalization effects, for which connected triple excitations are essential for a correct description. The best value for distance C1−C3 obtained in this work is 2.013 Å (estimated from the CCSD(T)/cc-pVTZ value of 2.026 and the CCSDT/6-31G(d,p) value of 2.093 Å).

Unlike the case of the the *p*-benzyne biradical, the choice of reference molecular orbitals has negligible impact on the predicted structure with RHF, UHF, and Brueckner determinants giving essentially identical results, both for the geometry and the vibrational spectrum. The fundamental infrared frequencies calculated for the first time at the CCSD(T) level are in excellent agreement with the measured values and confirm the monocyclic structure of *m*-benzyne. The biradical character of *m*-benzyne is significantly reduced relative to *p*-benzyne because of through-bond coupling leading to a delocalization of the unpaired electrons into the β-position σ^*(C−C) or the σ^*(C2−H7) orbitals.

The structure of tetrafluoro-*m*-benzyne, on the other hand, is somewhat more difficult to characterize. At the highest level of theory yet feasible, i.e. CCSD(T)/cc-pVTZ the molecule possesses a flat minimum at a C1−C3 distance of approximately 1.75 Å, which corresponds to weak bonding interaction to give a bicyclic structure. Although C−C bond lengths of that magnitude may no longer be considered to be "real" bonds, they still involve significant

C−C interactions considering the fact that typical transition state distances of breaking such bonds are 2.0 to 2.2 Å.

The CCSD(T)/6-31G(*d*,*p*) harmonic vibrational spectrum of tetrafluoro-*m*-benzyne compares reasonably well to the experimental difference spectrum of Wenk and Sander;[7,8] computations with larger basis sets are likely to resolve the remaining discrepancies. There are several features in the measured/calculated infrared spectrum that confirm the computed C1−C3 distance of 1.75 Å.

Chapter 4

Coupled Cluster Methods Including Triple Excitations for Excited-States of Radicals

4.1 Introduction

A variety of *ab initio* methods for computing molecular properties in electronically excited states have been developed over the last fifteen years, with a wide range of expected accuracy and computational expense. The simplest such approach is configuration interaction singles (CIS) or the Tamm-Dancoff approximation, in which the electronic Hamiltonian is diagonalized within the space of all singly excited determinants.[96] Although CIS excitation energies

are often significantly in error relative to experiment, the corresponding wave functions can sometimes provide a reasonable starting point for higher-level corrections, including the (D) correction for excited-state electron correlation effects.[10,97–99] The random-phase approximation (RPA) [also known as time-dependent Hartree-Fock (TDHF)][100] is similar to CIS in that it provides an approximate set of Hartree-Fock-like excited states, but is often viewed as incorporating the response into the orbitals while maintaining the single-determinant form of the wave function.[99] Among more advanced methods, the recently developed time-dependent density-functional theory (TDDFT) has had the greatest immediate impact.[101] TDDFT's formulation is similar to that of RPA, but its predictions for singly excited valence states are far superior. On the other hand, modern functionals such as B3LYP are notorious in their failures for "delocalized" excitations, such as diffuse Rydberg and charge-transfer states.[102,103] Among wave-function-based models that include electron correlation, second-order perturbation theory built upon a complete active space reference (CASPT2) has proved to be very useful for many applications.[104] A disadvantage of this approach, however, is the non-systematic selection of active spaces and the steep (factorial) scaling of the CAS wave function with system size. Excited states are also accessible via coupled cluster theory,[69,105–107] one of the most reliable quantum chemical methods, through its equation-of-motion (EOM-CC) or linear-response (LRCC) variants.[32,108] For many organic molecules, the singles and doubles truncation of the method (EOM-CCSD) has been shown to reproduce experimental excitation energies for single-excitation-dominated states to within 0.2 eV.[109]

Figure 4.1: Schematic diagram of the nine $M_S = \frac{1}{2}$ Slater determinants arising from the distribution of three electrons in three spatial orbitals (six spin-orbitals): (a) The ground doublet state, used as a reference determinant; (b) two "closed-shell" doublet determinants, both classified as single excitations relative to (a); (c) three "closed-shell" doublet determinants classified as double excitations relative to (a); and (d) three "low-spin" determinants that contribute to both doublet and quartet states, one of which is a double excitation relative to (a).

Unfortunately, the reliability and accuracy of most excited-state methods does not generally extend to radicals because of increases in both spin contamination and double-excitation character of excited-state wave functions. These problems are illustrated by the nine $M_S = \frac{1}{2}$ determinants shown in Fig. 4.1 for three electrons distributed among nine spin-orbitals. Ignoring spatial symmetry, and given a doublet ground state described by the single Slater determinant shown in Fig. 4.1(a), the "closed-shell" determinants given in Fig. 4.1(b) and Fig. 4.1(c) are all eigenfunctions of the $\hat{S}^2$ spin operator and may be classified as single- and double-excitations, respectively. As noted above, for excited states dominated by the singly excited determinants, methods such as EOM-CCSD perform admirably, but for those dominated by the doubly excited determinants, at least triple excitations are required to properly account for electron correlation effects within pairs of electrons that are both excited relative to the reference configuration. In addition, as noted by Szalay and Gauss,[110] the "low-spin" determinants in Fig. 4.1(d) contribute to both doublet and quartet excited states. If an approximate excited-state wave function fails to include these determinants in a spin-adapted manner, large spin contamination effects may result, potentially rendering the computed properties meaningless. Indeed, Maurice and Head-Gordon designed the extended CIS (XCIS) method specifically to deal with such cases,[10] and the spin-restricted coupled cluster (SR-CC) method recently developed by Szalay and Gauss includes such effects explicitly.

Coupled cluster treatments of the properties of excited states including the effects of triple excitations have been explored by several researchers. The first was reported in the mid-

1990s by Watts and Bartlett[111–113] who implemented an approximate EOM-CCSDT model (with a restriction to two-body elements in the triples blocks of the similarity-transformed Hamiltonian),[111] iterative EOM-CCSDT-1 and non-iterative EOM-CCSD(T) models,[112] and iterative EOM-CCSDT-3 and non-iterative EOM-CCSD($\tilde{\mathrm{T}}$).[113] They applied these methods to a variety of singlet and triplet excited states from closed-shell reference states and found significant improvement over EOM-CCSD for states with significant double-excitation character. At around the same time, Christiansen, Koch, Jørgensen and co-workers introduced the CC3 model,[2–4] which, like its EOM-CCSDT-1 and EOM-CCSDT-3 counterparts, is iterative and does not require explicit storage of triple-excitation amplitudes, but incorporates orbital relaxation effects through inclusion of singles at zeroth order (*vide infra*). The CC3 method has been applied to excitation energies out of closed-shell ground-states,[2,3,114] as well as to a variety of ground-state properties, including dipole moments[115] and both static- and frequency-dependent polarizabilities[3,116–118] and hyperpolarizabilities.[119] These same researchers have also developed a non-iterative method triples method known as CCSDR(3), which is closely related to the CC3 approach.[120] In 2001, Kucharski and co-workers[121] and Kowalski and Piecuch[122,123] independently implemented the first full EOM-CCSDT calculations. In addition, Stanton and Saeh developed a variant of the EOMIP-CCSD method (EOM-CCSD for ionized states) that is applicable to radicals and implicitly includes triple-excitation effects,[124] and Musial, Kucharski and Bartlett developed the EOMIP-CCSDT method which explicitly includes triples,[125] though these methods have not been used to explicitly calculate excitation energies. Finally, we note that Piecuch and co-workers have

extended the method of moments coupled cluster approach[126] to excited states, including corrections for triple and quadruple excitations.[127–129]

The purpose of the present work is to develop an open-shell version of the CC3 method and to benchmark its effectiveness in describing excited states of radicals. As noted above, such states often present greater difficulty than their closed-shell counterparts, and thus we anticipate that triple excitations should have even greater impact on the computed transition energies. We have implemented this method for both spin-unrestricted Hartree-Fock (UHF) and spin-restricted open-shell Hartree-Fock (ROHF) reference determinants and have applied it to a number of small molecules, including the allyl and nitromethyl radicals. This is the first time that an equation-of-motion (linear response) CC method for excitation energies that includes any treatment of connected triple excitations has been implemented for open-shell systems.

4.2 Theory

The CC3 model is an approximation to the full coupled cluster singles, doubles, and triples (CCSDT) approach defined based on a perturbation breakdown of the CCSDT amplitude equations that requires that single excitations are treated as zeroth order and triple excitations as second order in the perturbation potential.[4] The first requirement stems from the fact that single excitations, while second order in a standard many-body perturbational analysis of the correlation energy, become first order in the perturbation potential in the case

of non-Hartree-Fock orbitals, and zeroth order in an external (e.g. electric or magnetic field) potential. In addition, the desired pole structure of frequency-dependent response functions motivates the development of methods in which orbital response contributions are ignored to avoid artifactual poles introduced by the Hartree-Fock reference function itself. Thus, the singles play a pivotal role as orbital relaxation parameters, and thus should be included without truncation. The second requirement is motivated by efficiency considerations; assignment of triples to second-order leads to amplitude equations in which the triples do not couple into themselves. As a result, although the CC3 amplitudes must be determined iteratively, explicit storage of the complete set of triples amplitudes in each iteration is not necessary. In addition, the algebraic equations scale nominally as $\mathcal{O}(N^7)$ at most, similar to the popular non-iterative triples approximation, CCSD(T), and the closely related iterative CCSDT-n methods of Bartlett and co-workers.[40,130,131]

As discussed by Christiansen et al.,[3] CC3 excitation energies are obtained as the eigenvalues of a non-symmetric matrix (the "Jacobian"), which is an approximation to the CCSDT similarity-transformed Hamiltonian:

$$\bar{\mathbf{H}}_{\mathrm{CC3}} = \begin{pmatrix} \langle S| \left[\hat{H} + (\hat{H}T_2)_c\right] |S\rangle & \langle S|\hat{H}|D\rangle & \langle S|\hat{H}|T\rangle \\ \langle D| \left[\hat{H} + (\hat{H}T_2)_c + (\hat{H}T_3)_c\right] |S\rangle & \langle D| \left[\hat{H} + (\hat{H}T_2)_c\right] |D\rangle & \langle D|\hat{H}|T\rangle \\ \langle T|(\hat{H}T_2)_c|S\rangle & \langle T|\hat{H}|D\rangle & \langle T|\hat{F}|T\rangle \end{pmatrix} \tag{4.1}$$

where S, D, and T are all singly, doubly, and triply excited determinants, respectively, F is the one-electron spin-orbital Fock operator, and T_n denotes the n-th excited cluster operator obtained by solving the ground-state CC3 amplitude equations.[3,4] In addition, $\hat{H}$ is the

T_1-similarity-transformed operator,

$$\hat{H} = \exp(-T_1) H \exp(T_1), \tag{4.2}$$

and the subscript c indicates that only connected diagrams are included. Note that the equation above for $\bar{\mathbf{H}}_{\mathrm{CC3}}$ implicitly includes only those matrix elements for which the Hamiltonian is connected (in the diagrammatic sense) to the excited determinant on the right (*vide infra*).

Because we are generally interested only in the lowest few eigenvalues of the above matrix, these could be obtained by straightforward application of the Davidson algorithm, which involves repeated application of $\bar{\mathbf{H}}_{\mathrm{CC3}}$ to a set of guess vectors, $\mathbf{C}$:

$$\sigma = (\bar{\mathbf{H}}_{\mathrm{CC3}} \mathbf{C})_c, \tag{4.3}$$

Such an approach is computationally inefficient, however, because it would require explicit storage of the triples components of the σ and $\mathbf{C}$ vectors. Instead, as noted by Christiansen et al.,[3] one may adopt a Löwdin-like partitioning of the CC3 eigenvalue equation:

$$\begin{pmatrix} \mathbf{H}_{PP} & \mathbf{H}_{PQ} \\ \mathbf{H}_{QP} & \mathbf{H}_{QQ} \end{pmatrix} \begin{pmatrix} \mathbf{C}_P \\ \mathbf{C}_Q \end{pmatrix} = \omega \begin{pmatrix} \mathbf{C}_P \\ \mathbf{C}_Q \end{pmatrix} \tag{4.4}$$

where P denotes the direct sum of the singles and doubles spaces and Q denotes the triples space. This leads to a pair of matrix-vector equations:

$$\mathbf{H}_{PP}\mathbf{C}_P + \mathbf{H}_{PQ}\mathbf{C}_Q = \omega \mathbf{C}_P \tag{4.5}$$

and

$$\mathbf{H}_{QP}\mathbf{C}_P + \mathbf{H}_{QQ}\mathbf{C}_Q = \omega \mathbf{C}_Q. \tag{4.6}$$

Solving the second set of equations for $\mathbf{C}_Q$ and inserting the result into the first set leads to a new eigenvalue equation in only the P space:

$$\left[\mathbf{H}_{PP} + \mathbf{H}_{PQ}\left(\omega\mathbf{1}_{QQ} - \mathbf{H}_{QQ}\right)^{-1}\mathbf{H}_{QP}\right]\mathbf{C}_P = \omega\mathbf{C}_P, \tag{4.7}$$

where $\mathbf{1}$ denotes the identity matrix in the Q space. The matrix inverse appearing in Eq. 4.7 is trivial to evaluate as long as $\mathbf{H}_{QQ} = \langle T|F|T\rangle$ is diagonal, which is the case for canonical Hartree-Fock or semicanonical non-Hartree-Fock orbitals. One repercussion of the use of Eq. 4.7 to determine the eigenvalue ω is that, because the P-space matrix on the left-hand side of the equation depends on the eigenvalue itself, one may use the Davidson algorithm to determine only one excited state at a time. This is discussed in more detail below.

Using Eq. 4.1 and Eq. 4.7, the CC3 sigma singles and doubles equations become

$$\sigma_1^{\mathrm{CC3}} = \sigma_1^{\mathrm{CCSD}} + \langle S|\left(HX_3\right)_c|0\rangle + \langle S|\left(HY_3\right)_c|0\rangle \tag{4.8}$$

and

$$\sigma_2^{\mathrm{CC3}} = \sigma_2^{\mathrm{CCSD}} + \langle D|\left(\hat{H}X_3\right)_c|0\rangle + \langle D|\left(\hat{H}Y_3\right)_c|0\rangle + \langle D|\left(\left[HC_1\right]_c T_3\right)_c|0\rangle, \tag{4.9}$$

respectively. In Eqs. 4.8 and 4.9 above, σ^{CCSD} refers to the corresponding EOM-CCSD equations, which have been given several times in the literature.[32] The five additional terms involve the effective triple excitations, X_3, Y_3, and T_3, which may be written as

$$D_3(\omega)X_3 = \langle T|\left(\hat{U}'T_2\right)_c|0\rangle, \tag{4.10}$$

$$D_3(\omega)Y_3 = \langle T|\left(\hat{U}C_2\right)_c|0\rangle, \tag{4.11}$$

and

$$D_3(0)T_3 = \langle T| \left(\hat{U}T_2\right)_c |0\rangle, \tag{4.12}$$

where $\hat{U}$ is the T_1-similarity-transformed two-electron component of the Hamiltonian, $\hat{U}' = \left(\hat{U}C_1\right)_c$, and $D_3(\omega)$ is a three-electron orbital-energy denominator, shifted by the current guess at the eigenvalue, ω. All three of these classes of triples may be represented by the antisymmetrized diagrams shown in Fig. 4.2(a), with appropriate substitutions for the two-electron and double-excitation vertices.[105] Similarly, the contributions of these triples to Eqs. 4.8 and 4.9 are shown in the generalized diagrams in Fig. 4.2(b) and (c), respectively. We note that these diagrams are identical in structure to those required for the well-known (T) correction.

Each X_3, Y_3, and T_3 triples amplitude depends on six orbital indices, three occupied and three virtual. To avoid explicit storage of these amplitudes, we follow the same strategy used by Rendell, Lee, and Kormornicki and compute batches of amplitudes for fixed combinations of the occupied orbitals.[132] Furthermore, as the diagrams in Fig. 4.2 suggest, our implementation of Eqs. 4.8-4.12 makes use of general functions for constructing these batches and then determining their contributions to σ_1 and σ_2 on the fly. Specifically, in each iteration of the Davidson algorithm, we carry out the following steps:

1. Compute the necessary $\hat{U}'$ and $(HC_1)_c$ intermediates using the current single-excitation guess vector, C_1.

2. Loop over all combinations of three unique occupied indices.

3. Compute all X_3 amplitudes for the given occupied-index combination using $\hat{U}'$ and the ground-state T_2 amplitudes in Eq. 4.10 and determine their contributions to Eqs. 4.8 and 4.9.

4. Compute all Y_3 amplitudes for the given combination using $\hat{U}$ and the current C_2 guess vector in Eq. 4.11 and add their contributions to Eqs. 4.8 and 4.9.

5. Compute the ground-state T_3 amplitudes for the given combination using $\hat{U}$ and the ground-state T_2 amplitudes in Eq. 4.12 and determine their contributions to Eq. 4.9.

6. Return to step 2 for the next combination of occupied orbitals.

Once σ_1 and σ_2 have been computed for the current guess vector, the remaining steps of the Davidson algorithm proceed as usual for EOM-CCSD calculations. Because the value of omega changes in each iteration, if σ vectors from previous iterations are used, the Davidson subspace Hamiltonian (referred to as the G matrix in the literature[133]) will be comprised of dot products involving σ vectors corresponding to different values of ω. As the number of σ vectors increases, the procedure can become unstable or converge to an energy with significant error. This problem of reusing σ vectors is corrected by periodic "collapse" of the set of guess vectors to a single guess, with recomputation of the corresponding σ vector. We have found that for the excited states studied in this work, collapse after every eight iterations works efficiently.

We have also implemented a root-following algorithm to converge the solutions of excited states which are not the lowest of their spatial symmetry. At each iteration of the Davidson

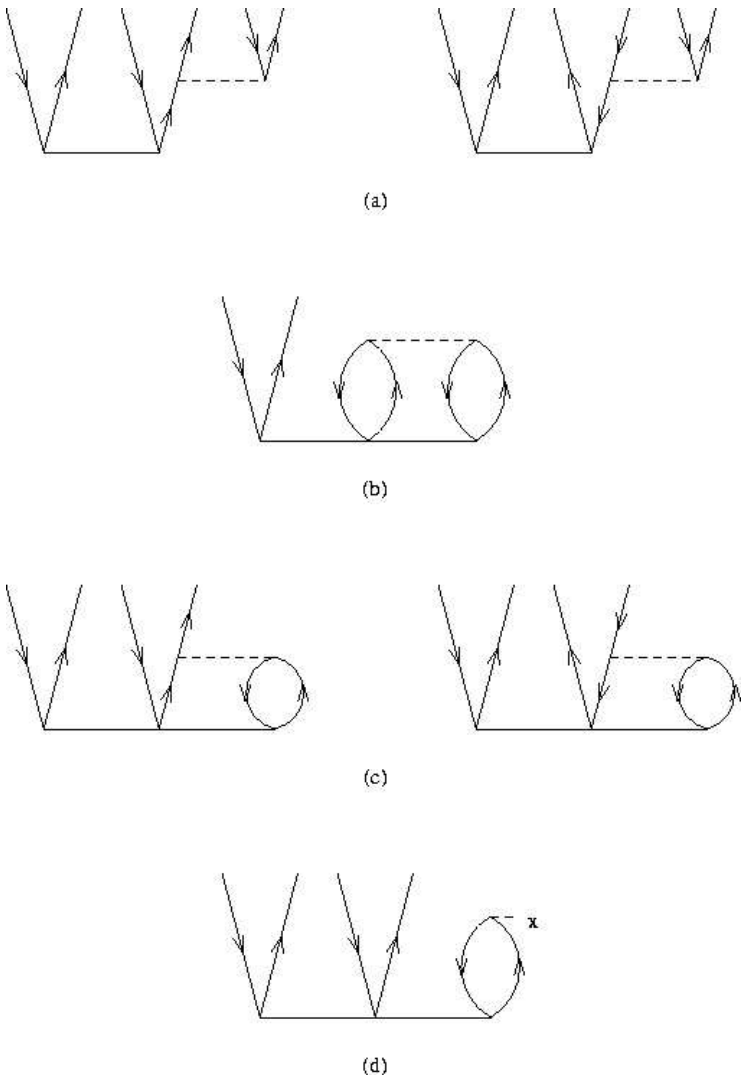

Figure 4.2: Generalized antisymmetrized diagrammatic representations of expressions for (a) X_3, Y_3 and T_3 triples given in Eqs. 4.10, 4.11, and 4.12; (b) triples contributions to Eq. 4.8; (c) triples contributions to Eq. 4.9 from two-electron intermediates; (d) triples contributions to Eq. 4.9 from the occupied-virtual block of the Fock matrix for non-Hartree-Fock references (e.g., ROHF).

algorithm, the eigenvectors of the G matrix are used to construct the current best-guesses for the eigenvectors of $\bar{\mathbf{H}}_{\mathrm{CC3}}$ (constructed only within the singles and doubles space). The desired eigenvector of G is chosen to be the one with maximum overlap with the converged EOM-CCSD eigenvector of the desired state.

We have implemented Eqs. 4.8-4.12 in the open-source PSI3 program package[31] using a spin-factored/spin-orbital approach that is useful for applications to excited-states of open-shell systems with either UHF or ROHF reference wave functions. The method is directly comparable to that described by Watts, Gauss, and Bartlett for the CCSD(T) method, for example.[134] For UHF orbitals, the implementation is straightforward and requires no special considerations beyond those described above. For ROHF orbitals, however, three complications should be noted. First, because the spin-orbital expression for the Fock operator appearing in Eq. 4.1 is not diagonal in the occupied-occupied and virtual-virtual blocks, we first semicanonicalize the ROHF orbitals,[83,134] resulting in a UHF-like reference determinant (though it remains an eigenfunction of $\hat{S}^2$). This allows a non-iterative construction of the triples amplitudes, thus avoiding their explicit storage. This same approach is used in a number of ROHF-CCSD(T) implementations.[134,135] Second, unlike for UHF orbitals, the occupied-virtual block of the Fock matrix is non-zero in an ROHF orbital basis, giving rise to additional $\mathcal{O}(N^6)$ terms in Eq. 4.9 of the form shown in Fig. 4.2(d). (Similar terms also arise in the ground-state CC3 amplitude equations, and these are included in our ROHF-CC3 implementation.)

Third, we note a potential complication in the fundamental definition of CC3 for ROHF

reference wave functions. In the perturbational analysis used to develop CC3 in Refs.[3] and ,[4] the zeroth-order Hamiltonian was taken to be the Fock operator, a typical approach for RHF- or UHF-based many-body perturbation theory (MBPT). For ROHF reference determinants, however, one could instead choose to shift the non-zero occupied-virtual blocks of F into the perturbation, thus defining ROHF-CC3 in direct analogy to the ROHF-MBPT and ROHF-CCSD(T) schemes of Bartlett and co-workers.[83,134,136]

However, as mentioned earlier, the CC3 method was also defined to include single-excitation contributions at zeroth order in the perturbation potential because of their unique role as orbital relaxation parameters. This suggests instead that the occupied-virtual blocks of the Fock matrix, which are the leading contributions to the singles amplitudes equations in an ROHF orbital basis, should instead be treated as zeroth order. Such an approach would require a term that couples T_3 into itself be included in the amplitude equations, namely

$$D_3 T_3 \leftarrow \langle T|(F T_1 T_3)_c|0\rangle. \tag{4.13}$$

As a result, either explicit storage of the triples amplitudes or an iterative $\mathcal{O}(N^8)$ algorithm would be required, thus rendering the method essentially useless.[137]

Given this choice between two variants of ROHF-CC3 — one that scales similarly to its UHF-CC3 counterpart, but does not include occupied-virtual Fock contributions in zeroth-order versus one that includes all such terms but requires dramatically greater storage or computational time — we have chosen to *define* the ROHF-CC3 method such that the term in Eq. 4.13 is ignored. It is likely that this term will have little to no numerical impact

on ground-state energies or excitation energies, though for response properties it could be more significant due to the presence of T_1 (which will become a perturbed T_1 in the response function) in Eq. 4.13.

4.3 Benchmark Calculations

We have performed numerical tests of the ROHF- and UHF-CC3 excitation energy approach described above using a number of representative open-shell systems, including the CH and CO^+ diatomics, the lowest valence $^2B_1$ state of the allyl radical, and three low-lying states of the nitromethyl radical. Each of these cases involves, to varying degrees, the double-excitation and/or spin-contamination complications described in the Introduction. Unless otherwise specified, all calculations were carried out using the PSI3 program package.[31]

4.3.1 The Valence $^2B_1$ State of the Allyl Radical

The excited states of the allyl radical provided our initial motivation for developing the UHF- and ROHF-CC3 approaches described above because of their interesting challenges to excited-state methods. The absorption maximum in the experimental UV spectrum occurs at 3.05 eV, but EOM-CCSD methods predict considerably higher values (*vide infra*). The three valence allyl π molecular orbitals transform as the b_1 (doubly occupied), a_2 (singly occupied), and b_1 (unoccupied) irreducible representations of the C_{2v} point group to which the $^2A_2$ ground-state equilibrium structure corresponds. As first shown by Yamaguchi, however, the

Table 4.1: CCSD and CC3 vertical and adiabatic excitation energies (in eV) of the valence $^2B_1$ state of the allyl radical, computed at the CCSD/cc-pVDZ optimized C_{2v} geometry for the ground state (vertical) and the cc-pVDZ/EOM-CCSD optimized geometry for the excited state (adiabatic). The experimental UV absorption maximum reported in Ref.[9] is 3.05 eV.

	ROHF						UHF					
	CCSD			CC3			CCSD			CC3		
	vertical	T_e	T_0	vertical	T_e	T_0	vertical	T_e	T_0	vertical	T_e	T_0
cc-pVDZ	3.427	3.171	3.110	3.387	3.085	3.023	3.634	3.457	3.395	3.440	3.172	3.111
aug-cc-pVDZ	3.378	3.125	3.064	3.342	3.042	2.980	3.580	3.400	3.339	3.393	3.123	3.062
cc-pVTZ	3.400	3.201	3.140	3.351	3.099	3.037	3.634	3.518	3.456	3.402	3.187	3.125

$^2B_1$ excited state breaks symmetry by twisting the end methylene groups, leading to a C_2-symmetric excited-state structure (properly labeled ^2B symmetry).[138] The corresponding vertical excitation is dominated by the two determinants shown in Fig. 4.1(b), both of which are singles relative to the reference state and are thus well described at the EOM-CCSD level. However, two of the three doubly excited determinants shown in Fig. 4.1(c) also contribute significantly and at least triple excitations are required to treat them adequately. We note that the third determinant in Fig. 4.1(c) and none of the "low-spin" determinants in Fig. 4.1(d) contribute to the $^2B_1$ state due to symmetry constraints.

Table 4.1 summarizes the CCSD and CC3 excitation energies (vertical and adiabatic) computed using the Dunning correlation-consistent polarized-valence double- and triple-zeta basis sets (cc-pVDZ and cc-pVTZ, respectively) as well as the cc-pVDZ basis augmented with diffuse s, p, and d-type functions (aug-cc-pVDZ).[78,139,140] The adiabatic excitation energies were computed using ground- and excited-state optimized structures obtained at the CCSD and EOM-CCSD levels of theory with the aug-cc-pVDZ basis set using analytic energy gradients[141,142] in the ACESII program package.[88] Zero-point energies were determined at these same levels of theory using harmonic vibrational frequencies computed using analytic energy second derivatives at the CCSD level for the ground state[84,85] and finite-differences of analytic energy first derivatives[142] in the excited state.

We first note that the basis set has only a small impact on the computed excitation energy (less than 0.06 eV in all cases), suggesting that the Rydberg character of the $^2B_1$ state is small. However, the ROHF-CCSD and UHF-CCSD excitation energies differ by more

than 0.2 eV for all three basis sets, indicative of significant spin-contamination in the latter. At the CC3 level, however, these differences are mostly removed, with both ROHF- and UHF-CC3 predicting a vertical excitation energy of 3.35-3.40 eV. (We note that "spin-flip" EOM-CCSD[143] and QRHF-EOM-CCSD calculations[32,71,144] for this state, performed at the same geometry with a 6-31++G** basis set give vertical excitation energies of 3.387 and 3.48 eV, in good agreement with these results.[145]) The adiabatic excitation energies, T_e and T_0, shift significantly downward (ca. 0.2-0.3 eV) relative to the vertical transitions because of the substantial geometry change upon excitation. While the UHF-CCSD values of T_e and T_0 are too high (approximately 0.3-0.4 eV above experiment), the corresponding UHF-CC3 values are in superb agreement with the experimental absorption maximum. The ROHF-CCSD adiabatic excitation energies, on the other hand, differ little from their ROHF-CC3 counterparts, again indicative of reduced spin contamination in the ROHF-based calculations.

4.3.2 The CH and CO^+ Radicals

The CH and CO^+ radicals have been considered previously by Maurice and Head-Gordon with the ROCIS and XCIS methods[10] and by Szalay and Gauss for the SR-CCSD method.[110] Table 4.2 summarizes CCSD and CC3 excitation energies for several low-lying states of both molecules using the Sadlej-pVTZ basis set[140,146] for comparison to MRCI data reported in Ref.[110] and the extrapolated experimental results reported in Ref.[10]

Table 4.2: CCSD and CC3 vertical excitation energies (in eV) of CO^+ and CH radicals with ROHF and UHF reference determinants.[2]

		CCSD		CC3			
	State	UHF	ROHF	UHF	ROHF	MRCI[3]	Expt.[4]
CO^+	$^2\Pi$	3.532	3.229	3.330	3.290	3.30	3.264
	$^2\Sigma^+$	6.192	6.002	5.811	5.725	5.88	5.819
CH	$^2\Delta$	3.221	3.215	3.173	3.160	2.96	2.880
	$^2\Sigma^-$	4.404	4.230	3.643	3.576	3.31	–
	$^2\Sigma^+$	5.312	5.199	4.517	4.472	4.03	3.943

For CO^+, the large difference between the UHF-CCSD and ROHF-CCSD excitation energies (0.2-0.3) is indicative of significant spin contamination in the former, as noted by Szalay and Gauss. At the CC3 level, this difference is mostly eliminated, suggesting that the spin contamination is greatly reduced by the inclusion of triples, as one would expect. The comparison between CC3 and the MRCI excitation energies is excellent, with differences of less than 0.1 eV for both states of CO^+ considered.

The CH radical presents a considerably more difficult test of the CC3 method. The $^2\Delta$ state is dominated by "low-spin" determinants analogous to the first two shown in Fig. 4.1(d). It is therefore reasonably well described even at the CCSD level, and the corresponding CC3

excitation energies shift downward by only about 0.05 eV, all in agreement with the 2.96 eV MRCI excitation energy. For the $^2\Sigma^-$ state, however, the third determinant in Fig. 4.1(d), which is a double excitation relative to the reference, contributes significantly. Thus, the UHF- and ROHF-CCSD excitation energies differ from the MRCI value of 3.31 eV by approximately 1.0 eV. The CC3 approach improves the comparison with MRCI considerably, though the error remains ca. 0.3 eV. (We note that both the $^2\Delta$ and $^2\Sigma^-$ states were computed as A_2 states in C_{2v} symmetry with our codes.) For the $^2\Sigma^+$ state, another double excitation contribution becomes important, analogous to the second determinant shown in Fig. 4.1(c). The CCSD results are essentially useless, with errors relative to MRCI of 1.2-1.3 eV. CC3 again improves upon this result, but the discrepancy is still approximately 0.5 eV. It is likely that a full treatment of triple excitations at the EOM-CCSDT level will be necessary to reduce the error to less than 0.2 eV.

4.3.3 Low-Lying Doublet States of the Nitromethyl Radical

Very little is known experimentally about the excitation spectrum of the nitromethyl radical. In the early 1990's, Metz, Cyr, and Neumark examined the ground $^2B_1$ and excited $^2A_2$ states using photoelectron spectroscopy of the $CH_2NO_2^-$ anion and *ab initio* calculations and determined that the $^2A_2$ state lies 1.591 eV above the ground state with a geometry similar in structure to the anion.[147] Later, Cyr and co-workers reported a photodissociation of nitromethyl following its production from the anion,[148] and tentatively estimated that the second $^2B_1$ state lies ca. 4.25 eV above the ground state based on earlier estimates of the

Table 4.3: CCSD and CC3 vertical excitation energies (in eV) of three low-lying states of the nitromethyl radical relative to the $^2B_1$ ground state.[6] ROCIS, XCIS and G2 results.[10]

	CCSD		CC3					
State	UHF	ROHF	UHF	ROHF	ROCIS[2]	XCIS[2]	G2	Expt.
$^2B_2$	2.403	2.401	2.048	2.033	4.557	2.607	1.990	—
$^2A_2$	2.624	2.627	2.418	2.407	6.183	1.512	2.476	1.591[7]
$^2A_1$	2.880	2.870	2.545	2.533	4.688	2.928	2.473	—
$^2B_1$	5.508	5.482	5.296	5.278	—	—	—	4.25[8]

dissociation threshold from matrix isolation studies by Jacox.[149] Later, Maurice and Head-Gordon used the nitromethyl radical as a benchmark case for the ROCIS and XCIS methods, though they made no comparison between their results and the limited experimental data.[10]

We have computed vertical excitation energies of CH_2NO_2 relative to its $^2B_1$ ground state at the CCSD and CC3 levels of theory using the Sadlej-pVTZ basis.[146] For comparison to the work of Maurice and Head-Gordon, all computations were carried out at the MP2/6-31++G(d,p) optimized geometry.[10,147] Core orbitals of the C, N, and O atoms were held frozen in all coupled cluster calculations.

Table 4.3.3 summarizes the CCSD and CC3 vertical excitation energies for comparison to the ROCIS, XCIS, and G2 results of Maurice and Head-Gordon.[10] For all four states, the choice of reference determinant makes little difference at either the CCSD or CC3 levels, suggesting

that spin contamination in these states is minimal. However, the difference between CCSD and CC3 results is large, up to 0.37 eV for the $^2B_2$ state, indicating that some double-excitation character is present in all four states. This is further supported by the ROCIS and XCIS results of Maurice and Head-Gordon. The ROCIS method gives poor results off by up to several eV, and the XCIS method, while a significant improvement over ROCIS, is still significantly in error for the $^2B_2$, $^2A_2$, and $^2A_1$ states. Interestingly, none of the methods compares well to the experimental result of 1.591 eV for the $^2A_2$ state, except for the XCIS method whose good agreement of 0.08 eV is likely fortuitous. It is likely that optimization of the excited state geometry would lower the CC3 result of 2.4 eV, though it is not clear that this would be sufficient to bring accord to theory and experiment for this state.

4.4 Conclusions

We have developed an open-shell variant of the CC3 method for computing excitation energies of open-shell systems. The method is defined for both UHF and ROHF reference determinants, and we have implemented it in the open-source PSI3 program package. The implementation is streamlined to use at most $\mathcal{O}(N^7)$ computational steps and avoids storage of the triple-excitation amplitudes for both ground and excited states. The excitation-energy program makes use of a Löwdin projection formalism (comparable to that of earlier implementations) that allows computational reduction of the Davidson algorithm to only the single- and double-excitation space, but limits the calculation to only one excited state at a

time.

Benchmark applications of the new methods to the lowest valence $^2B_1$ state of the allyl radical, low-lying states of the CH and CO^+ diatomics, and the nitromethyl radical show substantial improvement over ROHF- and UHF-based EOM-CCSD excitation energies for states with strong double-excitation character or cases suffering from significant spin contamination. Our future development efforts will focus on transition properties (such as oscillator strengths) and excited-state properties, including analytic energy gradients.

Chapter 5

Coupled Cluster Excitation Energies of the Allyl Radical Including Single- Double- and Approximate Triple Excitations

5.1 Introduction

Open-shell π-conjugated hydrocarbons are found in a multitude of fundamental organic reactions and exist as reactive intermediates. These radicals, for example, are found in the development of soot in high-temperature combustion reactions,[150] photochemistry,[151] atmo-

spheric and interstellar chemistry,[152,153] among others. Their clandestine role as meta-stable intermediates is thus essential for engineering a significant number of chemical products. Nevertheless, many of their molecular properties still remain poorly understood. While much research effort has been devoted towards understanding their properties, the accurate characterization of open-shell molecules - both experimentally and theoretically - is a particularly difficult research frontier. The complexity of these systems can be attributed to their underlying electronic framework; near degeneracies between low-lying states complicate the investigation of short-lived intermediates and lead to numerous theoretical problems, ranging from multireference character to convergence difficulties. Even geometrically simple molecules can have an electronic structure which makes their properties difficult to measure accurately.

As a first step towards understanding the complexity of such open-shell molecules, the allyl radical has been the focus of much research found in the literature. It is the simplest open-shell hydrocarbon possessing a π-conjugated system and is therefore an ideal candidate for understanding the intricate details of more complex systems. Although a considerable amount of data has been reported on its $\tilde{\mathrm{X}}^2A_2$ ground state, much less is known about its excited states. Flash photolysis studies by Currie and Ramsay revealed an electronic absorption peak at 408.3 nm (3.04 eV), which was assigned to the allyl radical's $\tilde{\mathrm{A}}^2B_1 \leftarrow \tilde{\mathrm{X}}^2A_2$ transtion.[154] Subsequent one-photon absorption experiments, *via* matrix isolation techniques and cavity ring-down spectroscopy, reported this transition at 408.5 nm (3.07 eV) and 408.3 nm (3.04 eV), respectively.[155,156] Multiphoton resonant ionization spectroscopy

investigations discovered three more absorptions assigned to the $2^2B_1 \leftarrow \tilde{\mathrm{X}}^2A_2$, $3^2B_1 \leftarrow \tilde{\mathrm{X}}^2A_2$ and a dipole forbidden $1^2A_1 \leftarrow \tilde{\mathrm{X}}^2A_2$ transition.[157–159] However, near- degeneracies between valence and Rydberg states complicates the resolution and detailed assignment for several of the electronic states. The increased complexity of such experimental conditions (e.g. short lifespan, resolution of close-lying states, unwanted side reactions) makes computational quantum chemistry an especially attractive approach for understanding the fundamental properties that govern a molecule's behavior.

Quantum chemical methods have been utilized to report vertical excitation energies of the allyl radical.[156,160,161] The apparent multiconfigurational nature of the Hartree-Fock wavefunction led previous computational efforts to focus on CASSCF (complete active space self-consistent field) methods. It was generally assumed that a simple three electron, three orbital CAS (comprising the bonding, anti-bonding, and non-bonding MO π-space) could accurately ascertain the first excited-state of the allyl radical: CASSCF(3,3)/TZV predicts a vertical excitation energy of 3.34 eV and an adiabatically corrected energy of 3.03 eV.[156,160] However, Roos *et al.* later reported that these results were fortuitous based on much larger CASSCF(3,7)/ANO computations where the predicted $\tilde{\mathrm{A}}^2B_1$ state lies 3.70 eV above the $\tilde{\mathrm{X}}^2A_2$ state.[161] Furthermore, they reported a series of CASPT2[162,163] and MS-CASPT2[164] valence and low-lying Rydberg states and addressed the importance of including dynamic electron correlation effects in the wavefunction.

Although multireference techniques may accurately predict the excited-state properties of radicals, as noted above there is no systematic approach for choosing an appropriate ac-

tive space. This becomes an especially complicated problem as the system size increases or when orbital degeneracies create a progressively complicated molecular wavefunction. Single-reference techniques can also reliably predict excited-state properties provided enough dynamic electron correlation is included in the wavefunction. The question is how much correlation is enough? Among the most reliable quantum chemical methods, coupled-cluster theory can ascertain excited states through variants of the equation-of-motion (EOM-CC)[32] or linear-response (LR-CC)[165] methods. The singles and doubles truncated EOM-CCSD method, for example, is capable of reproducing experimental excitation energies to within 0.2 eV when the excited-state wavefunction is dominated by single excitations. However, the accuracy of this model does not extend to cases when higher-excitations also contribute significantly.

When double-excitations or spin-contamination are pronounce, higher levels of correlation are required. For such cases, the inclusion of triples is found to dramatically improve excitation energies predicted by the EOM-CCSD model. Kucharski *et al.*[166] and Kowalski and Piecuch[167,168] were the first to report the implementation of the EOM-CCSDT method. Despite its promising results, the computational costs of the EOM-CCSDT method (i.e. storage requirements and $O(n^8)$ scaling) currently makes this technique unrealistic for most molecules. Watts and Bartlett have devoted much effort towards developing EOM-CC variants which approximate the effects of triples within the singles and doubles subspace: EOM-CCSDT-1, EOM-CCSDT-3, and EOM-CCSD(T), EOM-CCSD($\tilde{\text{T}}$).[39,41] These methods were found to improve excitation energies by up to 0.2 eV for a number of closed-shell molecules

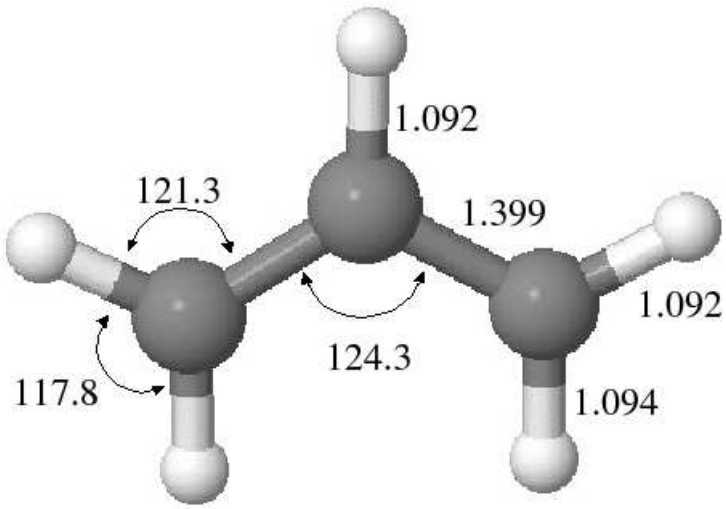

Figure 5.1: Geometric parameters were optimized at the CCSD(T)/aug-cc-pVDZ level; bond lengths are reported in Å; angles are reported in degrees.

while avoiding the expensive computation of the full treatment of triples.[169]

Recently, the CC3 method was extended to compute excitation energies for open-shell systems.[170] The method includes single-, double- and approximate triple-excitations in the correlated wavefunction. This method scales as an iterative $O(n^7)$ and avoids the explicite storage of the triples ampitudes. Utilizing this method, the first excited state of the allyl radical, and other open-shell molcules, displayed a significant improvements over the EOM-CCSD model. We have since adapted the single-reference CC3 model to investigate a series of valence and low-lying rydberg states of the allyl radical. ROHF- and UHF-reference vertical excitation energies were computed and compared to the CASPT2 results of Roos *et al.* and experiment when available. Systematic improvements (*via* electron correlation and basis set effects) to the excited-state wavefunction are used to measure the quality of the

CC3 model.

5.2 Computational Details

The allyl radical's ground state geometry was optimized at the CCSD(T)/cc-pVDZ level. EOM-CCSD and CC3 excitation energies are compared to Roos' CASPT2 results and experiment when available. The investigation entailed three different basis sets including aug-cc-pVDZ, aug-cc-pVTZ, and an ANO type basis set. The ANO basis set included the contracted set of 1s2p3d type functions on carbon and 1s2p type functions on hydrogen. Additionally, a single set of diffuse functions were placed at the center of mass. A spectrum of vertical excitation energies is reported utilizing the EOM-CCSD and CC3 methods. The CC3 method utilizes a Löwdin projection formalism in order to simplify computational costs of the linear-response sigma equations. As a tradeoff, however, only one state can be computed at a time. However, any state can be computed by keeping only the residual vectors produced within the Davidson algorithm with maximum overlap with the a particular EOM-CCSD state.

Table (5.1) summarizes the CCSD and CC3 vertical excitation energies computed using the Dunning correlation-consistent polarized-valence double- and triple-zeta basis sets (cc-pVDZ and cc-pVTZ, respectively) as well as the ANO basis augmented with diffuse s, p, and d-type functions (aug-cc-pVDZ).[78,139,140]

We have implemented the CCSD and CC3 methods in the open-source PSI3 program package[31] using a spin-factored/spin-orbital approach that is useful for applications to excited-

Table 5.1: Vertical exciation energies (eV) for each state of the allyl radical.

	aug-cc-pVDZ				Sadlej-pVTZ				ANO						
	CCSD		CC3		CCSD		CC3		CCSD		CC3				
	ROHF	UHF	ROHF	UHF	ROHF	UHF	ROHF	UHF	ROHF	UHF	ROHF	UHF	CASPT2	MSCASPT2	Experiment
$^2A_1$ states															
1 $(1a_2 \rightarrow 7a_1)$	4.904	5.006	4.871	4.887	4.910	5.014	4.870	4.887	4.978	5.086	4.922	4.941	5.11	5.11	4.97
2 $(1a_2 \rightarrow 8a_1)$	5.464	5.568	5.432	5.447	5.473	5.580	5.432	5.448	5.524	5.636	5.471	5.488	5.65	5.65	
3 $(1a_2 \rightarrow 9a_1)$	6.358	6.471	6.284	6.327	6.340	6.455	6.264	6.298	6.423	6.553	6.322	6.359	6.22		
4 $(6a_1 \rightarrow 1a_2)$	6.445	6.568	6.388	6.410	6.428	6.553	6.365	6.340	6.523	6.641	-	6.485	6.51	6.51	
5 $(1a_2 \rightarrow 11a_1)$	7.302	7.404	7.267	7.285	6.665	6.768	6.632	-	7.123	7.226	-	7.109	6.61	6.61	
$^2A_2$ states															
2 $(1b_1 \rightarrow 4b_1)$	6.288	6.378	5.948	6.007	6.261	6.352	5.919	5.980	6.263	6.359	5.911	5.971	6.60	6.61	
3 $(1a_2 \rightarrow 2a_2)$	7.505	7.595	7.472	7.490	7.288	7.382	7.251	7.270	7.116	7.219	7.095	7.104			
4 $(1b_1 \rightarrow 2b_1)$	8.879	8.911	8.667	8.719	8.763	8.796	8.573	8.620	8.653	8.732	8.597	8.619	8.34	8.36	
$^2B_1$ states															
1 $(1b_1 \rightarrow 1a_2)$	3.378	3.580	3.342	3.393	3.364	3.570	3.326	3.377	3.364	3.580	3.320	3.371	3.33	3.32	3.07
2 $(1a_2 \rightarrow 2b_1)$	5.776	5.832	5.743	5.751	5.735	5.798	5.700	5.709	5.887	5.941	5.838	5.847	5.83	5.73	(5.39-5.90)
3 $(1a_2 \rightarrow 3b_1)$	6.752	6.806	6.696	6.709	6.531	6.593	6.476	6.489	6.847	6.909	6.781	6.794	6.55	6.36	6.66
4 $(1a_2 \rightarrow 4b_1)$	8.255	8.346							7.151	7.252			6.59	6.90	
1 $(1a_2 \rightarrow 5b_2)$	5.559	5.658	5.525	5.543	5.564	5.665	5.523	5.541	5.651	5.755	5.594	5.614	5.76	5.76	
2 $(1a_2 \rightarrow 6b_2)$	6.519	6.620	6.503	6.474	6.522	5.626	6.474	6.498	6.608	6.722	6.530	6.562	6.56	6.56	
3 $(4b_2 \rightarrow 1a_2)$	6.639	6.767	6.592	6.553	6.630	6.759	6.553	6.584	6.692	6.819	6.625	6.648			

states of open-shell systems with either UHF or ROHF reference wave functions. The method is directly comparable to that described by Watts, Gauss, and Bartlett for the CCSD(T) method.[134] All adiabatic corrections were computed at the EOM-CCSD/aug-cc-pVDZ level using the AcesII programs package.

5.3 Discussion

The allyl radical's structural parameters listed in Table (5.1), were utilized throughout this investigation. Table (5.2) summarizes the CCSD and CC3 vertical excitation energies computed for the $^2A_1$, $^2A_2$, $^2B_1$, and $^2B_2$ excited states. Utilizing the CC3 model, we observe a reduction in spin contamination over the CCSD model. We compare our results to those reported by Roos *et al*, based solely on energetics, and experiment when possible. We note that we define each transitions based on Hartree-Fock molecular orbitals.

5.3.1 The $^2A_1$ States

The $^2A_1$ states are dipole forbidden transitions. As shown in Table (5.2), basis set effects appear minimal for states 1-4 with both CCSD and CC3: excitation energies utilizing the aug-cc-pVDZ, Sadlej-pVTZ and ANO basis sets are within 0.1 eV of each other. However, much larger effects are observed with state (5) where differences are nearly 0.5 eV between the aug-cc-pVDZ and the Sadlej-pVTZ basis sets. Although it is well known that the addition of diffuse functions are crucial in order to decrease these numerical effects, the extent of

sufficiently including such basis set corrections is not abundantly clear.

The (1) $^2A_1$ state has been assigned as a $1a_2 \rightarrow 3s$ Rydberg transition.[171] Indeed, ROHF- and UHF-based CCSD and CC3 calculations reveal significant s-type Rydberg character in the excited state wavefunction. Some spin contamination effects are observed in the UHF-reference with differences between ROHF- and UHF-CCSD on the order of 0.1 eV. We note that the excited state wavefunction posseses a rather large double excitation amplitude (0.111) which are known to be treated rather poorly at the CCSD level. The approximate excitation level (AEL) for this state, however, has a value of 1.08 indicating that the wavefunction is dominated primarily by single excitations. By including the effects of triples in the correlated wavefunction, differences between the predicted UHF- and ROHF-CC3 excitation energies are within 0.02 eV. Thus, it appears that CC3 largely removes spin contamination manifested in the CCSD wavefunction. Along with the fact that basis set effects are minimal, we therefore would expect the single-reference CC3 model to be reliable for predicting excitation energies for the (1) $^2A_1$ state. Nevertheless, CC3 predicts energies which are approximately 0.2 eV lower than the MSCASPT2 results of Roos *et al.* Furthermore, it is disturbing that the vertical excitation energies fall below the experimental results of Hudgens and Dulcey. Adiabatic corrections will further lower the predicted excitation energy and thus potentially bring into question the reliability of this method. However, Hudgens and Dulcey have also noted that these adiabatic corrections should be rather small for excitations out of a nominally nonbonding π electron into a weakly interacting Rydberg orbital.[159] A CCSD vibrational analysis of the (1) $^2A_1$ state indicates a large imaginary frequency along a b_1

type displacement (a disrotatory twist of the CH_2 end groups). Indeed, the ZEKE spectrum reported by Chen *et al.* implies a geometry change along this same coordinant path.[171] Furthermore, the reported MPI spectra indicates strong vibronic coupling between the (1) $^2A_1$ and (2) $^2B_1$ states leading to the nonplanar distortion. We have optimized the geometry of the (1) $^2A_1$ state *via* CCSD/aug-cc-pVDZ and discovered that the adiabatic corrections to the CCSD and CC3 models are approximately 0.11 eV. These models agree reasonably well with the experimental findings of Hudgens and Dulcey (within 0.2 eV).

The (2) $^2A_1$ state includes characteristics similar to those of the (1) $^2A_1$ state. According to the CCSD and CC3 calculations, the primary contribution to this excited state is an excitation out of the nominally singly occupied MO into an *s*-type Rydberg orbital. We note that although some *p*-type contributions are observed, their weight is significantly less than the *s*-type contributions. This is in contrast with the CASPT2 calculations of Roos *et al*, who assigned this Rydberg state as $3p_z$. Despite the fact that the (2) $^2A_1$ state poseses a large double excitation amplitude (0.114), with an AEL of 1.09 this state is primarily dominated by single replacement excitations. We would, therefore, expect the CCSD model to adequately describe this state, though small spin contamination effects are also observed at this level: differences between ROHF- and UHF-CCSD are approximately 0.1 eV. At the corresponding CC3 level, these differences are reduced to only 0.02 eV. Again, we observe descrepancies with the $1a_2 \rightarrow 3p_z$ Rydberg transition discribed by Roos *et al*: CC3 predicts the (2) $^2A_1$ state to lie 0.2 eV lower than the CASPT2 and MSCASPT2 models.

The (3) $^2A_1$ and (4) $^2A_1$ states are dominated by similar type excitations. The coupled-

cluster calculations predict that these excited states include significant contributions from alpha (from the singly occupied orbital) and beta (into the singly occupied orbital) spins. The largest alpha contributions involve excitations to a mixture of *s*- and *p*-type Rydberg orbitals. This is at odds with the CASPT2 calculations of Roos and co-workers: the (3) $^2A_1$ state was assigned as a valence transition while $3d_{x^2-y^2}$ Rydberg contributions were observed for the (4) $^2A_1$ state. Nevertheless, with a difference of less then 0.1 eV, both states are in excellent agreement with the CASPT2 and MSCASPT2 models.

For the (5) $^2A_1$ state, we observe that the dominant contribution is a single excitation out of the singly occupied MO into an *s*-type Rydberg orbital. Some *p*-type contributions are observed in the excited state wavefunction, however, their weight is significantly less. This again is in disagreement with the findings of Roos *et al*, who who assigned this Rydberg state as $3d_{z^2}$. Small spin contamination effects are observed at the CCSD level: differences between ROHF- and UHF-CCSD are approximately 0.1 eV. At the corresponding CC3 level, these effects are largely removed. Due to the large basis set dependance of this state, comparing our results to the CASPT2 results is quite difficult. Both the aug-cc-pVDZ and ANO basis sets produce results that differ by more than 0.6 eV with Roos *et al.* Only by utilizing the Sadlej-pVTZ basis set do the coupled cluster results agree with CASPT2 and MSCASPT2.

5.3.2 The $^2A_2$ States

The $^2A_2$ states are symmetric transitions. According to CCSD and CC3, the (2) $^2A_2$ excited state includes significant contributions from alpha and beta spins (both out of the HOMO-1 orbital). While Roos *et al.* has assigned this Rydberg state as $3d_{xy}$ we primarily observe *s*-type character and some *p*-type contributions. Both CCSD and CC3 display very little spin comtamination effects; differences between ROHF- and UHF- are less than 0.1 eV. The CC3 model's improved treatment of electron correlation does, however, significantly lower the predicted CCSD energy for the three $^2A_2$ states. Still, the coupled cluster vertical excitation energies are in complete disagreement with CASPT2 and MSCASPT2. CC3 predicts that this state is 0.5-0.6 eV more stable than the CAS models predict.

The (3) $^2A_2$ state does not appear to be assigned by Roos *et al*, *vide infra*. While spin-contamination appears minimal, there are large energetic differences (∼0.2 eV) between the basis sets. Thus, a more thorough investigation (e.g. higher levels of electron correlation, experimental data) is required before this state can be assigned with reasonable certainty.

CCSD and CC3 calculations on state (4) demonstrate a very strong contribution from beta-spin with some significant contributions of alpha spin as well (both out of the HOMO-1 orbital). The primary character of this state is of *p*-type but also includes some *s*-type Rydberg character. This is in agreement with Roos *et al.* who reported that this state as a $(1)b_1 \rightarrow 3p_y$ Rydberg transition. Dispite the fact that spin contamination appears negligible, dynamic correlation plays a significant role in this state with the CC3 model lowering the

CCSD energy by more than 0.2 eV. Nontheless, CASPT2 and MSCASPT2 both predict that the (4) $^2A_2$ state is approximately 0.3 eV more stable than predicted by CC3.

5.3.3 The $^2B_1$ States

The (1) $^2B_1$ state is the allyl radical's lowest lying excited state and has been indentified many times throughout the literature. Strong differences between ROHF- and UHF-CCSD indicates significant spin-contamination in the later. However, these differences are largely removed at the CC3 level. Furthermore, the CC3 energy is in excellent agreement with those of Roos *et al* and experiment. Compared to the results of Roos *et al*, while the CC3/Sadlej-pVTZ model agrees well with MSCASPT2, the CC3/ANO results compare best with CASPT2. However, unlike the reasonably well behaved (1) $^2B_1$ valence state, the Rydberg character of the (2) and (3) states make them ostensibly more challenging.

States (2) and (3), exhibit very little difference between ROHF- and UHF- for both CCSD and CC3. Basis set effects have a very small impact on the allyl radical's (1) and (2) $^2B_1$ states. The largest difference is observed in state (2) where the ANO basis set increases the CC3 energy by approximately 0.1 eV over the aug-cc-pVDZ and Sadlej-pVTZ basis sets. There are, however, significant basis set effects within state (3): the ANO basis set produces an energy that is 0.3 eV higher than with the Sadlej-pVTZ basis. The CC3/Sadlej-pVTZ model agrees best with both of the predicted CAS energies. Due to the large Rydberg character of these states, a more complete description of the basis set and correlated wavefunction

may be required.

5.3.4 The $^2B_2$ States

For the $^2B_2$ states, CC3 largely removes the multireference effects observed at the CCSD level: the largest difference between ROHF- and UHF-CC3 is 0.04 eV. Basis set effects, for both CCSD and CC3, are reasonably small (within 0.07 eV) for all three states. The CC3 energies for state (1) are approximately 0.1 eV lower than the corresponding CCSD energies. We note that in spite of the obstinately better CC3 model, CCSD is in better agreement with both CASPT2 and MSCASPT2.

For the (2) $^2B_2$ state, differences between ROHF- and UHF-CCSD are approximately 0.1 eV but are significantly reduced at the CC3 level. For this state, basis set effects are minimal and CC3 and CASPT3 are in excellent agreement with each other.

5.4 Conclusions

The electronic spectrum of the allyl radical has been obtained using the open-shell CC3 method. The assignment of the spectrum is in agreement with experiment to within 0.2 eV. The CC3 model's improved treatment of electron correlation reduced spin-contamination effects appearing in the EOM-CCSD model. However, significant discrepancies still exist with the predicted excitation energies of Roos and coworkers. For example, the (2) $^2A_2$ state

predicted by CC3 is 0.6 eV more stable than that predicted by CASPT2. However, we have concluded that accuracy of the coupled cluster results relies on the inclusion of triples for many states of the allyl radical. A more thorough analysis, including basis set effects, is still needed before the entire spectrum of allyl's states can be identified with certainty.

Chapter 6

One Electron Density Properties

> "God runs electromagnetics by wave theory on Monday, Wednesday, and Friday, and the Devil runs them by quantum theory on Tuesday, Thursday, and Saturday.[33]"
>
> -William Bragg

The response of a molecular system to external perturbations provides one of the principal sources of information on molecular behavior. The study of response functions, for both electric and magnetic perturbations, is thus of great importance in molecular science. However, in this chapter only the response to a electric field will be considered.

6.1 General Theory

For an electrostatic potential created at point $\mathbf{r}$ by the external field is $V(\mathbf{r})$, the perturbed Hamiltonian operator is,

$$H = H_0 + \sum_{\alpha} q^{\alpha} V(\mathbf{r}^{\alpha}), \tag{6.1}$$

where the sum is over all particles of the molecule; H_0 is the unperturbed Hamiltonian; q^{α} is the charge on the particle at $\mathbf{r}^{\alpha}$. The expansion of the external field $V(\mathbf{r})$ as a Taylor series in the displacement from the coordinate origin (commonly taken as the electronic charge centroid) leads to the following multipole expression,

$$H = H_0 - \mu_i F_i - \frac{1}{2} Q_{ij} F_{i,j} - \frac{1}{3!} \Omega_{ijk} F_{i,jk} - \ldots, \tag{6.2}$$

where F_i is the field parameter, $F_{i,j}{=}\partial F_i/\partial r_j$, and $F^{(2)}_{i,jk}{=}\partial^{(2)} F_i/\partial r_j \partial r_k$. The components μ_i, Q_{ij}, and Ω_{ijk} represent the dipole, quadrupole and octupole operators, respectively.

The total energy of the molecular system in the presence of a uniform field perturbation is defined as,

$$\begin{aligned} E &= \langle \Psi | H | \Psi \rangle \\ &= \langle \psi_0 + \psi | H | \psi_0 + \psi \rangle \end{aligned} \tag{6.3}$$

Where the unperturbed and perturbed normalized wave functions are denoted ψ_0 and ψ. The multipole components can thus be written directly as $\langle \psi | \mu_i | \psi \rangle$, $\langle \psi | Q_{ij} | \psi \rangle$, $\langle \psi | \Omega_{ijk} | \psi \rangle$, etc. Expanding the perturbed wave function ψ as a power series in the uniform field,

$$\psi = \psi^{(1)}_i F_i + \psi^{(2)}_{ij} F_{ij} + \psi^{(3)}_{ijk} F_{ijk} + \cdots, \tag{6.4}$$

leads to the formulation of the permanent dipole moment $\mu_i^{(0)}$, the linear polarizability α and the remaining hyperpolarizabilities,

$$\begin{aligned}
\langle\mu\rangle &= \langle\Psi|\mu|\Psi\rangle = \langle\psi_0 + \psi_i^{(1)}F_i + \psi_{ij}^{(1)}F_iF_j + \cdots|\mu|\psi_0 + \psi_i^{(1)}F_i + \psi_{ij}^{(1)}F_iF_j + \cdots\rangle \\
&= \langle\psi_0|\mu_i|\psi_0\rangle + \{2\langle\psi_j|\mu_i|\psi_0\rangle\}F_j \\
&\quad + \{2\langle\psi_{jk}^{(2)}|\mu_i|\psi_0\rangle + \langle\psi_j^{(1)}|\mu_i|\psi_k^{(1)}\rangle\}F_jF_k + \cdots \\
&= \mu_i^{(0)} + \alpha_{ij}F_j + \beta_{ijk}F_jF_k + \gamma_{ijkl}F_jF_kF_l + \cdots. \qquad (6.5)
\end{aligned}$$

If the wave function Ψ is calculated from a variational method, then it is straightforward to calculate these molecular properties in terms of analytic energy derivatives. Differentiating the energy - equation (6.3) - with respect to the field strength parameter gives,

$$\frac{\partial E}{\partial F_i} = \langle\Psi|\frac{\partial H}{\partial F_i}|\Psi\rangle + 2\langle\frac{\partial\Psi}{\partial F_i}|H|\Psi\rangle. \qquad (6.6)$$

For a variationally determined wave function the second term can be shown to vanish, giving the Hellman-Feynman theorem,

$$\frac{\partial E}{\partial F_i} = \langle\Psi|\frac{\partial H}{\partial F_i}|\Psi\rangle = \langle\Psi|\mu|\Psi\rangle = \left(\frac{\partial E}{\partial F_i}\right)_0 + \frac{1}{2}\left(\frac{\partial^2 E}{\partial F_i\partial F_j}\right)_0 F_j + \cdots \qquad (6.7)$$

Comparing equations (6.5) with (6.7), the permanent dipole moment and polarizabilities are now easily identified with derivatives of the energy at vanishing field strength.

It is important to note that the Hellman-Feynman theorem holds for variational methods where the energy is optimized with respect to all parameters in the wave function. For most calculations, the relevant parameters are the molecular orbital coefficients and the correlation amplitudes. For nonvariational methods such as coupled cluster theory, the dipole moment

calculated from equation (6.5) will differ from that of equation (6.7). The Hellman-Feynman theorem does however hold for the exact wave function. Therefore, as the truncated wave function in the coupled cluster method is improved, the differences between equations (6.5) and (6.7) will become negligible.

6.2 One-Particle Density Matrix

While the study of ground-state properties is well established and found in most quantum chemical software packages, the study of excited states is notoriously more difficult. However, the equation-of-motion formalism, discussed in chapter 2, can be exploited to determine properties of excited-states and transition probabilities among them.

The analytic derivation of equation (6.7) is formulated in terms of contracting the dipole moment integral with the reduced one-particle density matrix (opdm).

$$\rho_{pq} = \langle p^\dagger q \rangle = \langle L | \{ p^\dagger q \; exp(T) \}_c | R \rangle \tag{6.8}$$

Thus, properties other than energy can be computed provided the left- and right-states are considered. The R and L solutions satisfy the property of biorthogonality: a general property of non-Hermitian eigenvalue problems.[32]

$$\langle L^{(i)} | R^{(j)} \rangle = \delta_{ij} \tag{6.9}$$

However, the $L^{(i)}$ and $R^{(j)}$ are not orthogonal among themselves.

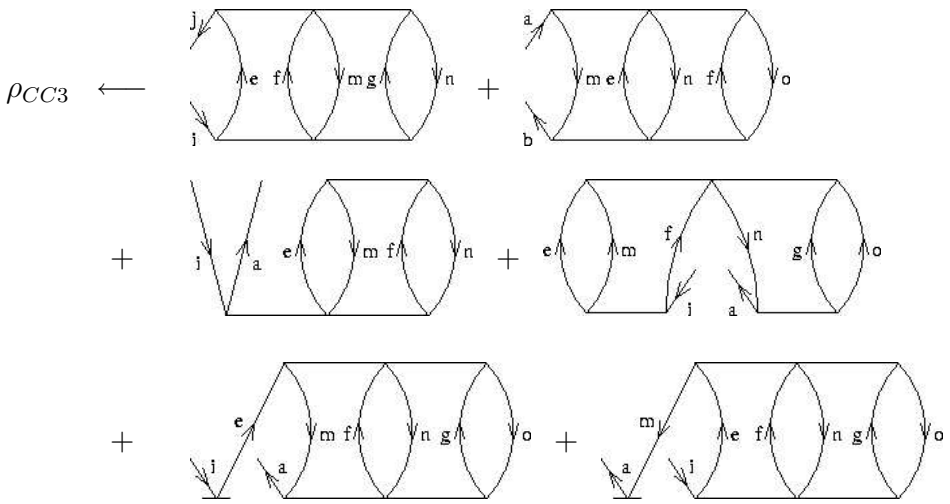

Figure 6.1: Triples contributions to the ground-state one-particle density matrix elements. The thin upper and lower lines represent λ and T vectors.

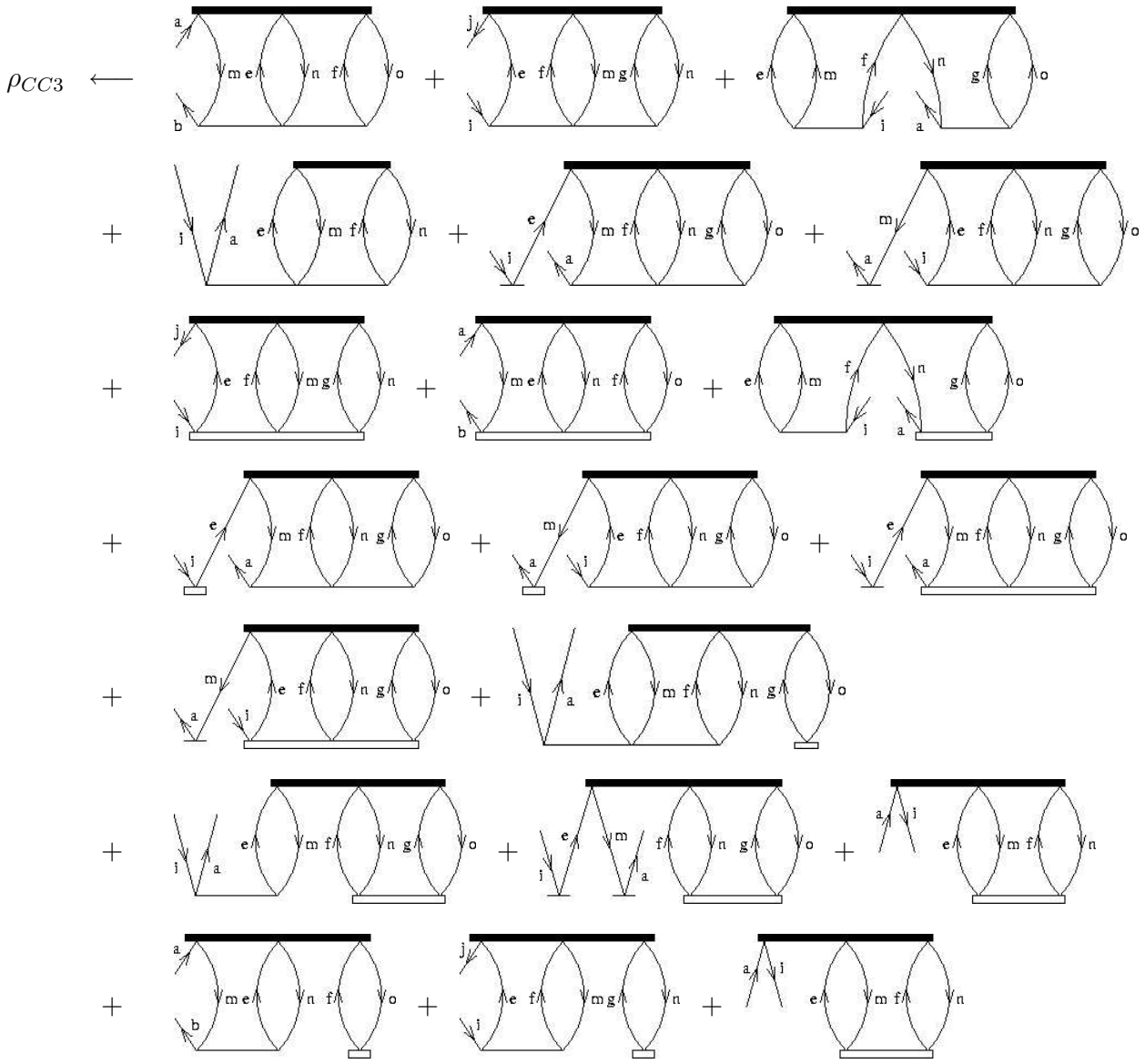

Figure 6.2: Triples contributions to the excited-state CC3 one-particle density matrix. The ground-state amplitudes (T_1, T_2, and T_3) correspond to the thin horizontal lines while the thick upper and lower lines represent the L and R vectors.

6.2.1 Transition Dipole Moments

The non-Hermitian nature of the EOM-CC approach leads to properties such as the dipole strength which can not be well defined. However, as Stanton and Bartlett noted, it is the "square" of these quantities that represent experimental observables.[32]

$$\begin{aligned} D_{xg} &= \langle L_g|\mu|R_x\rangle\langle L_x|\mu|R_g\rangle \\ D_{xg} &= \langle\Phi_0|L_g\{\mu\ exp(T)\}_c R_x|\Phi_0\rangle\langle\Phi_0|L_x\{\mu\ exp(T)\}_c R_g|\Phi_0\rangle \end{aligned} \tag{6.10}$$

The dipole strength D_{xg} is related to the oscillator strength in the dipole approximation *via*

$$f_L = \frac{2}{3}\omega_{g\to x} D_{xg} \tag{6.11}$$

where $\omega_{g\to x}$ is the excitation energy. Elements of the transition density matrix are identical to those shown in equation (6.10).

6.3 Computer Implementation

Figures (6.1) and (6.2) illustrate elements of the ground- and excited-state CC3 reduced opdm. Note that unlike the T-amplitudes, there is no connectivity requirement with the R-amplitudes and property operator. Fortunately, many of the excited-state density elements illustrated below, have the same diagrammatic structure of the ground-state equations. Therefore, after one has coded the ground-state density, many of the excited state density elements can easily be obtained.

We have recently added the ground- and excited-state CC3 opdm to the PSI3 chemical software package. However, convergence difficulties in the computation of the left-hand state, L, has complicated our goal of obtaining CC3 one-electron properties. For example, with CC3/DZ water, we were only able to converge L to 10^{-3}. For this case, L was solved from a linear set of equations. The convergence issues are currently under investigation. However, another approach is to solve L as an eigenvalue problem in an EOM like formalism. Our group is currently working on the L eigenvalue problem which may remove convergence problems.

Chapter 7

Summary and Concluding Remarks

> "If any student comes to me and says he wants to be useful to mankind and go into research to alleviate human suffering, I advise him to go into charity instead. Research wants real egotists who seek their own pleasure and satisfaction, but find it in solving the puzzles of nature.[33]"
>
> -Albert Szent-Györgi

The focus of this dissertation is on the general theory and development of approximate triples corrective models. We included a brief review on quantum chemical methods and the importance of adequately including electron correlation in the wave function. A particular emphasis was on coupled cluster theory and the equation-of-motion formalism. Adding triple excitations to the coupled cluster wave function, are known to play a vital role in improving the accuracy of the coupled cluster model. However, the costly CCSDT method stemmed

much research interest in the development of approximate triples methods. These methods are exact with respect to CCSDT in the singles and doubles space but approximate the costly triple excitations. Iterative and noniterative schemes were considered with a comparison of there defining triples equations. Using the diagrammatic rules discussed in Chapter 1, the derivation of the ground- and excited-state CCSD(T) and CC3 equations were illustrated. These methods were implemented within the PSI3 software package.

Utilizing the coupled cluster methods including triple excitations [CCSD(T) and CCSDT], the structures of *m*-benzyne and its fluorinated derivative, tetrafluoro-*m*-benzyne, were investigated using different reference wave functions (spin-restricted Hartree-Fock, spin-unrestricted Hartree-Fock, and Brueckner), and different basis sets [6-31G(*d*,*p*) and cc-pVTZ]. The inclusion of triple excitations in conjunction with *d*- and *f*-type polarization functions is paramount to correctly describe through-bond delocalization of the monocyclic form. At the highest level of theory, the C1−C3 distance of the minimum energy form of *m*-benzyne is 2.0 Å and the profile of the PES along the C1−C3 distance is that of an asymmetric, single-well, in agreement with previous density-functional theory and coupled cluster studies. In addition, the calculated CCSD(T) fundamental frequencies are in excellent agreement with the measured infrared frequencies, thus confirming the monocyclic form of *m*-benzyne. For tetrafluoro-*m*-benzyne, however, the increased eclipsing strain between the ring-external C−X bonds stabilizes the bicyclo[3.1.0]hexatriene form: the C1−C3 distance is calculated at the CCSD(T)/cc-pVTZ level to be approximately 1.75 Å, which is in the range of elongated CC bonds. Computed harmonic vibrational frequencies compare

reasonably well with the experimental neon-matrix difference spectrum and provide further evidence for the existence of a bicyclic form.

The coupled cluster iterative-triples model, CC3, is extended to include excited-states of open-shell molecules. We define the method for both spin-unrestricted Hartree-Fock (UHF) and spin-restricted open-shell Hartree-Fock (ROHF) reference determinants and discuss its efficient implementation in the PSI3 program package. The program is streamlined to use at most $\mathcal{O}(N^7)$ computational steps and avoids storage of the triple-excitation amplitudes for both the ground-and excited-state calculations. The excitation-energy program makes use of a Löwdin projection formalism (comparable to that of earlier implementations) that allows computational reduction of the Davidson algorithm to only the single- and double-excitation space, but limits the calculation to only one excited state at a time. However, a root-following algorithm may be used to compute energies for multiple states of the same symmetry. Benchmark applications of the new methods to the lowest valence $^2B_1$ state of the allyl radical, low-lying states of the CH and CO^+ diatomics, and the nitromethyl radical show substantial improvement over ROHF- and UHF-based CCSD excitation energies for states with strong double-excitation character or cases suffering from significant spin contamination. For the allyl radical, CC3 adiabatic excitation energies differ from experiment by less than 0.02 eV, while for the $^2\Sigma^+$ state of CH, significant errors of more than 0.4 eV remain.

The electronic spectrum of the allyl radical was computed by CCSD and CC3 combined with different reference wave functions (spin-restricted Hartree-Fock, spin-unrestricted Hartree-Fock), and different basis sets (aug-cc-pVDZ, ANO+, Sadlej-pVTZ). The complete Rydberg

series and the beginning of the second Rydberg series have been computed. The assignment of the spectrum is within 0.2 eV to experiment, however a few states reveal substantial discrepancies with previous CASPT2 and MSCASPT2 studies (0.6 eV). Nevertheless, for many states the single-reference CC3 model appears to be a promising tool to accurately characterize allyl's molecular structure.

The work that I have provided lays a foundation for future work in predicting high-accuracy electronic properties. There are many projects which can stem from the work which I have provided. The first is to fix the convergence problem with computing the CC3 left-hand state. This leads to the prediction of excited-state one-electron properties (dipole and multipole moments) and transition moments. However, the one-particle density matrix (opdm) should be streamlined to improve the programs efficiency. Currently, this code is doing at least twelve times more work than it needs to (a prefactor of $\frac{1}{12}$ appears in the occupied-occupied and virtual-virtual blocks of the matrix). Futhermore, the opdm includes a single N^8 step due to the format of the triples function (computes all possible A,B,C virtual orbital combinations for a given set of I,J,K occupied orbitals). This can be changed to an iterative N^7 step if the triples function is modified to compute all possible I,J,K combinations for a given set of A,B,C orbitals.

Bibliography

[1] S. Wilson, *Chemistry by Computer* (Springer-Verlag, New York, NY, 1986).

[2] H. Koch, O. Christiansen, P. Jørgensen, and J. Olsen, Chem. Phys. Lett. **244**, 75 (1995).

[3] O. Christiansen, H. Koch, and P. Jørgensen, J. Chem. Phys. **103**, 7429 (1995).

[4] H. Koch, O. Christiansen, P. Jørgensen, A. M. S. de Merás, and T. Helgaker, J. Chem. Phys. **106**, 1808 (1997).

[5] M. Winkler and W. Sander, J. Phys. Chem. A **105**, 10422 (2001).

[6] R. Marquardt, W. Sander, and E. Kraka, Angew. Chem. Int. Ed. Engl. **35**, 746 (1996).

[7] H. H. Wenk and W. Sander, Chem. Eur. J. **7**, 1837 (2001).

[8] H. H. Wenk and W. Sander, Eur. J. Org. Chem. 3927 (2002).

[9] C. L. Currie and D. A. Ramsay, J. Chem. Phys. **45**, 488 (1966).

[10] D. Maurice and M. Head-Gordon, J. Phys. Chem. A **100**, 6131 (1996).

[11] R. P. Feynman, *The Character of Physical Law*, 1st ed. (MIT Press, Cambridge, MA, 1967).

[12] M. Born and J. R. Oppenheimer, Annalen Der Physik **84**, 457 (1927).

[13] J. C. Slater, Phys. Rev. **32**, 339 (1928).

[14] J. C. Slater, Phys. Rev. **81**, 385 (1951).

[15] C. C. Roothaan, Rev. Mod. Phys. **23**, 69 (1951).

[16] J. A. Pople and R. Nesbit, J. Chem. Phys. **22**, 571 (1954).

[17] A. Szabo and N. S. Ostlund, *Modern Quantum Chemistry: Introduction to Advanced Electronic Structure Theory*, 1st ed. (McGraw-Hill, New York, 1989).

[18] T. D. Crawford, E. Kraka, J. F. Stanton, and D. Cremer, J. Chem. Phys. **114**, 10638 (2001).

[19] C. Møller and M. S. Plesset, Phys. Rev. **46**, 618 (1934).

[20] D. Cremer, E. Kraka, and Y. He, J. Mol. Structure **567**, 275 (2001).

[21] J. Olsen, O. Christiansen, H. Kock, and P. Jørgensen, J. Chem. Phys. **105**, 5082 (1996).

[22] B. Forsberg, Z. He, Y. He, and D. Cremer, Int. J. Quantum Chem. Symp. **76**, 306 (2000).

[23] J. Čížek, J. Chem. Phys. **45**, 4256 (1966).

[24] J. Čížek, Adv. Chem. Phys. **14**, 35 (1969).

[25] J. Čížek and J. Paldus, Int. J. Quantum Chem. Symp. **5**, 351 (1971).

[26] T. D. Crawford and H. F. Schaefer, Reviews in Compuational Chemistry **14**, 33 (2000).

[27] E. R. Davidson, J. Comp. Phys. **17**, 87 (1975).

[28] K. Hirao and H. Nakatsuji, J. Comp. Phys. **45**, 246 (1982).

[29] G. E. Scuseria, A. C. Scheiner, T. J. Lee, J. E. Rice, and H. F. Schaefer, J. Chem. Phys. **86**, 2881 (1987).

[30] J. F. Stanton, J. Gauss, J. D. Watts, and R. J. Bartlett, J. Chem. Phys. **94**, 4334 (1991).

[31] T. D. Crawford, C. D. Sherrill, E. F. Valeev, J. T. Fermann, M. L. Leininger, R. A. King, S. T. Brown, C. L. Janssen, E. T. Seidl, Y. Yamaguchi, W. D. Allen, Y. Xie, G. Vacek, T. P. Hamilton, C. B. Kellogg, R. B. Remington, and H. F. Schaefer, PSI 3.0, PSITECH, Inc., Watkinsville, GA 30677, U. S. A., 2000.

[32] J. F. Stanton and R. J. Bartlett, J. Chem. Phys. **98**, 7029 (1993).

[33] http://www.lhup.edu/ dsimanek/sciquote/htm.

[34] Z. He and D. Cremer, IJQCS **25**, 43 (1991).

[35] T. Helgaker, P. Jørgensen, and J. Olsen, *Molecular Electronic-Structure Theory*, 1st ed. (John Wiley and Sons Ltd, Baffins Lane, Chichester, West Sussex PO19 1UD, England, 2000).

[36] K. Raghavachari, G. W. Trucks, J. A. Pople, and M. Head-Gordon, CPL **157**, 479 (1989).

[37] Y. S. Lee, S. A. Kucharski, and R. J. Bartlett, J. Chem. Phys. **81**, 5906 (1984).

[38] J. Noga, R. J. Bartlett, and M. Urban, Chem. Phys. Lett. **134**, 126 (1987).

[39] J. D. Watts and R. J. Bartlett, Chem. Phys. Lett. **233**, 81 (1995).

[40] J. Noga, R. J. Bartlett, and M. Urban, Chem. Phys. Lett. **134**, 126 (1987).

[41] J. D. Watts and R. J. Bartlett, Chem. Phys. Lett. **258**, 581 (1996).

[42] G. Bucher, W. Sander, E. Kraka, and D. Cremer, Angew. Chem. Int. Ed. Engl. **31**, 1230 (1992).

[43] W. Sander, G. Bucher, H. Wandel, E. Kraka, D. Cremer, and W. S. Sheldrick, J. Am. Chem. Soc. **119**, 10660 (1997).

[44] W. Sander, Acc. Chem. Res. **32**, 669 (1999).

[45] W. Sander, M. Exner, M. Winkler, A. Balster, A. Hjerpe, E. Kraka, and D. Cremer, J. Amer. Chem. Soc. **124**, 13072 (2002).

[46] E. Kraka and D. Cremer, Chem. Phys. Lett. **216**, 333 (1993).

[47] E. Kraka and D. Cremer, J. Am. Chem. Soc. **116**, 4929 (1994).

[48] E. Kraka, D. Cremer, G. Bucher, H. Wandel, and W. Sander, Chem. Phys. Lett. **268**, 313 (1997).

[49] C. J. Cramer, J. J. Nash, R. R. Squires, and W. C. Lineberger, Chem. Phys. Lett. **277**, 311 (1997).

[50] E. Kraka, J. Anglada, A. Hjerpe, M. Filatov, and D. Cremer, Chem. Phys. Lett. **348**, 115 (2001).

[51] B. A. Hess, Chem. Phys. Lett. **352**, 75 (2002).

[52] L. V. Slipchenko and A. I. Krylov, J. Chem. Phys. **117**, 4694 (2002).

[53] Y. Shao, M. Head-Gordon, and A. I. Krylov, J. Chem. Phys. **118**, 4807 (2003).

[54] P. R. Schreiner, A. Navarro-Vasquez, and M. Prall, Acc. Chem. Res. **38**, 29 (2005).

[55] P. C. Hariharan and J. A. Pople, Theor. Chim. Acta **28**, 213 (1973).

[56] R. G. Parr and W. Yang, *Density-Functional Theory of Atoms and Molecules* (Oxford University, New York, 1989).

[57] A. D. Becke, J. Chem. Phys. **98**, 5648 (1993).

[58] C. Lee, W. Yang, and R. G. Parr, Phys. Rev. B. **37**, 785 (1988).

[59] A. D. Becke, Phys. Rev. A. **38**, 3098 (1988).

[60] J. Gräfenstein, E. Kraka, and D. Cremer, Chem. Phys. Lett. **288**, 593 (1998).

[61] J. Gräfenstein and D. Cremer, Phys. Chem. Chem. Phys. **2**, 2091 (2000).

[62] M. Prall, A. Wittkopp, and P. R. Schreiner, J. Phys. Chem. A **105**, 9265 (2001).

[63] J. Gräfenstein, E. Kraka, M. Filatov, and D. Cremer, Int. J. Mol. Sci. **3**, 360 (2002).

[64] V. Polo, E. Kraka, and D. Cremer, Theor. Chem. Acc. **107**, 291 (2002).

[65] V. Polo, E. Kraka, and D. Cremer, Mol. Phys. **100**, 1771 (2002).

[66] V. Polo, J. Gräfenstein, E. Kraka, and D. Cremer, Chem. Phys. Lett. **352**, 469 (2002).

[67] D. Cremer, M. Filatov, V. Polo, E. Kraka, and S. Shaik, Int. J. Mol. Sci. **3**, 604 (2002).

[68] A. P. Scott and L. Radom, J. Phys. Chem. **100**, 16502 (1996).

[69] R. J. Bartlett, in *Modern Electronic Structure Theory*, Vol. 2 of *Advanced Series in Physical Chemistry*, edited by D. R. Yarkony (World Scientific, Singapore, 1995), Chap. 16, pp. 1047–1131.

[70] G. D. Purvis and R. J. Bartlett, J. Chem. Phys. **76**, 1910 (1982).

[71] M. Rittby and R. J. Bartlett, J. Phys. Chem. **92**, 3033 (1988).

[72] K. Raghavachari, G. W. Trucks, J. A. Pople, and M. Head-Gordon, Chem. Phys. Lett. **157**, 479 (1989).

[73] R. J. Bartlett, J. D. Watts, S. A. Kucharski, and J. Noga, Chem. Phys. Lett. **165**, 513 (1990), erratum: **167**, 609 (1990).

[74] M. R. Hoffmann and H. F. Schaefer, Adv. Quantum Chem. **18**, 207 (1986).

[75] J. Noga and R. J. Bartlett, J. Chem. Phys. **86**, 7041 (1987), erratum: **89**, 3401 (1988).

[76] R. A. Chiles and C. E. Dykstra, J. Chem. Phys. **74**, 4544 (1981).

[77] N. C. Handy, J. A. Pople, M. Head-Gordon, K. Raghavachari, and G. W. Trucks, Chem. Phys. Lett. **164**, 185 (1989).

[78] T. H. Dunning, J. Chem. Phys. **90**, 1007 (1989).

[79] L. Adamowicz, W. D. Laidig, and R. J. Bartlett, Int. J. Quantum Chem. Symp. **18**, 245 (1984).

[80] A. C. Scheiner, G. E. Scuseria, J. E. Rice, T. J. Lee, and H. F. Schaefer, J. Chem. Phys. **87**, 5361 (1987).

[81] T. J. Lee and A. P. Rendell, J. Chem. Phys. **94**, 6229 (1991).

[82] G. E. Scuseria, J. Chem. Phys. **94**, 442 (1991).

[83] J. Gauss, W. J. Lauderdale, J. F. Stanton, J. D. Watts, and R. J. Bartlett, Chem. Phys. Lett. **182**, 207 (1991).

[84] J. Gauss and J. F. Stanton, Chem. Phys. Lett. **276**, 70 (1997).

[85] J. F. Stanton and J. Gauss, in *Recent Advances in Coupled-Cluster Methods*, edited by R. J. Bartlett (World Scientific Publishing, Singapore, 1997), pp. 49–79.

[86] P. G. Szalay, J. Gauss, and J. F. Stanton, Theor. Chim. Acta **100**, 5 (1998).

[87] J. F. Stanton, C. L. Lopreore, and J. Gauss, J. Chem. Phys. **108**, 7190 (1998).

[88] J. F. Stanton, J. Gauss, J. D. Watts, W. J. Lauderdale, and R. J. Bartlett, ACES II, 1993. The package also contains modified versions of the MOLECULE Gaussian integral program of J. Almlöf and P. R. Taylor, the ABACUS integral derivative program written by T. U. Helgaker, H. J. Aa. Jensen, P. Jørgensen and P. R. Taylor, and the PROPS property evaluation integral code of P. R. Taylor.

[89] R. Hoffman, A. Imamura, and W. J. Hehre, J. Amer. Chem. Soc. **90**, 1499 (1968).

[90] S. P. de Visser, M. Filatov, P. R. Schreiner, and S. Shaik, Eur. J. Org. Chem. 4199 (2003).

[91] J. M. Price, K. E. Nizzi, J. L. Campbell, H. I. Kenttämaa, M. Seierstad, and C. J. Cramer, J. Am. Chem. Soc. **125**, 131 (2003).

[92] P. G. Wenthold, R. R. Squires, and W. C. Lineberger, J. Am. Chem. Soc. **120**, 5279 (1998).

[93] C. J. Cramer and S. Debbert, Chem. Phys. Lett. **287**, 320 (1998).

[94] W. T. G. Johnson and C. J. Cramer, J. Phys. Org. Chem. **14**, 597 (2001).

[95] W. T. G. Johnson and C. J. Cramer, J. Am. Chem. Soc. **123**, 923 (2001).

[96] J. B. Foresman, M. Head-Gordon, J. A. Pople, and M. J. Frisch, J. Phys. Chem. A **96**, 135 (1992).

[97] M. Head-Gordon, R. J. Rico, M. Oumi, and T. J. Lee, Chem. Phys. Lett. **219**, 21 (1994).

[98] J. F. Stanton, J. Gauss, N. Ishikawa, and M. Head-Gordon, J. Chem. Phys. **103**, 4160 (1995).

[99] M. Head-Gordon and T. J. Lee, in *Recent Advances in Coupled-Cluster Methods*, edited by R. J. Bartlett (World Scientific Publishing, Singapore, 1997), pp. 221–253.

[100] D. J. Rowe, Rev. Mod. Phys. **40**, 153 (1968).

[101] M. E. Casida, in *Recent Advances in Density Functional Methods*, edited by D. P. Chong (World Scientific, Singapore, 1995), Vol. 1.

[102] D. J. Tozer, N. C. Handy, B. O. Roos, and L. Serrano-Andres, Mol. Phys. **97**, 859 (1999).

[103] A. Dreuw, J. L. Weisman, and M. Head-Gordon, J. Chem. Phys. **119**, 2943 (2003).

[104] B. Roos, M. Fülscher, P.-Å. Malmqvist, M. Merchán, and L. Serrano-Andrés, in *Quantum Mechanical Electronic Structure Calculations with Chemical Accuracy*, edited by S. Langhoff (Kluwer Academic Publishers, Dordrecht, 1995), pp. 357–438.

[105] T. D. Crawford and H. F. Schaefer, in *Reviews in Computational Chemistry*, edited by K. B. Lipkowitz and D. B. Boyd (VCH Publishers, New York, 2000), Vol. 14, Chap. 2, pp. 33–136.

[106] T. J. Lee and G. E. Scuseria, in *Quantum Mechanical Electronic Structure Calculations with Chemical Accuracy*, edited by S. R. Langhoff (Kluwer Academic Publishers, Dordrecht, 1995), pp. 47–108.

[107] J. Gauss, in *Encyclopedia of Computational Chemistry*, edited by P. Schleyer, N. L. Allinger, T. Clark, J. Gasteiger, P. A. Kollman, H. F. Schaefer III, and P. R. Schreiner (John Wiley and Sons, Chichester, 1998), pp. 615–636.

[108] H. Koch and P. Jørgensen, J. Chem. Phys. **93**, 3333 (1990).

[109] S. R. Gwaltney, M. Nooijen, and R. J. Bartlett, Chem. Phys. Lett. **248**, 189 (1996).

[110] P. G. Szalay and J. Gauss, J. Chem. Phys. **112**, 4027 (2000).

[111] J. D. Watts and R. J. Bartlett, J. Chem. Phys. **101**, 3073 (1994).

[112] J. D. Watts and R. J. Bartlett, Chem. Phys. Lett. **233**, 81 (1995).

[113] J. D. Watts and R. J. Bartlett, Chem. Phys. Lett. **258**, 581 (1996).

[114] K. Hald, P. Jørgensen, O. Christiansen, and H. Koch, J. Chem. Phys. **116**, 5963 (2002).

[115] K. Hald and P. Jørgensen, Phys. Chem. Chem. Phys. **4**, 5221 (2002).

[116] O. Christiansen, C. Hättig, and J. Gauss, J. Chem. Phys. **109**, 4745 (1998).

[117] O. Christiansen, J. Gauss, and J. F. Stanton, Chem. Phys. Lett. **292**, 437 (1998).

[118] K. Hald, P. Jørgensen, and C. Hättig, J. Chem. Phys. **118**, 1292 (2003).

[119] J. Gauss, O. Christiansen, and J. F. Stanton, Chem. Phys. Lett. **296**, 117 (1998).

[120] O. Christiansen, H. Koch, and P. Jørgensen, J. Chem. Phys. **105**, 1451 (1996).

[121] S. A. Kucharski, M. Wloch, M. Musial, and R. J. Bartlett, J. Chem. Phys. **115**, 8263 (2001).

[122] K. Kowalski and P. Piecuch, J. Chem. Phys. **115**, 643 (2001).

[123] K. Kowalski and P. Piecuch, Chem. Phys. Lett. **347**, 237 (2001).

[124] J. C. Saeh and J. F. Stanton, J. Chem. Phys. **111**, 8275 (1999).

[125] M. Musial, S. A. Kucharski, and R. J. Bartlett, J. Chem. Phys. **118**, 1128 (2003).

[126] P. Piecuch, K. Kowalski, I. S. O. Pimientia, and M. J. McGuire, Int. Rev. Phys. Chem. **21**, 527 (2002).

[127] K. Kowalski and P. Piecuch, J. Chem. Phys. **115**, 2966 (2001).

[128] K. Kowalski and P. Piecuch, J. Chem. Phys. **116**, 7411 (2002).

[129] K. Kowalski and P. Piecuch, J. Chem. Phys. **120**, 1715 (2004).

[130] Y. S. Lee, S. A. Kucharski, and R. J. Bartlett, J. Chem. Phys. **81**, 5906 (1984).

[131] M. Urban, J. Noga, S. J. Cole, and R. J. Bartlett, J. Chem. Phys. **83**, 4041 (1985).

[132] A. P. Rendell, T. J. Lee, and A. Komornicki, Chem. Phys. Lett. **178**, 462 (1991).

[133] C. D. Sherrill and H. F. Schaefer, The configuration interaction method: Advances in highly correlated approaches, in press.

[134] J. D. Watts, J. Gauss, and R. J. Bartlett, J. Chem. Phys. **98**, 8718 (1993).

[135] T. D. Crawford and H. F. Schaefer, J. Chem. Phys. **104**, 6259 (1996).

[136] W. J. Lauderdale, J. F. Stanton, J. Gauss, J. D. Watts, and R. J. Bartlett, Chem. Phys. Lett. **187**, 21 (1991).

[137] We note that the recent implementation of the CC3 linear response approach by Hald, Jørgensen, and Hättig (Ref.[118]) makes use of an $\mathcal{O}(N^7)$ algorithm that involves outer loops over pairs of virtual indices. It would be possible to use this algorithm to include the terms from Eq. 4.13 to obtain more optimal scaling, though the computational overhead of the algorithm is almost certainly greater than the one used for the other triples terms in this work, in which the outer loops involve groups of three occupied indices.

[138] M. Yamaguchi, J. Mol. Struct. (Theochem) **365**, 143 (1996).

[139] R. A. Kendall, T. H. Dunning, and R. J. Harrison, J. Chem. Phys. **96**, 6796 (1992).

[140] Basis sets were obtained from the Extensible Computational Chemistry Environment Basis Set Database, Version 12/03/03, as developed and distributed by the Molecular Science Computing Facility, Environmental and Molecular Sciences Laboratory which

is part of the Pacific Northwest Laboratory, P.O. Box 999, Richland, Washington 99352, USA, and funded by the U.S. Department of Energy. The Pacific Northwest Laboratory is a multi-program laboratory operated by Battelle Memorial Institute for the U.S. Department of Energy under contract DE-AC06-76RLO 1830. Contact David Feller or Karen Schuchardt for further information.

[141] J. Gauss, J. F. Stanton, and R. J. Bartlett, J. Chem. Phys. **95**, 2623 (1991).

[142] J. F. Stanton and J. Gauss, J. Chem. Phys. **99**, 8840 (1993).

[143] S. V. Levchenko and A. I. Krylov, J. Chem. Phys. **120**, 175 (2004).

[144] We note that similar QRHF-EOM-CCSD calculations were used by Williams, Harding, Stanton and Weisshaar to reduce the spin contamination in excited-state calculations on the methylvinoxy radical, whose electronic structure bears strong similarity to that of the allyl radical..[172,173]

[145] S. V. Levchenko and A. I. Krylov, private communication.

[146] A. J. Sadlej, Theor. Chim. Acta **79**, 123 (1991).

[147] R. B. Metz, D. R. Cyr, and D. M. Neumark, J. Phys. Chem. **95**, 2900 (1991).

[148] D. R. Cyr, D. J. Leahy, D. L. Osborn, R. E. Continetti, and D. M. Neumark, J. Chem. Phys. **99**, 8751 (1993).

[149] M. E. Jacox, J. Phys. Chem. **87**, 3126 (1983).

[150] K. M. Leung and R. P. Lindstedt, Combust. Flame **102**, 129 (1995).

[151] H.-J. Deyerl, I. Fischer, and P. Chen, J. Chem. Phys. **110**, 1450 (1999).

[152] P. R. Westmorel, A. M. Dean, J. B. Howard, and J. P. Longwell, J. Phys. Chem. **93**, 817 (1989).

[153] A. Webster, Mon. Not. R. Astron. Soc. **265**, 421 (1993).

[154] C. L. Currie and D. A. Ramsay, J. Chem. Phys. **45**, 488 (1966).

[155] G. Maier, H. P. Reisenauer, B. Rohde, and K. Dehnicke, Chem. Ber. **116**, 732 (1983).

[156] K. Tonokura and M. Koshi, J. Phys. Chem. A **104**, 8456 (2000).

[157] A. Callear and H. Lee, Trans. Faraday Soc. **64**, 308 (1968).

[158] T.-K. Ha, H. Baumann, and J. Oth, J. Chem. Phys. **85**, 1438 (1986).

[159] J. Hudgens and C. Dulcey, J. Phys. Chem. **89**, 1505 (1985).

[160] M. Yamaguchi, J. Mol. Structure **365**, 143 (1996).

[161] F. Aquilante, K. P. Jensen, and B. O. Roos, Chem. Phys. Lett. **380**, 689 (2003).

[162] K. Andersson, P.-A. Malmqvist, B. Roos, A. Sadlej, and K. Wolinski, J. Phys. Chem. **94**, 5483 (1990).

[163] K. Andersson, P.-A. Malmqvist, and B. Roos, J. Chem. Phys. **96**, 1218 (1992).

[164] J. Finley, P.-A. Malmqvist, B. Roos, and L. Serrano-Andesr, Chem. Phys. Lett. **288**, 299 (1997).

[165] H. Koch and P. Jørgensen, J. Chem. Phys. **93**, 3333 (1990).

[166] S. A. Kucharski, M. Wloch, M. Musial, and R. J. Bartlett, J. Chem. Phys. **115**, 8263 (2001).

[167] K. Kowalski and P. Piecuch, J. Chem. Phys. **115**, 8263 (2001).

[168] K. Kowalski and P. Piecuch, Chem. Phys. Lett. **347**, 247 (2001).

[169] M. Musial, Stanislaw, and R. J. Bartlett, J. Chem. Phys. **118**, 1128 (2003).

[170] C. E. Smith, R. A. King, and T. D. Crawford, J. Chem. Phys. **122**, 054110 (2005).

[171] D. W. Minsek and P. Chen, J. Phys. Chem. **97**, 13375 (1993).

[172] S. Williams, L. B. Harding, J. F. Stanton, and J. C. Weisshaar, J. Phys. Chem. A **104**, 9906 (2000).

[173] S. Williams, L. B. Harding, J. F. Stanton, and J. C. Weisshaar, J. Phys. Chem. A **104**, 10131 (2000).

Vita

Christopher Edward Smith was born to Charles and Nancy Smith on September 18, 1977 in Paducah Kentucky and was raised with a sister Christina Smith. Christopher grew up in Pensacola Florida and went on to attend the University of Florida where he graduated from in May 2000 with a Bachelor of Science degree in Engineering Science. Christopher moved to Blacksburg, Virginia to begin graduate study in August 2001 where he began his research efforts under the guidance of Dr. Daniel Crawford in theoretical chemistry in pursuit of a Ph.D. Upon completion of his graduate studies at Virginia Tech, Christopher plans on moving to Northern Virginia and work for an Engineering or Government contracting organization.